ESTIMATION OF WAVE-INDUCED SHIP HULL BENDING MOMENT FROM SHIP MOTION MEASUREMENTS

JINSONG XU

INFORMATION TO USERS

This manuscript has been reproduced from the microfilm master. UMI films the text directly from the original or copy submitted. Thus, some thesis and dissertation copies are in typewriter face, while others may be from any type of computer printer.

The quality of this reproduction is dependent upon the quality of the copy submitted. Broken or indistinct print, colored or poor quality illustrations and photographs, print bleedthrough, substandard margins, and improper alignment can adversely affect reproduction.

In the unlikely event that the author did not send UMI a complete manuscript and there are missing pages, these will be noted. Also, if unauthorized copyright material had to be removed, a note will indicate the deletion.

Oversize materials (e.g., maps, drawings, charts) are reproduced by sectioning the original, beginning at the upper left-hand corner and continuing from left to right in equal sections with small overlaps.

Photographs included in the original manuscript have been reproduced xerographically in this copy. Higher quality 6" x 9" black and white photographic prints are available for any photographs or illustrations appearing in this copy for an additional charge. Contact UMI directly to order.

ProQuest Information and Learning
300 North Zeeb Road, Ann Arbor, MI 48106-1346 USA
800-521-0600

UMI®

Estimation of Wave-Induced Ship Hull Bending Moment from Ship Motion Measurements

By

© Jinsong Xu, M. Eng.

A thesis submitted to the School of Graduate Studies
in partial fulfillment of the requirement
for the degree of Ph.D.

Faculty of Engineering and Applied Science
Memorial University of Newfoundland
November 2000

St. John's Newfoundland Canada

Abstract

A time-domain technique is developed for the real-time estimation of wave-induced vertical bending moment from the coupled heave and pitch motion measurements. The estimated values can be compared with those obtained from the strain gauge readings to ensure the validity of Hull Response Monitoring Systems (HRMS).

A general time-domain relationship between the vertical bending moment and the coupled heave and pitch motions was formulated through a Fourier transform of the frequency-domain mathematical model. The instantaneous bending moment value was approximated by a function of the heaving and pitching displacements, velocities, and accelerations. A neural network technique was developed to identify this unknown function through a learning process.

The application of the proposed technique to the experimental data demonstrated the validity of the methodology. The simulation results suggested that this technique could be used in conjunction with a time-domain simulation package to provide a numerical estimation model.

Acknowledgements

I am grateful to Dr. Haddara for his guidance and encouragement in preparing this thesis.

I am also grateful to Dr. Lye and Dr. Swamidas for their help in this work.

Special thanks to Mr. Andrew Kuczora for his technical support in the experiments.

Table of Contents

List of Figures

List of Tables

List of Abbreviations

ABS	American Bureau of Shipping (USA)
DNV	Det Norske Veritas (Norway)
HRMS	Hull Response Monitoring System
IMO	International Maritime Organization
ISSC	The International Ship and Offshore Structure Congress
ITTC	The International Towing Tank Conference
Lloyd's	Lloyd's Register of Shipping (UK)
MLP	The Multilayer Perceptron
MUN	Memorial University of Newfoundland
NSRDC	Naval Ship Research and Development Center (USA)
ONR	Office of Naval Research (USA)
RAO	Response Amplitude Operator
RINA	The Royal Institution of Naval Architects (UK)
SNAME	The Society of Naval Architects and Marine Engineers (USA)

1. Introduction

1.1 Objective

The growth in the size and complexity of ship structures has provided an impetus for the increased use of Hull Response Monitoring Systems (HRMS). These systems are intended to enhance ship operational safety by monitoring and displaying ship response information. Since ship structural design is mainly based on the magnitude of the allowable hull girder bending moment, it would be preferable for the HRMS systems to display the instantaneous bending moment against allowable values in real time.

In most HRMS systems, bending moment values are obtained from strain gauge measurements. These transformations are usually based on the theoretical strain-moment relationship and need to be validated by some other estimation methods. Significant research has been conducted in an attempt to estimate hull girder bending moments from ship motion data. These estimated values can be compared with those transformed from the strain gauge readings to prevent any significant errors.

The main objective of this work is to develop a time-domain technique for estimating the wave-induced vertical bending moment from the coupled heave and pitch motions.

1.2 Research Outline

Ship response analysis could be carried out in three different domains, namely, the time domain, the frequency domain, and the probability domain. Numerous transformation techniques allow the researchers to move from one domain to another.

For real-time estimation in this work, a time-domain relationship between the wave-induced bending moment and vertical ship motions has to be established. It is convenient to determine a mathematical model in the frequency domain first, and then transform the model into the time domain. The frequency-domain model for the rigid-body ship motions and the wave-induced bending moment can be formulated using a strip theory. Through Fourier transform, the wave-induced bending moment is approximated by a function of the heaving and pitching displacements, velocities, and accelerations in the time domain. This function can be identified using artificial neural networks.

The important feature of neural networks is their ability to approximate arbitrary functions through on-line and off-line learning processes. A multilayer perceptron (MLP) network is employed in this work, and the backpropagation learning algorithm is used. The training data must be maximally representative and informative. For the present system, it is proved that the auto- and cross-correlation functions of the bending moment and ship motions are suitable training data. The correlation functions can be estimated from the ship response time histories.

The proposed technique is applied to experimental data as well as to simulated data. Model tests of 'R-class Icebreaker' ship model are carried out in the wave tank at Memorial University of Newfoundland. The model consists of two segments joined at the midship section by an aluminum bar. Four strain gauges are mounted on the joint bar to measure the midship bending moment. After the training process, the neural network produces the accurate estimates of the instantaneous bending moment. The simulation

results suggest that this technique can be used in conjunction with a time-domain simulation package to provide a numerical estimation model.

This work is based on a mathematical model for the rigid ship hull and a linear relationship between the wave-induced bending moment and the ship motions in the vertical plane. The high-frequency vibratory loads due to whipping and springing are not considered in the current work. It is promising to extend the present technique to include the high-frequency loads in the final estimation.

1.3 Organization

An extensive review of previously published work and available techniques is presented in Chapter 2. A full description of the ship model and the experimental program follows in Chapter 3. The mathematical formulation as well as the experimental analysis in the frequency domain is described in Chapter 4. The time-domain estimation technique is developed in Chapter 5. A numerical simulation procedure and the results are given in Chapter 6. Finally, the conclusions and recommendations are presented in Chapter 7.

More details of the numerical computations, the computer programs, and the experimental results are presented in Appendix I to Appendix III.

2. Literature Review

2.1 Hull Response Monitoring System

2.1.1 HRMS Overview

Ship response to the sea environment is a main concern for ship designers and operators. With the growth in ship size and structural complexity, it has been difficult for mariners to monitor various ship responses through their physical senses. Hull Response Monitoring Systems (HRMS) have been developed to measure and display the real-time ship motions and hull structural responses. The recorded data is also valuable for more sophisticated onshore analysis to develop and verify ship design criteria. HRMS development is spurred by regulatory bodies, classification societies, academic organizations, and ship owner/operators. IMO is developing a set of HRMS rules for bulk carriers over 20,000 DWT. ABS, Lloyd's, and DNV have offered guidelines for HRMS systems. Some technical issues are also addressed in recent ISSC proceedings (Moan and Berge, 1997). A survey result from Slaughter *et al.* (1997) shows that there are more than 200 HRMS installations around the world. Representative installations include four crude oil tankers for BP Oil Company (Witmer and Lewis, 1995), and two other crude oil tankers for ARCO Marine (Lacey and Chen, 1995).

Ashcroft (1996) and Slaughter *et al.* (1997) present an overview of Hull Response Monitoring Systems. There are four major components in a basic HRMS system: a microprocessor, a visual display, data storage equipment, and a suite of sensors. Long baseline strain gauges are typically used to measure primary hull girder strain on the main deck. Accelerometers are used to measure ship motions. Some environmental sensors are

also available for installation. The microprocessor analyzes the raw data and interprets the signals. Immediate comparison can be made between measured and allowable values. Suitable information is displayed in real time. The storage of monitored data allows more sophisticated post voyage analysis. The basic HRMS system may be expanded to incorporate a wide variety of additional sensors. Some more extensive systems include automatic downloading of weather forecast information via satellite and advanced voyage-planning capability based on weather information. It is expected that HRMS systems will become a standard feature in future ships.

2.1.2 Characteristics of Major Ship Responses

The major environmental factor for a floating vessel is ocean waves. The wave elevation in a realistic seaway is always irregular and never repeats itself. Ship responses that may require monitoring are mainly ship motions, hull girder stresses, and wave loads. They are also random processes (Slaughter *et al.*, 1997).

The six-degree-of-freedom ship motions are three translational (surge, sway, and heave) and three rotational (roll, pitch, and yaw). Roll, pitch, and heave are generally of most concern for ship motion analysis. Roll motion reduces reserve transverse stability and causes crew discomfort. The coupled heaving and pitching generate the vertical cargo acceleration and increase relative bottom velocity with respect to the waves. A detailed description of ship motions is given in Lewis (1989).

Full-scale stress data from Little and Lewis (1971), Vulovich *et al.* (1989) and other research programs have clarified the characteristics of hull girder stresses under actual service conditions. These characteristics are summarized by Mansour (1990). A typical

stress time history is the combination of three independent components: static stress, low-frequency wave-induced stress, and high-frequency vibratory stress. The static stress results mainly from the stillwater loads caused by the loading condition in stillwater and the thermal loads due to temperature difference in water and air. The wave-induced stress is associated with the loads resulting from the motions of the ship as a rigid body. The frequency range is relatively low and close in magnitude to the wave encounter frequency for a wave having a length nearly equal to the ship length. The vibratory stress is associated with loads resulting from the two-node mode vibration of the hull girder. The frequency range is relatively high and close to the two-node mode natural frequency of the hull girder. The vibration can be continuous "springing" excited by the high-frequency wave components. It also can be the transient "whipping" caused by bottom or bow flare slamming. The wave-induced stress and the vibratory stress do not always occur simultaneously. Quite often only the wave-induced component appears in a stress record. Due to the random nature of the ocean waves, both wave-induced stress and vibratory stress are random processes.

Wave loads exerted on a ship hull girder include bending moments and shear forces (Bhattacharyya, 1978). Similar to the hull girder stresses, the total bending moment consists of a static component, a wave-induced component, and a vibratory component (due to whipping and springing). From full-scale measurements and model tests results, the whipping bending moment may be as large as the wave-induced bending moment, while the springing bending moment is usually of low magnitude. Only in very long flexible ships such as Great Lakes bulk carriers, the springing loads are found to be

important. Jenson and Dogliani (1996) shows that a design wave bending moment probably can be derived without considering springing for normal merchant ship types. In most cases, only static and wave-induced bending moments are superimposed on each other. At an arbitrary longitudinal section, total wave-induced bending moments can be resolved into three components: vertical bending moment, horizontal bending moment, and torsional moment. Vertical bending moment dominates the structural design. Horizontal bending moment is generally much less important because of its smaller magnitude and the greater hull strength. Torsional moment is usually insignificant. Therefore, the wave-induced vertical bending moment represents a major component of hull girder bending moment for a ship at sea.

2.1.3 Monitoring Hull Girder Bending Moments

With the drastic increase in ship size since 1960's, overloading of hull structures has been highlighted in many marine losses. Since ship structural design is based mainly on the magnitude of the allowable bending moment, it would be preferable for the HRMS system to display the instantaneous bending moment against allowable values in real time (Witmer and Lewis, 1995). The recorded data is also valuable for the structural reliability analysis, which requires more specific information about wave loads (Mansour, 1990).

In most full-scale measurements, the bending moment values are obtained from the strain gauge readings. Strains experienced by a ship's deck structure normally comprise three components, namely, primary hull strain due to hull girder bending moments, secondary grillage strains and tertiary strains in local plate panels. Long baseline strain gauges are typically designed to measure primary hull strain by measuring the displacement of a

metal rod of about two meters in length. The rod is rigidly fixed at one end and free to move at the other. The coefficient of thermal expansion of the rod and deck material should be matched to minimize errors caused by thermal expansion. Experience has shown that long baseline strain gauges are more durable in exposed locations and less susceptible to local strain effects (Ashcroft, 1996). As long as the ship structure remains elastic, hull girder bending moment varies linearly with the primary hull strain. Ideally the transformation from strain readings to bending moment values should be based on a full-scale calibration. That is, a known bending moment is applied on the ship in calm water while the corresponding change in strain gauge reading is recorded (Little and Lewis, 1971). The "known" bending moments are usually applied in either of two ways: special ballast changes or normal cargo discharges. Full-scale calibration frequently takes several days and the strain gauges are responsive to thermal effects that may cause a gross change in hull stress. It is thus required to conduct full-scale calibrations on overcast, windless nights after the hull structure has reached a steady-state temperature. Even if the calibration were "thermal effects free", the final measurements may still be affected by the diurnal thermal stress changes, particularly in the more tropic regions. Such thermal contamination has been fully discussed by Shi *et al.* (1996). As an alternative to full-scale calibrations, some HRMS systems obtain the linear strain-moment relationship from the structural analysis results. Witmer and Lewis (1995) used simple beam theory to obtain the bending moment as the product of the measured bending stress and the calculated section modulus. The use of finite element analysis should provide more accurate results. As indicated by Ashcroft (1996), an HRMS system should include a means for checking the system results to ensure its validity. Significant

research has been conducted in an attempt to estimate hull girder bending moments from wave information or ship motion measurements.

Theoretically it is easier to estimate the hull girder bending moment from wave information rather than from ship motion measurements. But shipboard environmental sensors are much less accurate than ship motion sensors. Some researchers are even back-calculating sea states as a function of ship motion parameters (Hua and Palmquist, 1995). It is expected that values of hull girder bending moments estimated from ship motion measurements should be more accurate than those estimated from wave information. Slaughter *et al.* (1997) quoted a technique proposed by Lovdahl, Lacey, and Chen in their presentation "Advances in Computer Based Onboard Voyage Planning" to the 1995 SNAME Joint California Sections Meeting. Their approach is based on the work of Kaplan (1995), but the accuracy of this approach is not within ABS guidelines for real-time value display. In Kaplan (1995), both wave-induced loads and slam-induced vibratory loads are incorporated into time-domain simulations. The rigid-body ship motion characteristics are calculated in the frequency domain using a linear strip theory. Although time histories of ship motions and wave loads are generated, the general time-domain relationships between the wave loads and ship motions are not established. Without a time-domain mathematical model, it is not convenient to estimate the instantaneous bending moments from ship motion measurements in real time.

2.2 Theories for Ship Response Analysis

2.2.1 Frequency-domain Theories

Extensive research has been conducted to study ship response in regular waves. The strip theory for heave and pitch motions in head waves (Korvin-Kroukovsky and Jacobs, 1957) was the first motion theory suitable for numerical computations with adequate accuracy. This theory was later extended by Jacobs (1958) to include wave-induced bending moments and shear forces for a ship in regular head seas. The more rigorous approach of Salvesen *et al.* (1970) has been widely accepted for computing the motions and loads of a rigid-body ship advancing at constant mean forward speed with arbitrary heading in regular sinusoidal waves.

Strip theory is used to determine the coefficients and exciting forces in the linear equations of ship motion. It is assumed that the vessel is a slender body moving in high-frequency waves. Consequently, the fluid flow velocities in the transverse direction are much greater than in the longitudinal direction, and the flow field around any cross section of the ship may be approximated by the assumed two-dimensional flow in that plane. If the ship body is divided into many narrow strips, the total effect on the ship is the integration of the effects on all individual strips. The essence of strip theory is thus to reduce a three-dimensional hydrodynamic problem to a series of two-dimensional problems. The most popular methods for solving the two-dimensional hydrodynamic problems are the boundary integral method (Frank, 1967) and the Lewis-form method (Lewis, 1929). Frank's method allows a more accurate description of the hull cross section, but requires more computational effort compared with the Lewis-form approach.

Strip theory methods have been extended to study the springing loads in flexible ship hulls. Troesch (1984) carried out both experiments and computations for springing response on a ship model joined amidships. Jensen and Dogliani (1996) performed springing load calculations within the framework of a nonlinear, quadratic strip theory. The complete solution to the springing problem requires consideration of the hull structural properties as well as the hydrodynamic excitation.

For ship motions in low-frequency waves, the ordinary slender-body theory has to be used instead of the strip theory. Newman and Sclavounos (1980) developed a unified theory to cover the whole frequency range. At low frequencies, the unified theory approaches the ordinary slender-body theory and yields terms that involve longitudinal interference between sections. For high frequencies, this longitudinal interference disappears and the results are identical to the strip theory.

The advent of large, high-speed computers has allowed the application of three-dimensional calculation methods, which take into account the 3-D effects and improve the accuracy of both local and global force predictions. The Rankine source methods and 3-D panel methods are being developed to replace the strip theory (Tan *et al.*, 1996).

The equations for regular-wave responses involve frequency-dependent coefficients. For a given frequency they are all constants and the system has a solution. Essentially we are solving the problems in the frequency domain, and the regular-wave equations constitute a frequency-domain mathematical model (Ogilvie, 1964).

2.2.2 Linear-Random Theory

The theory for the response of a linear system to random excitation was developed in the realm of electrical engineering (Rice, 1944). It is essentially a combination of linear system theory and random process theory. St. Denis and Pierson (1953) first introduced this linear-random theory to the marine field for the study of irregular ship motions. Later application for the wave load evaluation helped in the development of the structural reliability analysis for marine structures (Mansour, 1990).

Lewis (1989) gives a description of the linear-random theory for marine applications. There are two crucial assumptions underlying the theory. First, the short-term ocean waves are stationary, zero-mean, Gaussian random processes. Secondly, ship responses are linear transformations of the wave elevation or slope. Based on these assumptions the probability structure and the statistical parameters of the wave elevation and the ship response are constant in the short term. Linear-random theory is intended for predicting the stationary statistics of the ship response. In a stationary, zero-mean, Gaussian process the only necessary statistical parameter is the variance. It is uniquely determined by the power spectrum. Because of the linearity assumption, the response spectrum is related to the wave spectrum through a Response Amplitude Operator (RAO). The Response Amplitude Operator is conventionally defined as the modulus of the frequency response function, and physically interpreted as the ratio of the response amplitude to the amplitude of a harmonic wave. The RAOs represent the frequency-domain relationship between ship responses and wave elevations. They can be obtained from either theoretical calculations or regular-wave experiments. Once the wave spectrum and RAOs are available, the ship response spectra and statistics can be easily determined.

The essence of linear-random theory is transforming the frequency-domain results into a probability domain. The statistical parameters as well as extreme values are suitable for use in reliability analyses and performance assessments.

2.2.3 Time-domain Theories

Although the application of linear strip theory in the frequency and probability domains has achieved remarkable success, there are a number of ship response problems that can not be satisfactorily analyzed using such techniques. Bottom slamming, bow flare impact, and the resulting whipping are obvious examples. They are commonly dealt with in the time domain using estimated motion history and impact forces (Oliver, 1990). A comprehensive review of the theories and techniques for impact loading is given in Daidola and Mishkevich (1995). In order to analyze the combined responses, even linear rigid-body results have to be expressed in the form of a time history.

Kaplan (1995) describes a quasi-linear analysis procedure to determine both the rigid-body and hydroelastic vibratory responses due to slamming impacts. The rigid-body ship motions and wave loads are calculated in the frequency domain using a linear strip theory. These outputs in frequency response form are then expressed in time history form in order to be combined with the slam-induced responses that are determined in the time domain. The transformation is performed using a time-domain simulation method. A wave spectrum is considered as a sum of sinusoidal components, and the response time history is obtained as the linear superposition of responses to these individual wave components. The general time-domain equations are not formulated in this procedure.

In Oliver (1990), the simulation of ship motions and the hull girder loads is based on the time-domain equations. The assumed equation form is similar to that of the frequency domain, but the coefficients are calculated at each time step. The frequencies at which the coefficients are evaluated can be selected to be either peak frequencies of response spectra or the average frequencies during the previous two cycles of response. Here the time-domain equations are actually approximated using the frequency-domain models.

For the ship response in ocean waves, it is usually convenient to formulate a mathematical model in the frequency domain first, and then transform the results into the time domain (Hutchison, 1990). The frequency-domain equations are generally differential equations with frequency-dependent coefficients. Tick (1959) and Ogilvie (1964) have shown that these equations can be transformed to the time domain as convolution integral equations. Under certain conditions, they may be approximated by the constant-coefficient differential equations.

2.3 Experiments for Ship Response Analysis

2.3.1 Full-scale Measurements and Ship Model Tests

Full-scale measurement is the most direct approach to study ship response in actual seaways. More and more design criteria are based on the results of full-scale measurements. Typical programs are presented in Little and Lewis (1971) and Vulovich *et al.* (1989). This approach, however, has some disadvantages and difficulties. First of all, full-scale measurements are very expensive and difficult to implement. Secondly, it is difficult to measure the sea state, in particular the directional wave spectrum. Thirdly, it is impossible to fully control the experimental environment. Finally, full-scale measurements can not be used as a design tool for predicting the behavior of a proposed new design (Hutchison, 1990).

In contrast to full-scale measurements, ship model tests are controlled experiments. The desired sea environment can be achieved and maintained during the test. This approach is a useful design tool and relatively inexpensive. One major problem is the errors caused by scale effect due to viscous and surface tension forces. In some experiments, the physical dimensions of the test facility make it difficult to obtain long duration test runs for a model with forward speed (Hutchison, 1990).

During model tests, the motion measurements are relatively straightforward. But the experimental study of the hull girder bending moment requires a specially designed ship model. Lewis (1954) used a wooden model to determine the wave-induced bending moment. The model was segmented amidships and the bending moment was determined by measuring the relative deflection between the two segments. This model is essentially

rigid and does not include any hydroelastic effects. De Does (1960) measured bending moments at three locations along the model length. The models were made of fiberglass with wire resistance strain gauges imbedded in the walls. Wachnik and Schwartz (1963) segmented a ship model at seven stations and interconnected the model parts using an aluminum flexure beam. These models are essentially hydroelastic models and the hull vibratory responses are included in the measurements.

Recently, Hermanski (1993) measured the wave-induced bending moment on a rigid ship model. McTaggart (1997) used a hydroelastic model with a continuous flexible backbone to determine both the wave-induced and whipping bending moments.

2.3.2 Experimental Data Analysis and System Identification

Ship response data are recorded during ship model tests and full-scale measurements. Data analysis and system identification techniques have been employed to determine the response characteristics and the coefficients of the assumed mathematical model. Hutchison (1990) mentioned some applications in determining resistance and maneuvering characteristics for a full-scale ship. Application to the rolling model tests showed some good results.

A typical procedure for conducting system identification is described in Ljung (1999). The most fundamental step is the careful design of the experiments. The recorded response data must be representative and informative. After data acquisition and preparation, the form of the mathematical model has to be determined. This is the most difficult step in the procedure. In some cases, a model with several unknown physical parameters may be constructed using basic physical laws and other well-established

relationships. This is a "gray box" model. In other cases some standard mathematical structures, such as a linear time-invariant model and artificial neural networks, are assumed without reference to the physical background. The parameters of these models have no physical interpretation. This is a "black box" model. The final step in the procedure is to identify the unknown parameters using the experimental data through the application of estimation methods. The quality of the model is assessed from the performance when the model is used to reproduce the experimental data.

The analysis of the experimental data could be carried out in three different domains, namely, the time domain, the frequency domain, and the probability domain. Numerous transformation and analysis techniques allow the researchers to move from one domain to another (Hutchison, 1990). Typical data processing techniques include data filtering, mean and variance analysis, probability density analysis, auto-correlation analysis, cross-correlation analysis, auto-spectral density analysis, cross-spectral density analysis, impulse response analysis, and frequency response analysis. The details of data analysis techniques are fully presented in Bendat and Piersol (1986), and Ljung (1999).

2.4 Real-time Techniques for Ship Response Analysis

2.4.1 Application of Real-time Techniques

Real-time techniques have been developed rapidly in the past decades. Their application in the marine field has helped to improve the operational safety and efficiency. Real-time estimation is widely used in HRMS systems for monitoring instantaneous ship response. Real-time forecasting is developed for predicting motions or other responses over an interval of several seconds. Tan *et al.* (1993) gives a brief review of these techniques. The early attempts for real-time prediction of ship responses were made using Kalman filtering techniques. The mathematical model of the ship response is provided using seakeeping theory and based on the knowledge of the encountered wave spectrum and response transfer functions. The main difficulty in this approach is the estimation of the wave spectrum. Later development involved the application of on-line system identification techniques. Chung *et al.* (1990) developed an algorithm in which the wave excitation information is extracted from the ship motion data. The estimated wave excitation is extrapolated for the forecasting of the ship motions. Broome and Pittaras (1990) used the ARMAX models (Auto Regressive Moving Average with eXogenous input) to identify the ship motion equations in real time. No previous knowledge of the ship response is required. The mathematical model is formed on-line and conveniently updated whenever it is necessary.

Recent development is closely associated with the real-time control of ship response and machinery. The application details and technical issues are presented in Wilson (1997).

The focus of the real-time techniques is the construction of a mathematical model in the time domain.

2.4.2 Artificial Neural Networks

Artificial neural networks are a group of cellular computational structures that can be implemented in both hardware and software forms. One of their capabilities is to approximate arbitrary functions through an on-line or off-line learning process. This provides a means to identify and model complex systems without a priori knowledge of the physical mechanisms. In the past decade, they have become a very popular choice as a universal "black box" model for nonlinear systems (Ljung, 1999). A full discussion about network structures, functional capabilities, learning algorithms, and generalization performance is presented in Hush and Horne (1993).

Artificial neural networks are constructed from individual neurons, which are the basic computing units in the structure. Static networks are characterized by neuron equations that are memoryless, thus the output is a function only of the current inputs. Dynamic networks, on the other hand, are systems with memory. Their neuron equations are typically described by differential or difference equations. In the multilayer perceptron (MLP) network, which is the most widely used static network, individual neurons are arranged in successive layers with the sigmoid nonlinearity as neuron equation. Quite often each layer is fully connected to the adjacent layers and information is passed only forward from the input layer through the hidden layer(s) to the output layer. Linear neurons are commonly used in the output layer to make learning easier. The connecting weights between the layers are the trainable network parameters that fully determine the

relationship between the inputs and the outputs. During the supervised learning process, the neural network is presented with a set of input-output points and trained to implement a mapping that matches the sample points as closely as possible. The most popular learning method for the MLP is the backpropagation algorithm, which uses a gradient search technique to find the optimum values for the connecting weights. It is an iterative process of computing the gradient and adjusting the weight values until a minimum error is located. This learning process finally selects a "black box" model suitable for the underlying system.

The most important issue for the network implementation is the generalization performance, which is a measure of how well the network performs on the actual data outside the training set. A particular method, cross-validation, has been developed to monitor generalization performance during the learning process. It works by splitting the sample data into two sets: a training set that is used to train the network, and a test set that is used to measure the generalization performance of the network. During the learning process the performance of the network on the training data will continue to improve, but its performance on the test data will only improve to a point, beyond which it will start to degrade. It is at this point where the network starts to memorize the data instead of to learn the function. This is the point at which the learning process should be stopped. Cross-validation not only avoids any premature termination, but also improves the generalization performance of the network.

In the marine field, the MLP networks have been used for ship motion identification by Haddara & Hinchey (1995), and Haddara & Xu (1999). More applications are associated

with ship control systems. Hardier (1997) developed a maneuverability model using recurrent neural networks. Zhang *et al.* (1997) described an on-line trained neutral network controller (NNC) for the automatic ship control. The focus of these developments is to take advantage of the learning ability of the neural networks.

2.5 Review Summary

An extensive review of the literature indicates that Hull Response Monitoring System (HRMS) is a developing technology to measure and display the real-time ship response information. The major ship responses that may require monitoring are ship motions, hull girder stresses, and wave loads. The results of full-scale measurements and model tests have shown that the wave-induced vertical bending moment is the significant wave load component. Since ship structural design is mainly based on the magnitude of allowable bending moment, it would be preferable for the HRMS system to display the instantaneous bending moment against allowable values in real time. In most HRMS systems, the bending moment values are determined from the strain gauge readings based on linear strain-moment relationship. The transformation results may be affected by the calibration process and the computational inaccuracies. They need to be validated by some other estimation results. Significant research has been conducted in an attempt to estimate hull girder bending moments from ship motion readings.

Ship response analysis could be carried out in three different domains, namely, the time domain, the frequency domain, and the probability domain. Numerous theories and transformation techniques allow the researchers to move from one domain to another. Strip theory, unified theory, and 3-D theories have been developed to solve the regular-wave problems and formulate the frequency-domain equations. Linear-random theory transforms the frequency-domain results into probability domain. The resulting statistical parameters and extreme values are suitable for reliability analysis and performance assessment. The time-domain results are also transformed from the frequency domain.

Numerical simulations and Fourier transforms are most common techniques. In addition to theoretical analysis, full-scale measurements and ship model tests provide the experimental methods for ship response analysis. System identification techniques have been combined with the experimental data to determine the unknown coefficients and terms in ship response models.

More and more real-time techniques have been developed for estimation, forecasting, and control of ship responses. The fundamental element of the real-time techniques is the construction of a mathematical model in the time domain. Artificial neural networks have become a popular choice as a universal "black box" model of nonlinear systems. The peculiar advantage lies in their capability to approximate arbitrary functions through an on-line or off-line learning process. This provides a good means to identify and model the complex systems without a priori knowledge of physical mechanisms.

3. Model Tests

3.1 Experimental Set-up

3.1.1 General Arrangement

The objective of the present work is to identify the time-domain relationship between wave-induced vertical bending moment and coupled heave and pitch motions. Time histories of bending moment and ship motions have to be measured during model tests. The experimental technique involving a segmented model, as seen in Lewis (1954) and Hermanski (1993), is used in this work.

Model tests were carried out in MUN's wave tank using a 1:40 'R-class Icebreaker' ship model. The testing facility consists of a wave tank, an instrumented towing carriage, and a fully equipped control room. The wave tank has inside dimensions of 58.27m in length, 4.57m in wide, and 3.04m in depth. At one end of the wave tank is a hydraulically operated, piston type wave generator. At the other end is a parabolic beach for absorbing and dissipating the incident wave energy. Waves are created in the tank by the translatory motion of a waveboard, which is electronically controlled from the control room. The available wave frequencies range from 0.3Hz to 1.2Hz. The towing carriage over the wave tank is equipped with a dynamometer, which is able to measure the vertical motion up to 0.4m and rotations within a ±30°.

During the model tests, an 'R-class Icebreaker' ship model was positioned along the centerline of the wave tank, and attached to the towing carriage through the dynamometer. The model was free to move only in the vertical plane, and the forward

speed was provided by the towing carriage. In every test run, five parameters were measured and recorded in the form of time history. They are:

- Model Speed (m/sec)
- Wave Elevation (cm)
- Heave Displacement (cm)
- Angular Pitch Displacement (degree)
- Wave-induced Midship Bending Moment (Nm)

In order to measure the wave-induced bending moment amidships, the ship model was segmented at the midship section. The two segments were joined together by an aluminum bar, and the hull gap was sealed with medium-resistive latex medical band. The general arrangement is illustrated in Figure 1.

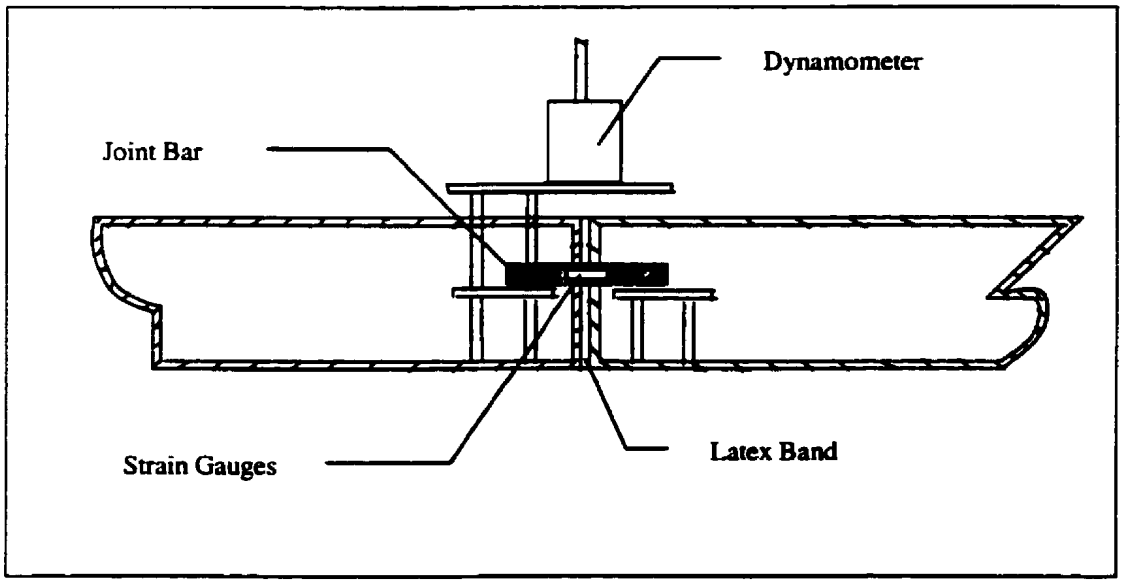

Figure 1: Illustration of General Arrangement

3.1.2 Model Description

The model used for the tests is a 1:40 scale 'R-class Icebreaker'. The hydrostatic particulars of the ship model are presented in Table 1, and the body plan is shown in Figure 2. The model hull was made of glass reinforced plastic and segmented at the midship section. A gap of about 5mm was left between the segments to allow the small deflection of the joint bar. This gap was sealed with medium-resistive latex medical band, which was attached to the hull surface using duct tape. When the ship model was out of the tank, three auxiliary bars were added to prevent the overload of the midship section. They were removed before each calibration and test run.

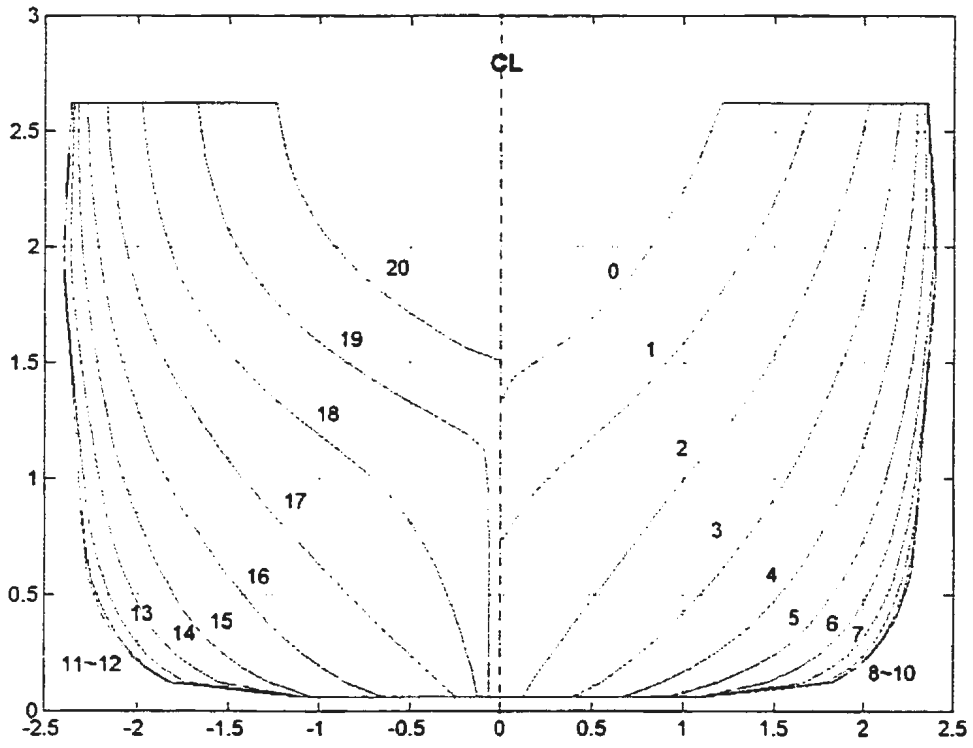

Figure 2: Body Plan of 'R-class Icebreaker' Ship Model

Table 1: Hydrostatic Particulars for 'R-class Icebreaker' Ship Model

Length between perpendiculars (LPP), m	2.1985
Length of waterline (LWL), m	2.3250
Waterline beam at midships, m	0.4840
Waterline beam at maximum section, m	0.4840
Maximum waterline beam, m	0.4845
Draft at midships, m	0.1735
Draft at maximum section, m	0.1745
Draft at aft perpendicular, m	0.1790
Draft at forward perpendicular, m	0.1675
Equivalent level keel draft, m	0.1735
Maximum section forward at midships, m	-0.1850
Area of maximum section, m^2	0.0773
Center of buoyancy forward of midships (LCB), m	-0.0080
Center of buoyancy above keel, m	0.0970
Wetted surface area, m^2	1.3347
Volume of displacement, m^3	0.1190
Center of floatation forward of midships (LCF), m	-0.0175
Center of floatation above keel, m	0.1735
Area of waterline plane, m^2	0.899
Transverse metacentric radius (BM), m	0.122
Longitudinal metacentric radius (BML), m	2.4
Center of area of profile plane forward of midships, m	-0.0195
Center of area of profile plane above keel, m	0.0895
Area of profile plane, m^2	0.3580

The platform structure, the aluminum bar, and the dynamometer formed a considerable proportion of the ballast on the model. Other lead ballast weights were distributed along

the model length and placed as low as possible to assure maximum transverse stability. The individual weight locations are listed in Table 2, and the model longitudinal weight distribution is plotted in Figure 3.

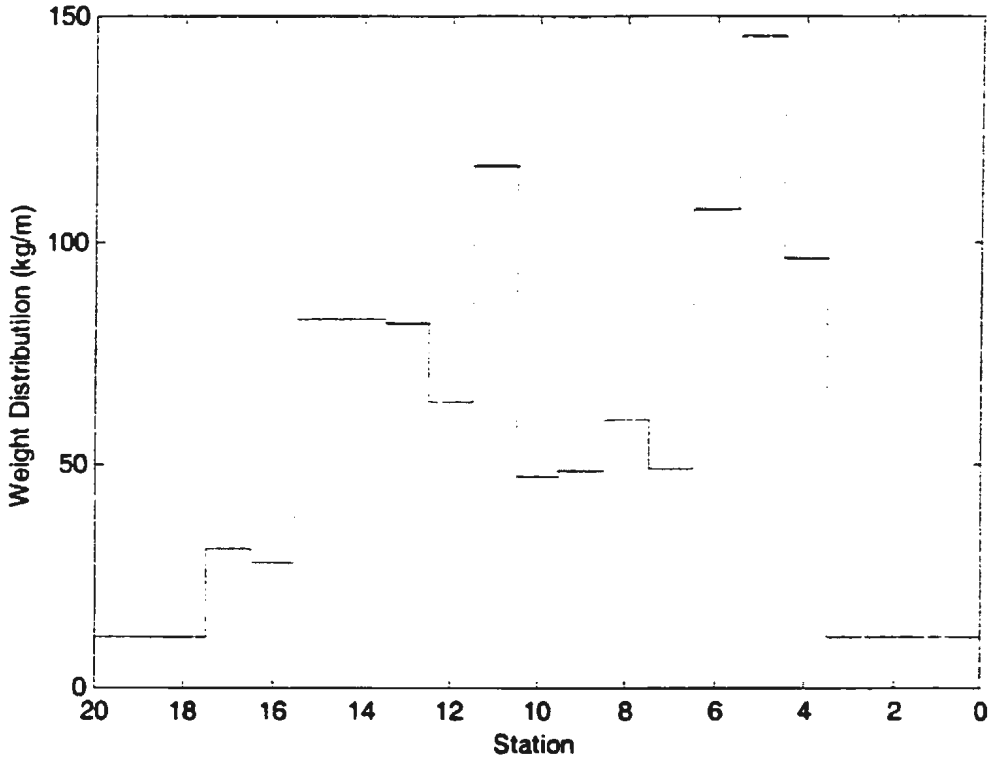

Figure 3: Weight Distribution of 'R-class Icebreaker' Model

Table 2: Weight Locations in 'R-class Icebreaker' Model

Component	Mass (kg)	Aft-edge (cm) (from midship)	Fore-edge (cm) (from midship)	Length (cm)
Ballast-1	12.005	42.5	70.5	28
Ballast-2	8.381	42.5	64.5	22
Ballast-3	1.964	42.5	51.5	9
Ballast-4	4.056	32.5	42.5	10
Ballast-5	4.075	32.5	42.5	10
Ballast-6	4.110	-14	-3	11
Ballast-7	4.285	-14	-3	11
Ballast-8	1.998	-36.5	-31.5	5
Ballast-9	1.996	-36.5	-31.5	5
Ballast-10	8.607	-58.5	-36.5	22
Ballast-11	12.005	-63.5	-36.5	27
Ballast-12	2.096	-83.5	-74.5	9
Dynamometer	7.3	-8	8	16
Aft-platform	11.33	-27.5	-7.5	20
Center-platform	1.643	-7.5	7.5	15
Fore-platform	8.667	7.5	27.5	20
Joint bar	2.348	-22.5	22.5	45
Ship Hull	24.5	-110	110	220
Total	**121.366**			

3.1.3 Instrumentation

Five parameters were recorded during model tests. The wave elevation was measured using a capacitance type wave probe, which was installed on the carriage at a fixed location about 0.5m away from the model at the midship section. The forward speed was

measured by a velocity meter on the towing carriage. Heave displacement and angular pitch displacement were measured using the dynamometer located on the vertical line through the center of gravity. The wave-induced bending moment was determined from the strain of the aluminum bar, which was equipped with four strain gauges at the center. During model tests, a computer on the towing carriage was used to record the experimental data at a frequency of 50Hz.

The aluminum bar actually functioned as a bending moment transducer. It was machined from an aluminum 6061 T6 stock. The elastic part is 150mm long and extends 75mm fore-and-aft from the midship section. Its cross-sectional shape is 20mm×20mm square. The strain values were measured using four metal-foil strain gauges mounted along the longitudinal center of the bar. The four matched gauges were connected to form a full Wheatstone bridge, which compensated for temperature effects and other environmental noise. A schematic diagram is shown in Figure 4. This design is based on the work of Wachnik and Schwartz (1963).

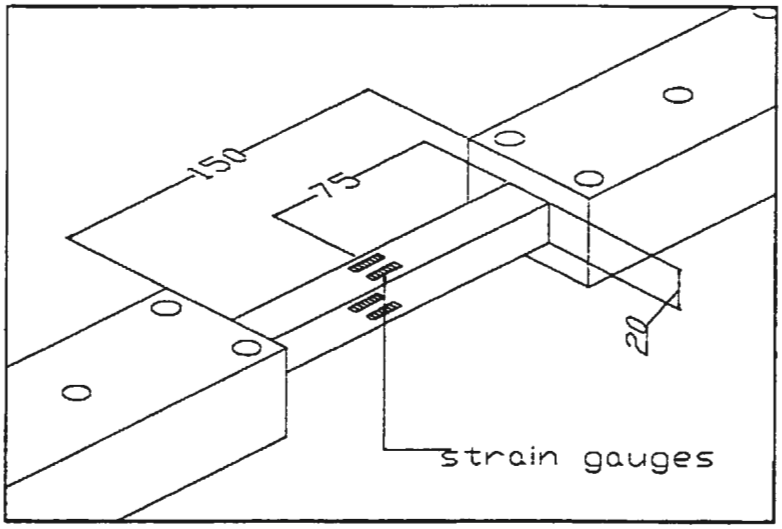

Figure 4: Schematic Diagram of the Aluminum Bar

To install both the aluminum bar and the dynamometer across the midship section, a platform structure with three levels was mounted on the two segments. The upper-most level is the dynamometer platform, which has a cantilever form to avoid any disturbance to the moment transducer. The second level consists of two separate platforms mounted each on a different segment. The aluminum bar was rigidly bolted to these platforms at the two ends, leaving the middle part to deflect elastically. On the lowest level, the installation space was left for three auxiliary bars that were added after the experiments. These bars provided a protection for the model hull against breakage when the model was out of the tank. The whole platform structure was bolted to large wooden plates that were securely fastened to the ship model bottom with wood screws and epoxy bonding material. Figure 5 shows the ship model out of the wave tank with the auxiliary bars added in the lowest level. Figure 6 shows the ship model in the wave tank with the dynamometer attached to the cantilever platform.

Figure 5: Ship Model out of the Wave Tank

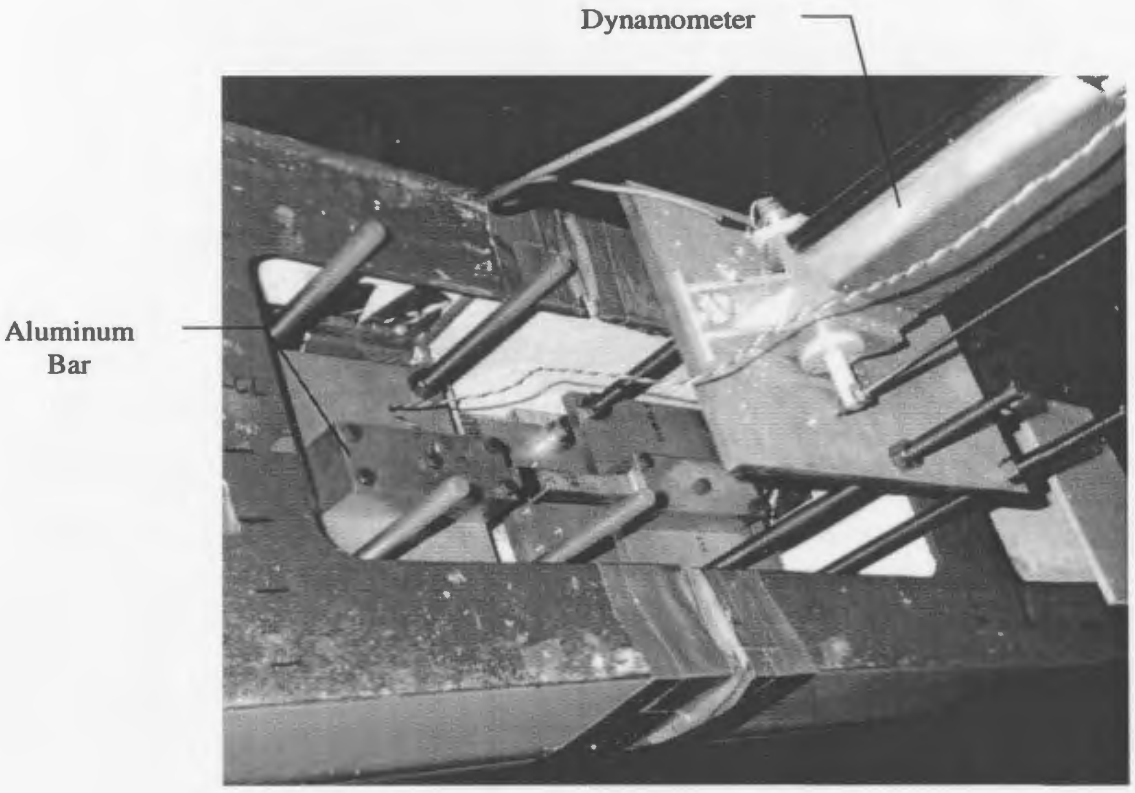

Figure 6: Ship Model in the Wave Tank

3.2 Experimental Preparation

3.2.1 Bending Moment Calibration

Prior to the model tests, one major concern is the calibration of the bending moment transducer. Since the bending moment is linearly proportional to the strain of the aluminum bar, the calibration was performed by applying a series of known loads to the bar. The calculated bending moments were combined with the strain gauge readings to determine the slope and offset constants using a least-square linear fit. In this experiment, two types of calibration were carried out for validating each other. They are the bench calibration and the in-situ calibration.

For the bench calibration the aluminum bar was removed from the model and set up as a cantilever beam. Several known weights were placed at the free end, and the corresponding bending moments at the strain gauge location were calculated as the product of loads and distance. These calculated values represent dynamic bending moments rather than total bending moments. The sagging moments were recorded as positive values, and the hogging moments were negative. The applied weights, calculated bending moments, and the strain gauge readings are listed in Table 3.

Table 3: Bench Calibration Results for Dynamic Bending Moment

Load W (kg)	Distance L (m)	Dynamic BM M (Nm)	Digital Reading X
0	0.215	0	31420
1	0.215	-2.107	31051
3	0.215	-6.321	30300
4	0.215	-8.428	29928
5	0.215	-10.535	29553

The in-situ calibration took place in the wave tank with the aluminum bar and the strain gauges mounted on the fully outfitted model. Some known weights were placed initially at the midship section, and the bending moment was recorded as zero. The weights were then separated into two equal sets, and moved the same distance in opposite directions. The calibration process is illustrated in Figure 7. The changes of the midship bending moment due to the weight movements were calculated as the product of the moved weight and the distance to the midship section. The changes in the sag direction were recorded as positive values, and those in the hog direction were negative. The final results of the in-situ calibration are listed in Table 4.

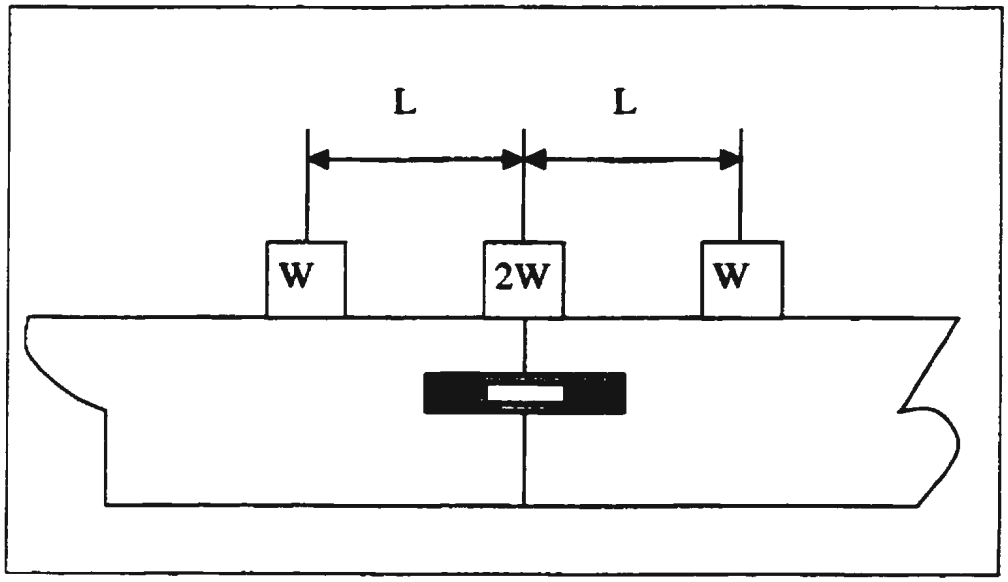

Figure 7: In-situ Calibration Illustration

Table 4: In-situ Calibration Results for Dynamic Bending Moment

Moved Weight W (kg)	Distance L (m)	Dynamic BM M (Nm)	Digital Reading X
4	0	0	36534
4	0.25	-9.8	35007
4	0.4	-15.68	33991
4	0.5	-19.6	33326
4	0.6	-23.52	32649
4	0.7	-27.44	31910
4	0.8	-31.36	31254
4	0.9	-35.28	30534
4	1.0	-39.2	29827

Both bench calibration data and in-situ calibration data are plotted together in Figure 8. There is a perfect linear relationship between the midship dynamic bending moment and the strain gauge readings. The straight line passing through the bench calibration points is parallel to the line through the in-situ calibration points. After performing the least-squares linear fit, we got the bench calibration equation

$$M = 0.005637X - 177.13 \qquad (1)$$

and the in-situ calibration equation

$$M = 0.005800X - 212.8 \qquad (2)$$

The slope values in two equations are very close to each other. The difference in offset values is caused by the zero adjustment of the instrument. In bench calibration the initial value of the digital reading was set to 31420, while for in-situ calibration it was 36534.

These offset values, however, have no effect on the final results since wave-induced bending moments are always taken as the relative change with respect to the stillwater measurements. Therefore, the bench and in-situ calibrations are in excellent agreement.

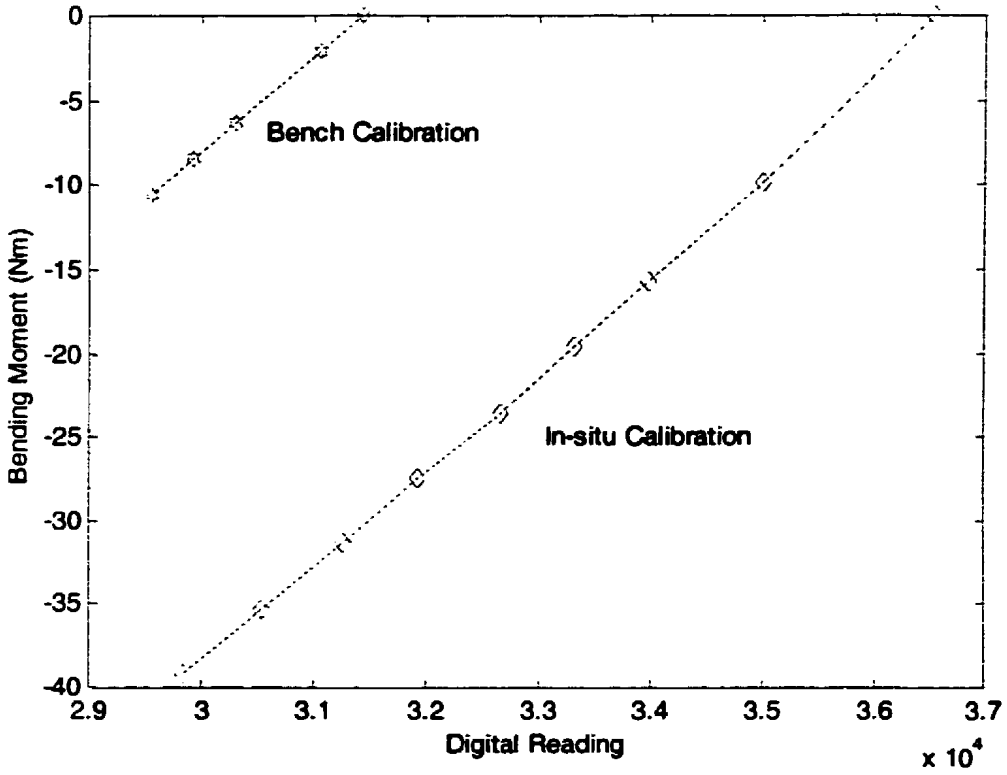

Figure 8: Calibration Results for Bending Moment

Before the model tests, other measuring instruments were also calibrated. The positive direction for the heave displacement and the wave elevation was set vertically upward. For the angular pitch displacement, the positive direction was set bow upward.

3.2.2 Free Response Tests

Prior to the model tests in the waves, the free response tests were carried out to determine the natural frequencies of the ship responses. The model was excited and released in calm

water, and the declining responses were recorded. The coupled heave and pitch responses are shown in Figure 9, and the midship bending moment response is shown in Figure 10.

From the free response results, the natural frequency of the coupled heave and pitch motions is about 1.0Hz. For the midship bending moment, there are two components present in its free response data. While the low-frequency component corresponds to the coupled heave and pitch motions, the high-frequency component is associated with two-node mode ship hull vibration. The two-node mode natural frequency is about 6.5Hz.

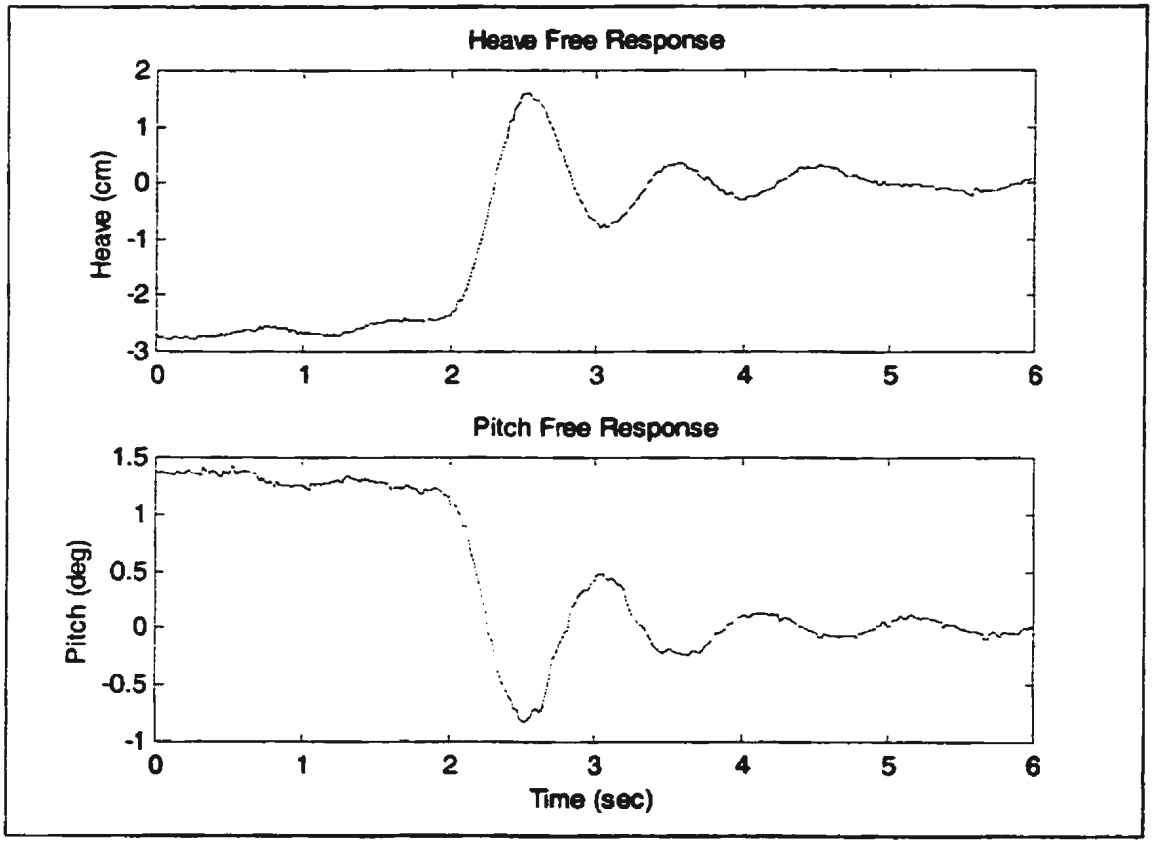

Figure 9: Coupled Heave and Pitch Free Responses

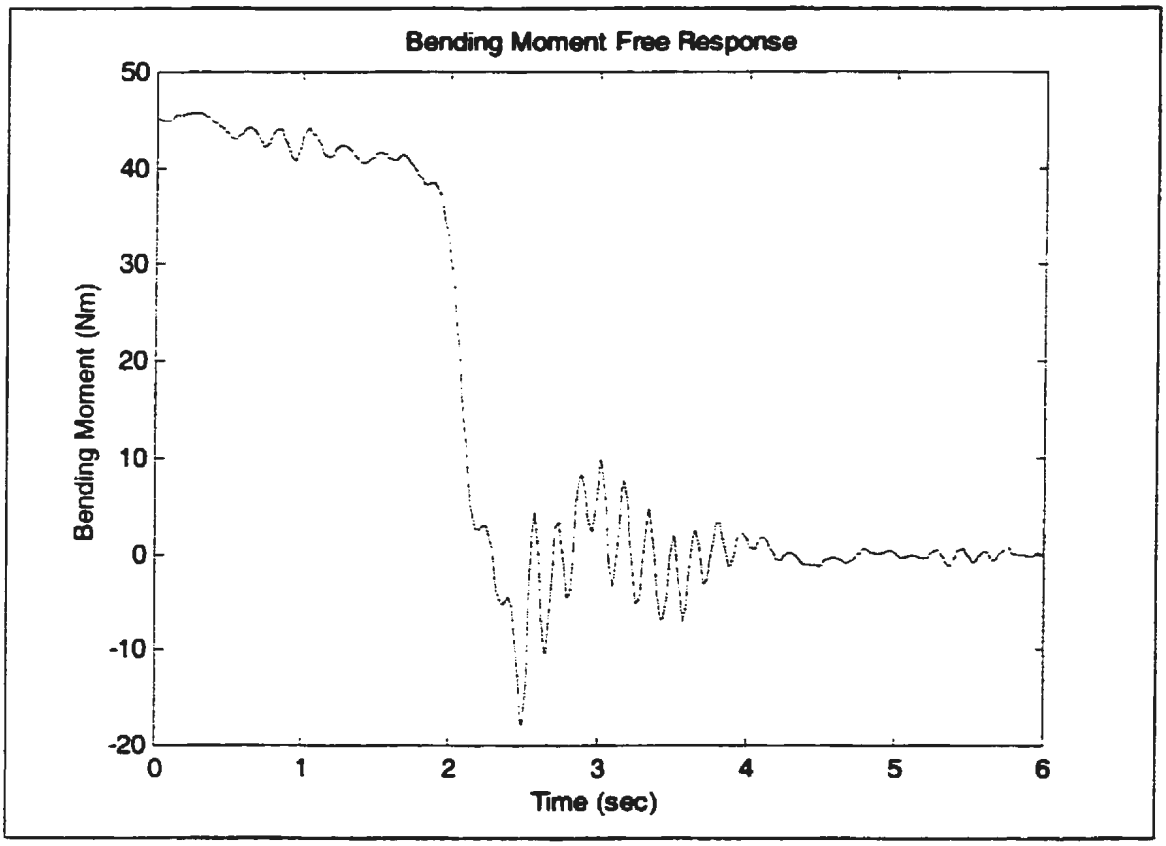

Figure 10: Midship Bending Moment Free Response

3.3 Scope of the Experiments

3.3.1 Stationary Tests in Head Waves

Stationary tests were carried out in regular head waves, JONSWAP random head waves, and broad-band random head waves.

Regular head waves with different frequencies were generated in the wave tank. In each test run, 120sec long experimental data were recorded in five channels. The initial part of the time history was obtained in calm water, which was used as the zero value for data analysis. The data files of regular wave tests are listed in Table 5.

Table 5: Stationary Tests in Regular Head Waves

Wave Frequency (Hz)	Wave Height (cm)	Data Files
0.3	6	W3h6.dat
0.4	6	W4h6.dat
0.5	6	W5h6.dat
0.6	6	W6h6.dat
0.7	6	W7h6.dat
0.8	6	W8h6.dat
0.9	6	W9h6.dat
1.0	6	W10h6.dat
1.1	6	W11h6.dat

Six groups of JONSWAP head waves were generated in the wave tank. For the test runs within the same group, the wave time histories were generated from the same spectrum. In each test run, 500sec long experimental data were recorded in five channels. The initial

part of the time history was obtained in calm water, which was used as the zero value for data analysis. The data files of JONSWAP wave tests are listed in Table 6.

Table 6: Stationary Tests in JONSWAP Head Waves

Peak Frequency F_m (Hz)	**Significant Wave Height H_s (cm)**	**Data Files**
0.7	5.0	J7h5c.dat
0.7	7.5	J7h75a.dat, J7h75b.dat J7h75c.dat
0.5	5.0	J5h5a.dat, J5h5b.dat J5h5c.dat
0.5	7.5	J5h75a.dat, J5h75b.dat J5h75c.dat
0.6	5.0	J6h5a.dat, J6h5b.dat J6h5c.dat
0.6	7.5	J6h75a.dat, J6h75b.dat J6h75c.dat

Two groups of broad-band random wave tests were carried out in the wave tank. For the test runs within the same group, the wave time histories were generated from the same spectrum. In each test run, 500sec long experimental data were recorded in five channels. The initial part of the time history was obtained in calm water, which was used as the zero value for data analysis. The data files for broad-band random wave tests are listed in Table 7.

Table 7: Stationary Tests in Broad-band Random Head Waves

Frequency Range F (Hz)	Significant Wave Height H_s (cm)	Data Files
0.3 ~ 1.2	7.5	B75a.dat, B75b.dat B75c.dat
0.3 ~ 1.2	5.0	B5a.dat, B5b.dat B5c.dat

3.3.2 Stationary Tests in Following Waves

Stationary tests were carried out in regular following waves, JONSWAP random following waves, and broad-band random following waves.

Regular following waves with different frequencies were generated in the wave tank. In each test run, 120sec long experimental data were recorded in five channels. The initial part of the time history was obtained in calm water, which was used as the zero value for data analysis. The data files for regular wave tests are listed in Table 8.

Six groups of JONSWAP waves were generated in the wave tank. For the test runs within the same group, the wave time histories were generated from the same spectrum. In each test run, 500sec long experimental data were recorded in five channels. The initial part of the time history was obtained in calm water, which was used as the zero value for data analysis. The data files for JONSWAP wave tests are listed in Table 9.

Table 8: Stationary Tests in Regular Following Waves

Wave Frequency (Hz)	Wave Height (cm)	Data Files
0.3	6	fw3h6.dat
0.4	6	fw4h6.dat
0.5	6	fw5h6.dat
0.6	6	fw6h6.dat
0.7	6	fw7h6.dat
0.8	6	fw8h6.dat
0.9	6	fw9h6.dat
1.0	6	fw10h6.dat
1.1	6	fw11h6.dat

Table 9: Stationary Tests in JONSWAP Following Waves

Peak Frequency F_m (Hz)	Significant Wave Height H_s (cm)	Test Data Files
0.5	5.0	Fj5h5a.dat, Fj5h5b.dat
0.5	7.5	Fj5h75a.dat, Fj5h75b.dat
0.6	5.0	Fj6h5a.dat, Fj6h5b.dat
0.6	7.5	Fj6h75a.dat, Fj6h75b.dat
0.7	5.0	Fj7h5a.dat, Fj7h5b.dat
0.7	7.5	Fj7h75a.dat, Fj7h75b.dat

Two groups of broad-band random wave tests were carried out in the wave tank. For the test runs within the same group, the wave time histories were generated from the same spectrum. In each test run, 500sec long experimental data were recorded in five channels. The initial part of the time history was obtained in calm water, which was used as the

zero value for data analysis. The data files for broad-band random wave tests are listed in Table 10.

Table 10: Stationary Tests in Broad-band Random Following Waves

Frequency Range F (Hz)	Significant Wave Height H_s (cm)	Test Data Files
0.3 ~ 1.2	5.0	Fb5a.dat, Fb5b.dat
0.3 ~ 1.2	7.5	Fb75a.dat, Fb75b.dat

3.3.3 Towing Tests in Head Waves

Towing tests were carried out in calm water, regular head waves, and JONSWAP random head waves with a forward speed 0.5m/sec.

A towing test in calm water was carried out prior to each group of test runs. The purpose of these tests is to measure the ship responses due to the model wave system in calm water. In each test run, 90sec long experimental data were recorded in five channels. The initial part of the time history was obtained in stationary state, which was used as the zero value for data analysis.

Regular head waves with different frequencies were generated in the wave tank. In each test run, 90sec long experimental data were recorded in five channels. The initial part of the time history was obtained in calm water stationary state, which was used as the zero value for data analysis. Prior to each group of test runs, a towing test in calm water was carried out. The data files for the towing tests in regular wave and the corresponding calm water tests are listed in Table 11.

Table 11: Towing Tests in Regular Head Waves

Wave Frequency (Hz)	Wave Height (cm)	Calm Water Test	Data Files
0.3	6	C05b.dat	S5w3h6.dat
0.4	6	C05b.dat	S5w4h6.dat
0.5	6	C05b.dat	S5w5h6.dat
0.6	6	C05b.dat	S5w6h6.dat
0.7	6	C05b.dat	S5w7h6.dat
0.7	5	C05c.dat	S5w7h5.dat
0.8	5	C05c.dat	S5w8h5.dat
0.9	5	C05c.dat	S5w9h5.dat
1.0	5	C05c.dat	S5w10h5.dat
1.1	5	C05c.dat	S5w11h5.dat

JONSWAP random waves were generated in the wave tank. Due to the limited length of the wave tank, a single test run did not provide a data record long enough for random data analysis. Therefore, a JONSWAP wave time history of 450sec long was divided into seven segments, which were generated sequentially in the wave tank. A separate towing test was performed for each wave segment. The time histories from the seven segment runs were finally joined together to form an experimental data record of 350sec length. In each segment run, 120sec long experimental data were recorded in five channels. The initial part of the time history was obtained in calm water for the stationary model. This was used as the zero value for data analysis. Prior to each segment run, a towing test in

calm water was also carried out. The data files for towing tests in JONSWAP wave segments and the corresponding calm water tests are listed in Table 12.

Table 12: Towing Tests in JONSWAP Head Waves

JONSWAP Wave	Calm Water Tests	Test Segments Data
$F_m = 0.7Hz$ $H_s = 7.5cm$	C05c.dat	S5j7r1.dat, S5j7r2.dat S5j7r3.dat, S5j7r4.dat
	C05d.dat	S5j7r5.dat, S5j7r6.dat S5j7r7.dat

4. Frequency-domain Analysis

4.1 Mathematical Model

For a ship advancing at constant mean forward speed with arbitrary heading in regular waves, the six-degree-of-freedom motion responses and the wave-induced bending moment could be computed theoretically. Under the assumption of linear response and ship port/starboard symmetry, the vertical-plane motions are uncoupled from the horizontal-plane motions. Both the wave excitation forces and the resultant oscillatory motions are assumed to be linear and harmonic at the frequency of wave encounter ω_e,

$$\omega_e = \omega_0 - \frac{\omega_0^2 U}{g}\cos\mu \qquad (3)$$

where ω_0 is the wave circular frequency, U is the ship forward speed, and μ is the wave direction angle. The equations of coupled vertical motions and wave-induced bending moment can be formulated using a strip theory. It is customary to use two sets of coordinate systems as shown in Figure 11: an inertia system (x_0, y_0, z_0) and a body system (x, y, z). The origin of the body system is attached to the center of gravity of the ship, with its x-axis pointing forward, y-axis pointing to port and z-axis pointing upward. The inertial system is fixed in space with its coordinate axes parallel to that of the body system before the ship motion starts.

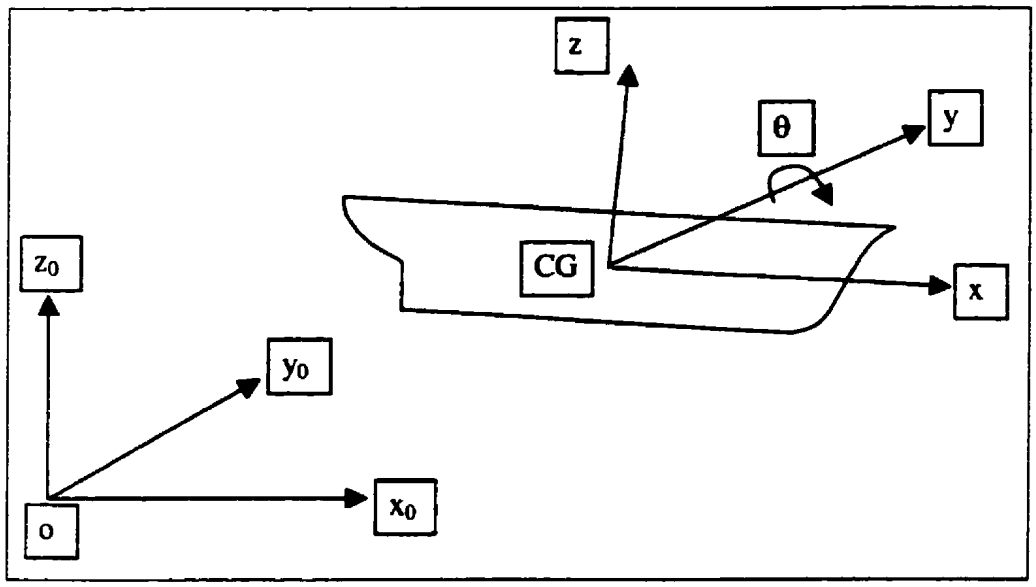

Figure 11: Ship Motions Coordinate Systems

In this work we use the equations given in Lewis (1989), which are based on the work of Salvesen *et al.* (1970). The equations of motion for a rigid-body ship are expressed as

$$\begin{aligned}(M + A_{33})\ddot{z} + B_{33}\dot{z} + C_{33}z + A_{35}\ddot{\theta} + B_{35}\dot{\theta} + C_{35}\theta &= F_3 e^{i\omega t} \\ A_{53}\ddot{z} + B_{53}\dot{z} + C_{53}z + (I + A_{55})\ddot{\theta} + B_{55}\dot{\theta} + C_{55}\theta &= F_5 e^{i\omega t}\end{aligned} \qquad (4)$$

where z is the heave displacement of the center of gravity, θ is the angular pitch displacement, M is the mass of the ship, I is the mass moment of inertia; F_3 and F_5 are complex amplitudes of the exciting force and moment, respectively. The force and moment are given by the real part of $F_j e^{i\omega t}$ (j=3, 5). The positive direction for z is vertically upward, and for θ is bow downward. The added mass and moment A_{jk}, damping coefficients B_{jk}, and restoring coefficients C_{jk} are expressed in terms of the sectional coefficients as follows:

$$A_{33} = \int_L a_{33} d\xi \qquad B_{33} = \int_L b_{33} d\xi \tag{5}$$

$$A_{35} = -\int_L \xi a_{33} d\xi - \frac{U}{\omega_e^2} B_{33} \qquad B_{35} = -\int_L \xi b_{33} d\xi + U A_{33}$$

$$A_{53} = -\int_L \xi a_{33} d\xi + \frac{U}{\omega_e^2} B_{33} \qquad B_{53} = -\int_L \xi b_{33} d\xi - U A_{33}$$

$$A_{55} = \int_L \xi^2 a_{33} d\xi + \frac{U^2}{\omega_e^2} A_{33} \qquad B_{55} = \int_L \xi^2 b_{33} d\xi + \frac{U^2}{\omega_e^2} B_{33}$$

$$C_{33} = \int_L c_{33} d\xi = \int_L \rho g B(\xi) d\xi$$

$$C_{35} = C_{53} = -\int_L \xi c_{33} d\xi = -\int_L \xi \rho g B(\xi) d\xi$$

$$C_{55} = \int_L \xi^2 c_{33} d\xi = \int_L \xi^2 \rho g B(\xi) d\xi$$

For head sea conditions (μ=180deg), the wave excitation forces F_3 and F_5 can be simplified as

$$F_3 = \varsigma_a \int_L e^{ik\xi} e^{-kT(\xi)} [c_{33} - \omega_0(\omega_e a_{33} - i b_{33})] d\xi \tag{6}$$

$$F_5 = \varsigma_a \int_L e^{ik\xi} e^{-kT(\xi)} \left\{ \xi [c_{33} - \omega_0(\omega_e a_{33} - i b_{33})] - \frac{U}{i\omega_e} \omega_0(\omega_e a_{33} - i b_{33}) \right\} d\xi$$

In equations (5) and (6), a_{33} is the sectional heave added mass, b_{33} is the sectional heave damping, c_{33} is the sectional restoring force ρgB, B is the sectional waterline beam, T is the mean sectional draft *S/B*, and ς_a is the incident wave amplitude. The sectional coefficients a_{33} and b_{33} are obtained by solving the two-dimensional hydrodynamic problems. All coefficients are frequency-dependent.

For a rigid ship hull, the wave-induced vertical bending moment at an arbitrary longitudinal location x_0 can be expressed in terms of the resulting motions. If the sag direction is taken positive, the expression is

$$y(x_0) = A_y\ddot{z} + B_y\dot{z} + C_y z + D_y\ddot{\theta} + E_y\dot{\theta} + H_y\theta + y_\zeta e^{i\omega_e t} \tag{7}$$

where

$$\begin{aligned}
A_y &= -\int_{x_0}^{bow}(m_n + a_{33})(\xi - x_0)d\xi + \int_{x_0}^{bow}\frac{U}{\omega_e^{\,2}}b_{33}d\xi \\
B_y &= -\int_{x_0}^{bow} b_{33}(\xi - x_0)d\xi - \int_{x_0}^{bow} Ua_{33}d\xi \\
C_y &= -\int_{x_0}^{bow} c_{33}(\xi - x_0)d\xi \\
D_y &= \int_{x_0}^{bow}(m_n + a_{33})\xi(\xi - x_0)d\xi + \int_{x_0}^{bow}\frac{U^2}{\omega_e^{\,2}}a_{33}d\xi - \int_{x_0}^{bow}\frac{U}{\omega_e^{\,2}}b_{33}x_0 d\xi \\
E_y &= \int_{x_0}^{bow} b_{33}\xi(\xi - x_0)d\xi + \int_{x_0}^{bow}\frac{U^2}{\omega_e^{\,2}}b_{33}d\xi + \int_{x_0}^{bow} Ua_{33}x_0 d\xi \\
H_y &= \int_{x_0}^{bow} c_{33}\xi(\xi - x_0)d\xi
\end{aligned} \tag{8}$$

The bending moment component $y_\zeta e^{i\omega e t}$ results from the wave excitation forces, and the complex amplitude y_ζ can be simplified for head sea conditions as

$$y_\zeta = \zeta_a \int_L e^{ik\xi} e^{-kT(\xi)} \left\{ (\xi - x_0)[c_{33} - \omega_0(\omega_e a_{33} - ib_{33})] - \frac{U}{i\omega_e}\omega_0(\omega_e a_{33} - ib_{33}) \right\} d\xi \tag{9}$$

In linear theory, the steady-state harmonic responses z, θ, and $y(x_0)$ have the same encounter frequency ω_e, but different phase shifts. Consequently, they can be expressed in the complex form as

$$\begin{aligned}
z &= z_a e^{i\omega_e t} \\
\theta &= \theta_a e^{i\omega_e t} \\
y(x_0) &= y_a(x_0) e^{i\omega_e t}
\end{aligned} \tag{10}$$

The complex amplitudes z_a, θ_a, and $y_a(x_0)$ are functions of both the magnitude and phase of the responses. Substituting expression (10) into equations (4) and (7), and eliminating the common term $e^{i\omega_e t}$, the resulting equations are

$$\begin{aligned}
&[-\omega_e^2(M+A_{33})+C_{33}+i\omega_e B_{33}]z_a+(-\omega_e^2 A_{35}+C_{35}+i\omega_e B_{35})\theta_a = F_3 \\
&[-\omega_e^2(I+A_{55})+C_{55}+i\omega_e B_{55}]\theta_a+(-\omega_e^2 A_{53}+C_{53}+i\omega_e B_{53})z_a = F_5
\end{aligned} \qquad (11)$$

and

$$y_a(x_0)=(-A_y\omega_e^2+C_y+i\omega_e B_y)z_a+(-D_y\omega_e^2+H_y+i\omega_e E_y)\theta_a+y_\zeta \qquad (12)$$

Equations (11) and (12) constitute the frequency-domain model for vertical ship motions and bending moment. The solution to equation (11) is easily obtained as

$$\begin{aligned}
z_a &= \frac{F_3 S - F_5 Q}{PS - QR} \\
\theta_a &= \frac{F_5 P - F_3 R}{PS - QR}
\end{aligned} \qquad (13)$$

where

$$\begin{aligned}
P &= -\omega_e^2(M+A_{33})+C_{33}+i\omega_e B_{33} \\
Q &= -\omega_e^2 A_{35}+C_{35}+i\omega_e B_{35} \\
R &= -\omega_e^2 A_{53}+C_{53}+i\omega_e B_{53} \\
S &= -\omega_e^2(I+A_{55})+C_{55}+i\omega_e B_{55}
\end{aligned} \qquad (14)$$

Substitution of (13) into (12) gives the solution for the wave-induced bending moment amplitude $y_a(x_0)$. The ratios between the complex response amplitudes and the wave amplitude are frequency response functions as shown below,

$$H_z(\omega_e) = \frac{z_a}{\zeta_a} \qquad (15)$$

$$H_\theta(\omega_e) = \frac{\theta_a}{\zeta_a}$$

$$H_y(\omega_e) = \frac{y_a(x_0)}{\zeta_a}$$

The modulus of the frequency response function is a Response Amplitude Operator (RAO). These frequency-domain solutions could be obtained either from theoretical computations of two-dimensional hydrodynamic problems, or from experimental model tests in a wave tank.

4.2 Regular Waves Data Analysis

4.2.1 Frequency Analysis Method

Following Ljung (1999), if the input signal u(t) to a linear system has the form

$$u(t) = u_0 \cos(\omega t + \alpha) \qquad (16)$$

then the output signal y(t) will be given by

$$y(t) = u_0 |H(\omega)| \cos[\omega t + \alpha + \arg H(\omega)] + v(t) + transient \qquad (17)$$

where v(t) is noise. The transient response eventually decays and only the steady state response remains. The amplitude and the phase of H(ω) are related to the amplitudes and phase angles of u(t) and y(t). This provides a means to estimate the frequency response function H(ω) from a series of sinusoidal-wave tests with different frequencies.

For each sinusoidal-wave test, the amplitudes and phase angles of u(t) and y(t) can be determined first from the time histories of the input u(t) and the output y(t), respectively. The existence of noise v(t) in the signal makes it difficult to determine the required parameters accurately. Since the steady state part of y(t) is harmonic, it is possible to average out the noise using the correlation method described by Ljung (1999). From the amplitudes and phase angles of u(t) and y(t), the frequency response function H(ω) can be calculated. The following algorithm was used in this work

$$|H(\omega)| = \frac{y_0(\omega)}{u_0(\omega)} \qquad (18)$$

$$\arg H(\omega) = \arg y(\omega) - \arg u(\omega)$$

where

$$y_0(\omega) = 2\sqrt{I_c^{\,2}(y) + I_s^{\,2}(y)} \qquad (19)$$

$$\arg y(\omega) = -\arctan\frac{I_s(y)}{I_c(y)} + k\pi, (k = 0,1)$$

$$I_c(y) = \frac{1}{N}\sum_{n=1}^{N} y[n]\cos(\frac{\omega}{f_s}n)$$

$$I_s(y) = \frac{1}{N}\sum_{n=1}^{N} y[n]\sin(\frac{\omega}{f_s}n)$$

and

$$u_0(\omega) = 2\sqrt{I_c^{\,2}(u) + I_s^{\,2}(u)} \qquad (20)$$

$$\arg u(\omega) = -\arctan\frac{I_s(u)}{I_c(u)} + k\pi, (k = 0,1)$$

$$I_c(u) = \frac{1}{N}\sum_{n=1}^{N} u[n]\cos(\frac{\omega}{f_s}n)$$

$$I_s(u) = \frac{1}{N}\sum_{n=1}^{N} u[n]\sin(\frac{\omega}{f_s}n)$$

Here ω is the circular encounter frequency and f_s is the sampling frequency taken as 50Hz. The effect of the noise v(t) diminishes to zero as the number of data points, N approaches infinity.

4.2.2 Results of Regular Wave Tests

From the frequency analysis of the regular wave tests data, we could determine the amplitudes and phase angles of the wave elevation, the heave displacement, the angular pitch displacement, and the wave-induced midship bending moment. Based on these values, the frequency response functions can be estimated. The modulus (RAO) was

calculated as the ratio of the response amplitude to the wave amplitude, and the phase angle of $H(\omega)$ is the phase difference between the response and the wave elevation.

The results of stationary tests in head waves are presented in Table 13 and Table 14. The results of stationary tests in following waves are presented in Table 15 and Table 16.

For each towing test in regular waves, a towing test in calm water was always performed previously. The mean values of the calm water test data were subtracted from the regular wave test data to determine the wave-induced responses. Since the wave probe was fixed to the towing carriage, the identified frequency was the wave encounter frequency. The results of towing tests in head waves are presented in Table 17 and Table 18.

Table 13: Results of Stationary Tests in Regular Head Waves

	F (Hz)	Wave Amp. (cm)	BM Amp. (Nm)	BM Pha. (deg)	Heave Amp. (cm)	Heave Pha. (deg)	Pitch Amp. (deg)	Pitch Pha. (deg)
W3h6	0.294	3.40	3.27	221	3.29	6.0	0.91	73.5
W4h6	0.392	3.31	3.83	205	3.05	5.8	0.75	87.5
W5h6	0.490	3.56	7.39	203	3.02	9.0	1.28	81.1
W6h6	0.588	2.82	8.89	205	1.94	8.5	2.06	92.1
W7h6	0.685	2.70	10.48	196	1.35	16.6	2.37	101.7
W8h6	0.784	3.28	13.75	188	0.88	23.8	2.36	106.2
W9h6	0.882	3.30	10.82	194	0.52	83.3	1.82	104.1
W10h6	0.980	4.13	6.14	222	2.22	181.3	1.32	132.2
W11h6	1.077	3.32	6.63	230	0.54	150.1	0.79	166.3

Table 14: Frequency Response Functions of Stationary Tests in Regular Head Waves

F (Hz)	$\lvert H_y \rvert$ (Nm/cm)	ang(H_y) (deg)	$\lvert H_z \rvert$ (cm/cm)	ang(H_z) (deg)	$\lvert H_\theta \rvert$ (deg/cm)	ang(H_θ) (deg)
0.294	0.962	221	0.968	6.0	0.268	73.5
0.392	1.157	205	0.921	5.8	0.226	87.5
0.490	2.076	203	0.848	9.0	0.360	81.1
0.588	3.152	205	0.688	8.5	0.730	92.1
0.685	3.881	196	0.500	16.6	0.878	101.7
0.784	4.192	188	0.268	23.8	0.720	106.2
0.882	3.279	194	0.158	83.3	0.551	104.1
0.980	1.487	222	0.538	181.3	0.320	132.2
1.077	1.997	230	0.163	150.1	0.238	166.3

Table 15: Results of Stationary Tests in Regular Following Waves

	F (Hz)	Wave Amp. (cm)	BM Amp. (Nm)	BM Pha. (deg)	Heave Amp. (cm)	Heave Pha. (deg)	Pitch Amp. (deg)	Pitch Pha. (deg)
fw3h6	0.295	3.49	2.91	109	3.21	1.96	0.89	255.5
fw4h6	0.393	3.03	3.63	149	2.68	2.51	0.62	279.3
fw5h6	0.491	3.98	7.09	159	3.23	3.30	1.38	271.6
fw6h6	0.590	3.04	8.14	163	1.79	-2.01	1.89	271.2
fw7h6	0.689	3.09	11.29	177	1.41	2.07	2.35	277.7
fw8h6	0.787	3.40	13.69	190	0.72	-0.41	2.30	285.4
fw9h6	0.886	3.70	17.68	218	0.65	72.7	2.13	287.1
fw10h6	0.983	2.49	16.74	241	3.14	124.6	1.43	284.2
fw11h6	1.081	2.94	10.57	272	0.51	125.1	0.72	337.4

Table 16: Frequency Response Functions of Stationary Tests in Regular Following Waves

F (Hz)	$\lvert H_y \rvert$ (Nm/cm)	ang(H_y) (deg)	$\lvert H_z \rvert$ (cm/cm)	ang(H_z) (deg)	$\lvert H_\theta \rvert$ (deg/cm)	ang(H_θ) (deg)
0.295	0.834	109	0.920	1.96	0.254	255.5
0.393	1.198	149	0.884	2.51	0.203	279.3
0.491	1.781	159	0.812	3.30	0.347	271.6
0.590	2.678	163	0.589	-2.01	0.620	271.2
0.689	3.652	177	0.456	2.07	0.760	277.7
0.787	4.027	190	0.212	-0.41	0.676	285.4
0.886	4.778	218	0.176	72.7	0.576	287.1
0.983	6.723	241	1.261	124.6	0.576	284.2
1.081	3.595	272	0.172	125.1	0.246	337.4

Table 17: Results of Towing Tests in Regular Head Waves

	En. F (Hz)	Wave Amp. (cm)	BM Amp. (Nm)	BM Pha. (deg)	Heave Amp. (cm)	Heave Pha. (deg)	Pitch Amp. (deg)	Pitch Pha. (deg)
S5w3h6	0.333	2.82	2.30	232.0	2.90	6.12	0.81	92.3
S5w4h6	0.450	2.23	3.12	218.9	2.24	7.65	0.96	94.4
S5w5h6	0.573	2.61	5.84	207.8	2.53	10.56	1.64	98.7
S5w6h6	0.702	3.02	9.71	190.0	2.41	7.56	2.22	99.2
S5w7h6	0.840	2.95	12.39	167.6	1.99	8.43	3.26	103.0
S5w7h5	0.841	2.57	11.73	163.1	1.68	3.04	2.77	99.7
S5w8h5	0.987	1.37	13.09	79.7	1.31	306.9	3.20	24.3
S5w9h5	1.135	2.90	4.86	-4.6	0.34	356.3	1.98	23.6
S5w10h5	1.292	3.23	7.65	-108.1	0.43	76.95	0.26	64.7
S5w11h5	1.454	3.12	4.65	-113.2	0.25	108.3	0.19	159.2

Table 18: Frequency Response Functions of Towing Tests in Regular Head Waves

En. F (Hz)	$\lvert H_y \rvert$ (Nm/cm)	ang(H_y) (deg)	$\lvert H_z \rvert$ (cm/cm)	ang(H_z) (deg)	$\lvert H_\theta \rvert$ (deg/cm)	ang(H_θ) (deg)
0.333	0.82	232.0	1.03	6.12	0.29	92.3
0.450	1.40	218.9	1.00	7.65	0.43	94.4
0.573	2.24	207.8	0.97	10.56	0.63	98.7
0.702	3.22	190.0	0.80	7.56	0.74	99.2
0.840	4.20	167.6	0.67	8.43	1.11	103.0
0.841	4.56	163.1	0.65	3.04	1.08	99.7
0.987	9.55	79.7	0.96	306.9	2.34	24.3
1.135	1.68	-4.6	0.12	356.3	0.68	23.6
1.292	2.37	-108.1	0.13	76.95	0.08	64.7
1.454	1.49	-113.2	0.08	108.3	0.06	159.2

4.3 Random Waves Data Analysis

4.3.1 Spectral Analysis Method

The Response Amplitude Operators (RAOs) can be estimated from the random test data using a spectral analysis method (Ljung, 1999). An algorithm in continuous form is given in Thomson (1981) as

$$X(\omega) = \lim_{T\to\infty}\int_0^T x(t)e^{-i\omega t}dt \qquad (21)$$

$$Y(\omega) = \lim_{T\to\infty}\int_0^T y(t)e^{-i\omega t}dt$$

$$S_{xx}(\omega) = \lim_{T\to\infty}\frac{1}{T}X(\omega)X^*(\omega)$$

$$S_{yy}(\omega) = \lim_{T\to\infty}\frac{1}{T}Y(\omega)Y^*(\omega)$$

$$|H(\omega)| = \sqrt{\frac{S_{yy}(\omega)}{S_{xx}(\omega)}}$$

The discrete form used in this work is as follows,

$$X(k) = \sum_{n=1}^{N} x[n]e^{-ik\frac{2\pi}{N}n} \qquad (22)$$

$$Y(k) = \sum_{n=1}^{N} y[n]e^{-ik\frac{2\pi}{N}n}$$

$$S_{xx}(k) = \frac{1}{Nf_s}X(k)X^*(k)$$

$$S_{yy}(k) = \frac{1}{Nf_s}Y(k)Y^*(k)$$

$$|H(k)| = \sqrt{\frac{S_{yy}(k)}{S_{xx}(k)}}$$

$$f(k) = f_s\frac{k}{N}, (0 \le k \le N-1)$$

From linear-random theory, the above RAO values should have a good agreement with the frequency response functions estimated from the regular wave tests.

4.3.2 Results of Random Wave Tests

For each stationary test in random waves, 500sec long experimental data were recorded in five channels. Since the initial 50sec segment consisted of the calm water data and the transient response data, only the latter 450sec long experimental data could be used for spectral analysis. For the towing test in random waves, 350sec long time histories were formed by joining seven segments. The estimated frequency was the encounter frequency.

For stationary tests in head waves, representative results of the JONSWAP random wave tests and the broad-band random wave tests are plotted in Figure 12 and Figure 13, respectively. The circle points in the figures are RAO values obtained from the stationary tests in regular head waves. Other test results are presented in Appendix III.

For stationary tests in following waves, representative results of the JONSWAP random wave tests and the broad-band random wave tests are plotted in Figure 14 and Figure 15, respectively. The circle points in the figures are RAO values obtained from the stationary tests in regular following waves. Other test results are presented in Appendix III.

For towing tests in head waves, the results of the JONSWAP random wave tests are plotted in Figure 16. The circle points in the figure are RAO values obtained from the towing tests in regular head waves.

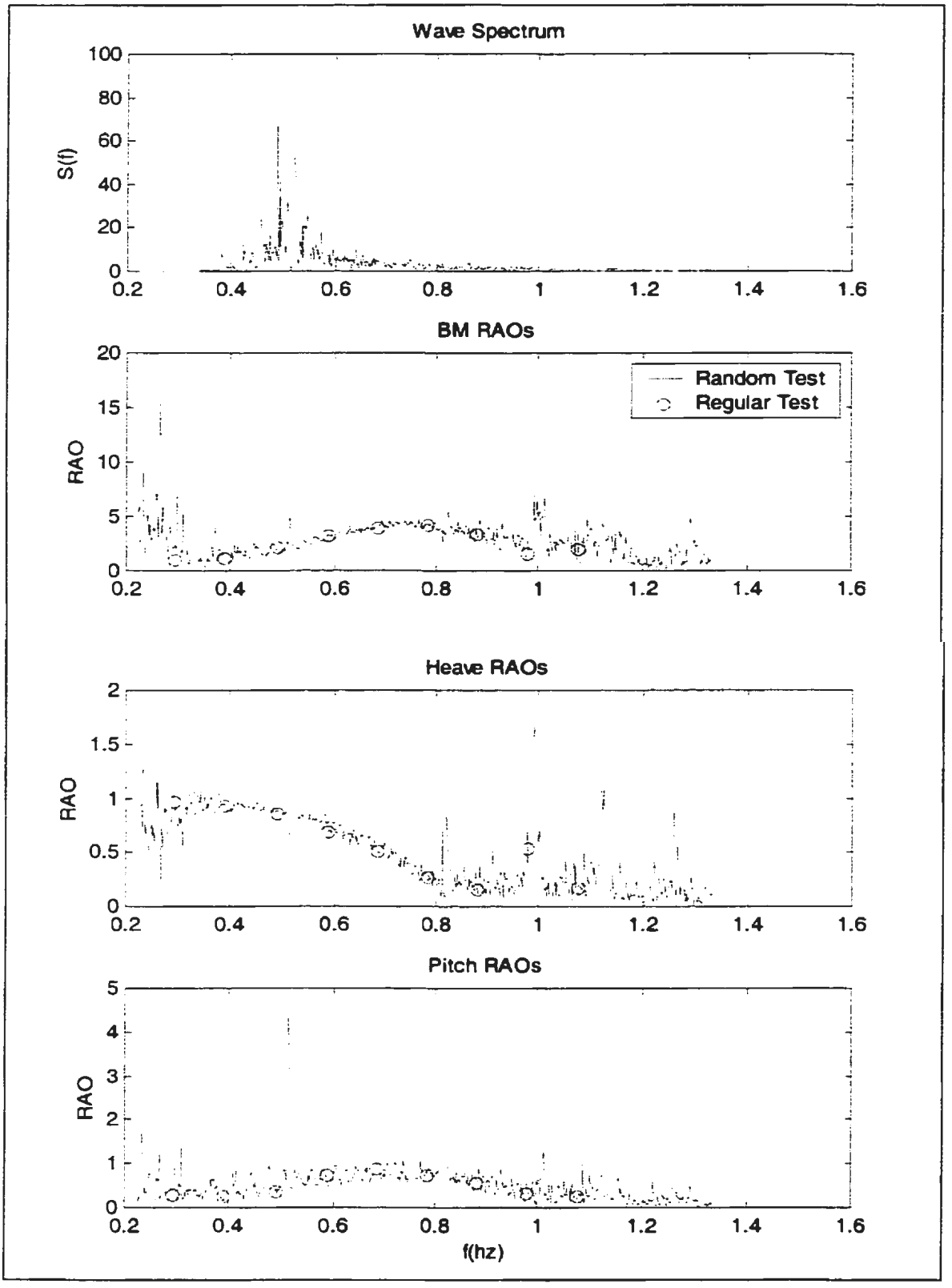

Figure 12: Spectral Analysis Results of J5h75a.dat

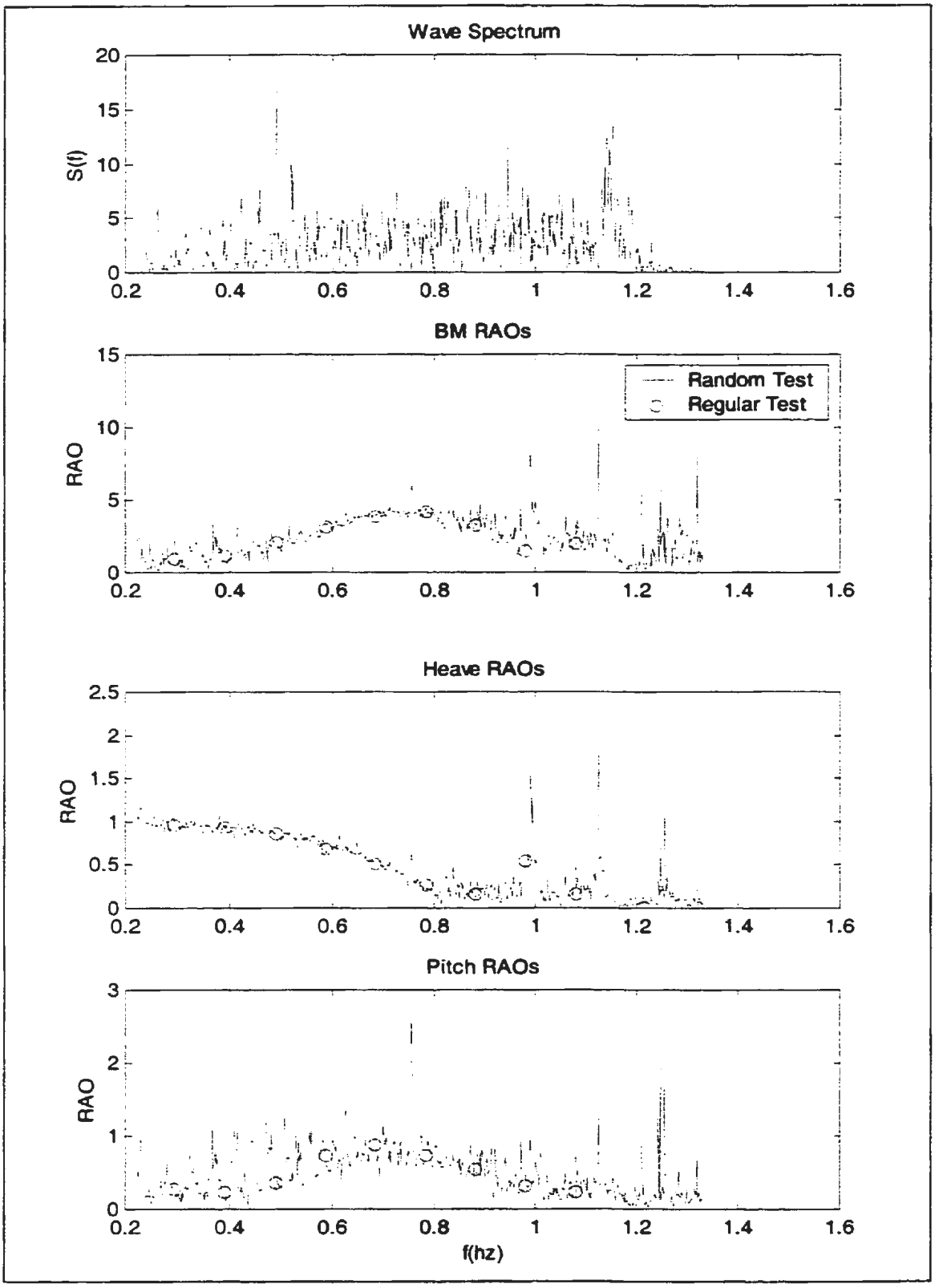

Figure 13: Spectral Analysis Results of B75a.dat

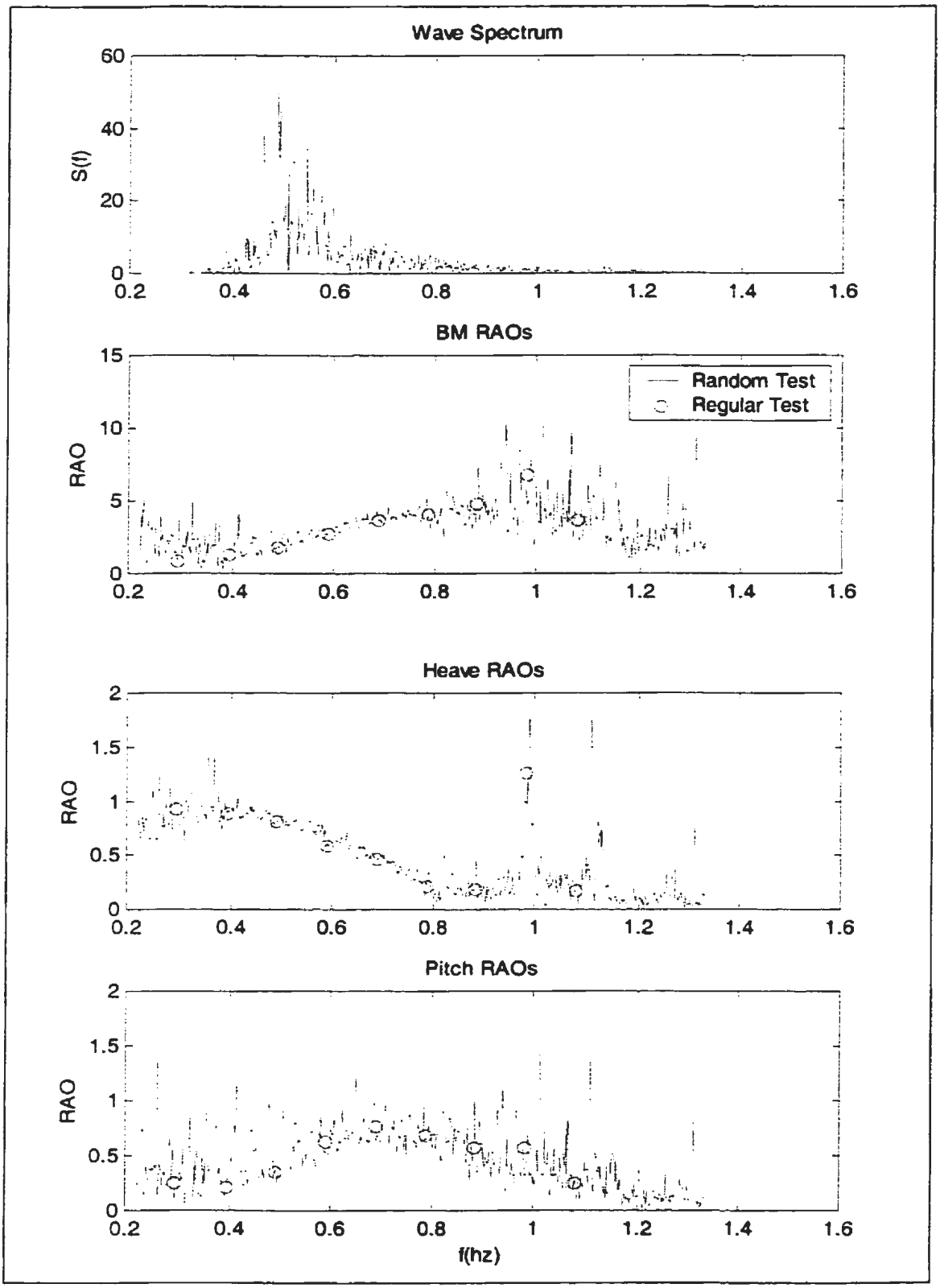

Figure 14: Spectral Analysis Results of Fj5h75a.dat

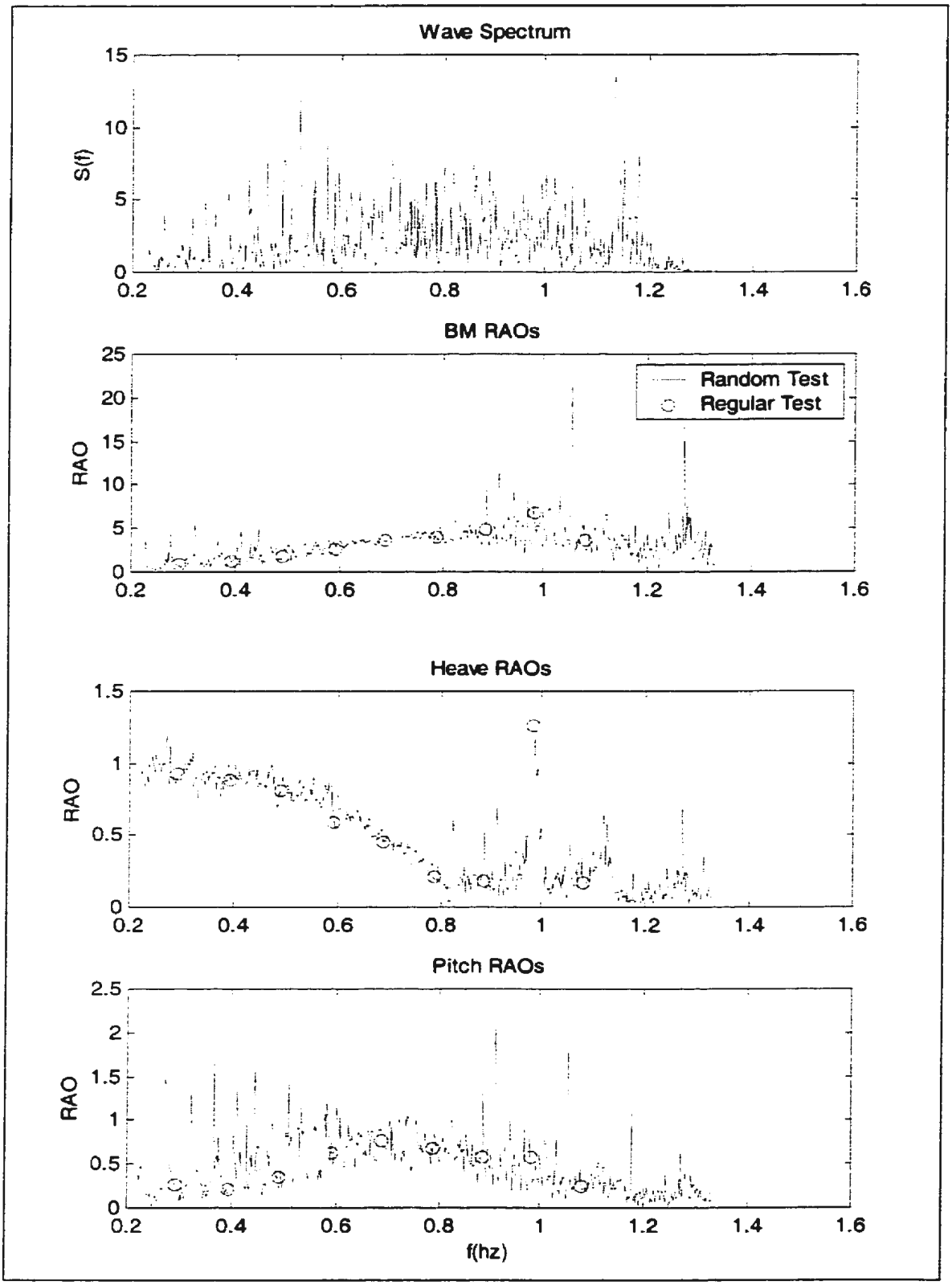

Figure 15: Spectral Analysis Results of Fb75b.dat

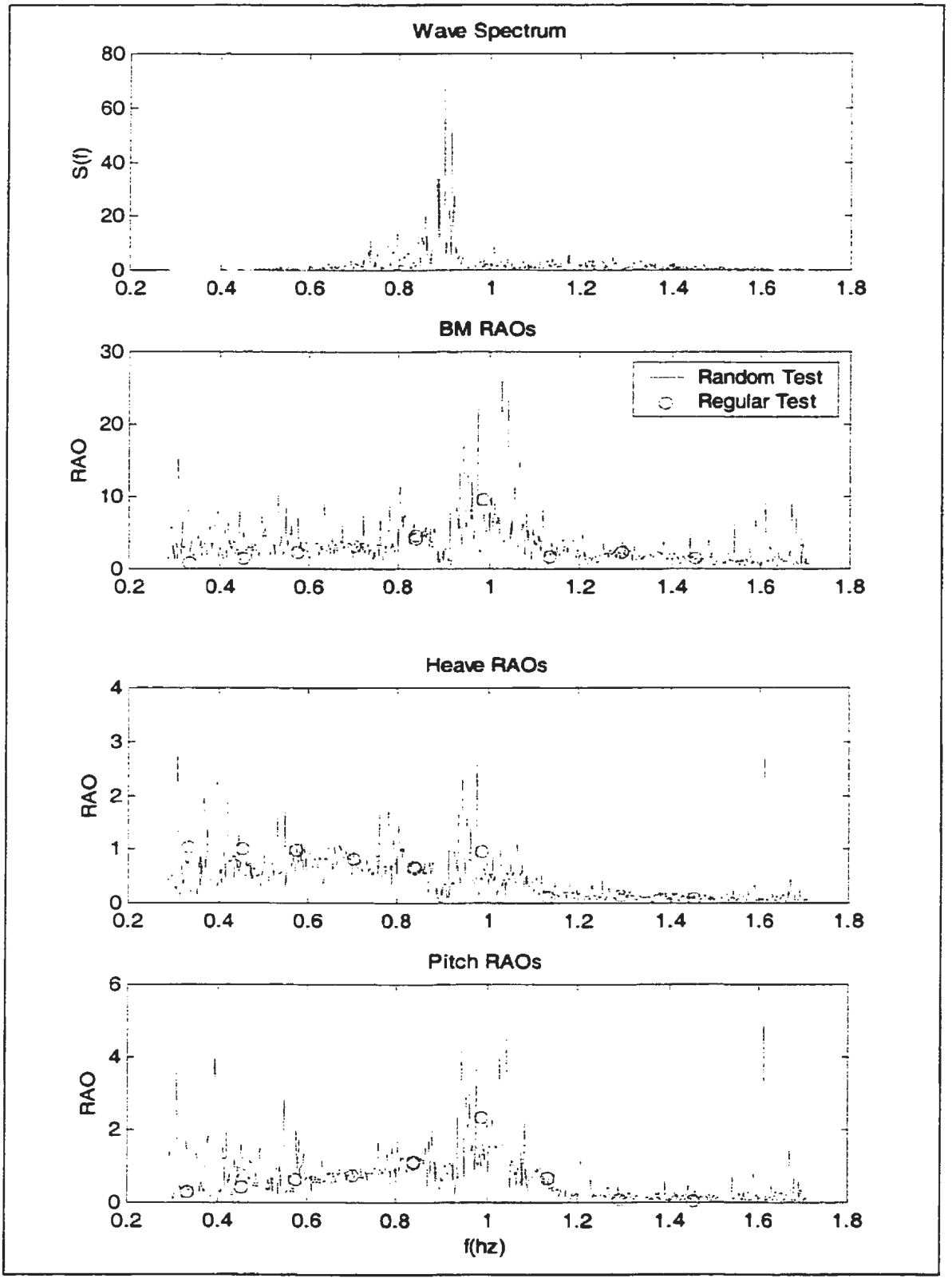

Figure 16: Spectral Analysis Results of JONSWAP Wave Towing Test

From Figure 12 to Figure 16, there is an excellent agreement between the RAOs obtained from both regular wave tests and random wave tests. According to linear-random theory, this agreement validates the assumption of linearity that is adopted in the current work. In addition, the accuracy of the experimental measurements is also validated.

4.4 Numerical Computations

In order to validate the experimental results theoretically, the frequency response functions of heave, pitch, and midship bending moment for head sea stationary conditions were computed using a strip theory. The two-dimensional sectional coefficients and excitation forces were determined by Lewis-form method. The computation details are described in Appendix I, and the results of the frequency response functions are presented in Table 19. The comparisons between the calculated results and the experimental results obtained from the regular wave tests are shown in Figure 17 to Figure 19. It should be noted that the positive direction for angular pitch displacement is bow downward in the computations, but bow upward in the experiments. This causes a 180° difference in pitch phase angles, as seen in Figure 19.

Table 19: Frequency Response Functions from Numerical Computations

F (Hz)	$\|H_y\|$ (Nm/cm)	ang(H_y) (deg)	$\|H_z\|$ (cm/cm)	ang(H_z) (deg)	$\|H_\theta\|$ (deg/cm)	ang(H_θ) (deg)
0.392	0.6829	181.75	0.921	-1.18	0.389	267.68
0.490	1.345	185.64	0.848	-2.54	0.537	266.17
0.588	2.130	188.70	0.749	-4.89	0.662	263.81
0.685	3.208	191.35	0.542	-8.16	0.761	260.61
0.784	3.939	196.74	0.258	-8.05	0.721	256.64
0.882	4.017	205.55	0.119	111.62	0.527	249.03
0.980	3.566	221.71	0.332	110.95	0.167	241.30
1.077	2.695	232.95	0.271	85.75	0.224	41.04

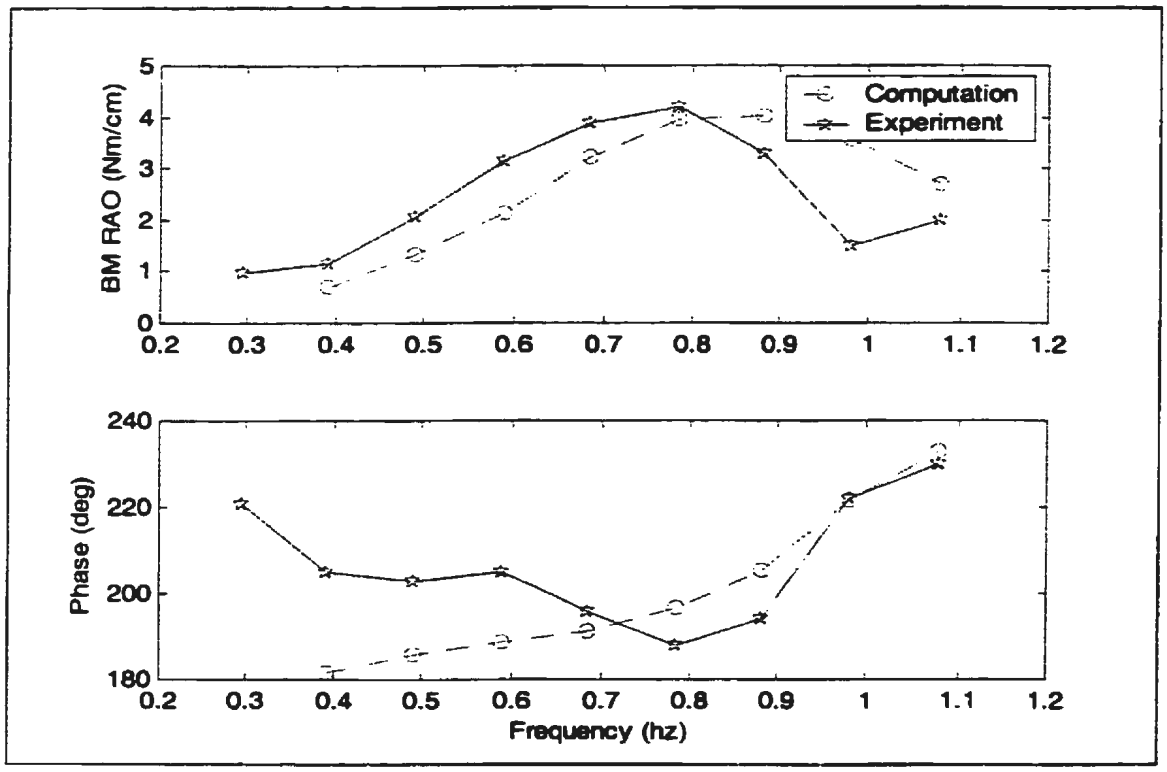

Figure 17: Frequency Response Functions for Midship Bending Moment

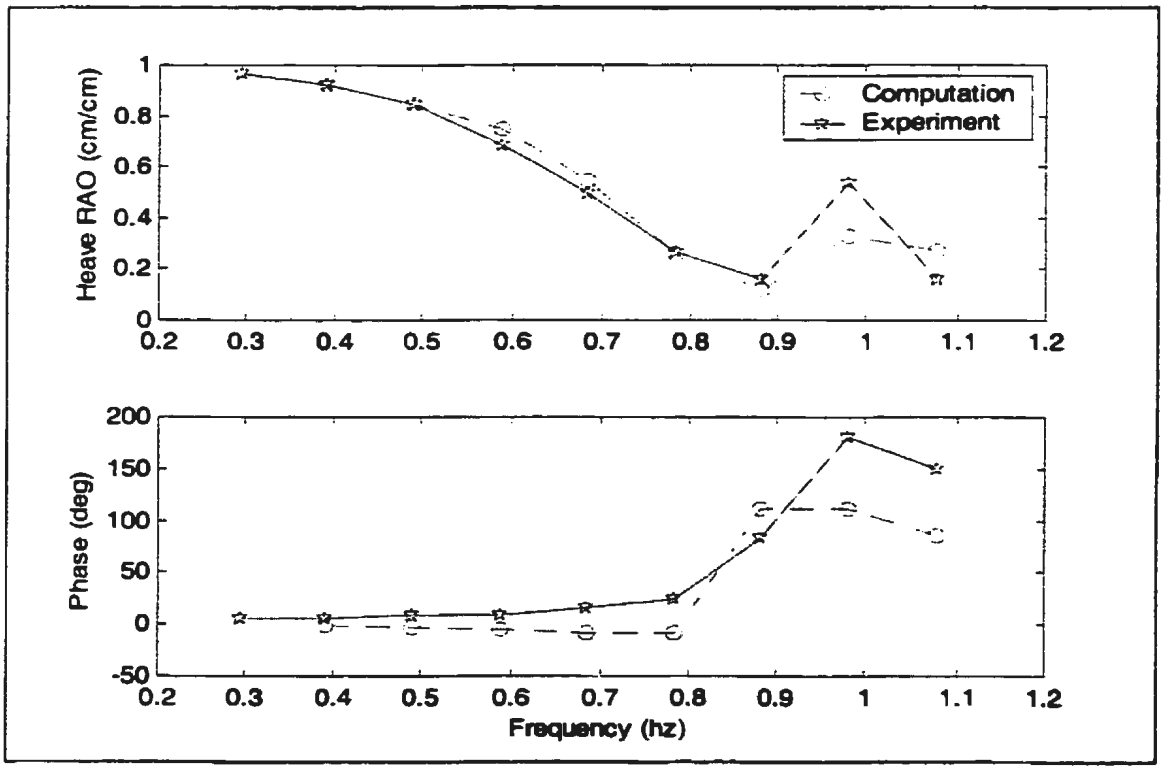

Figure 18: Frequency Response Functions for Heave

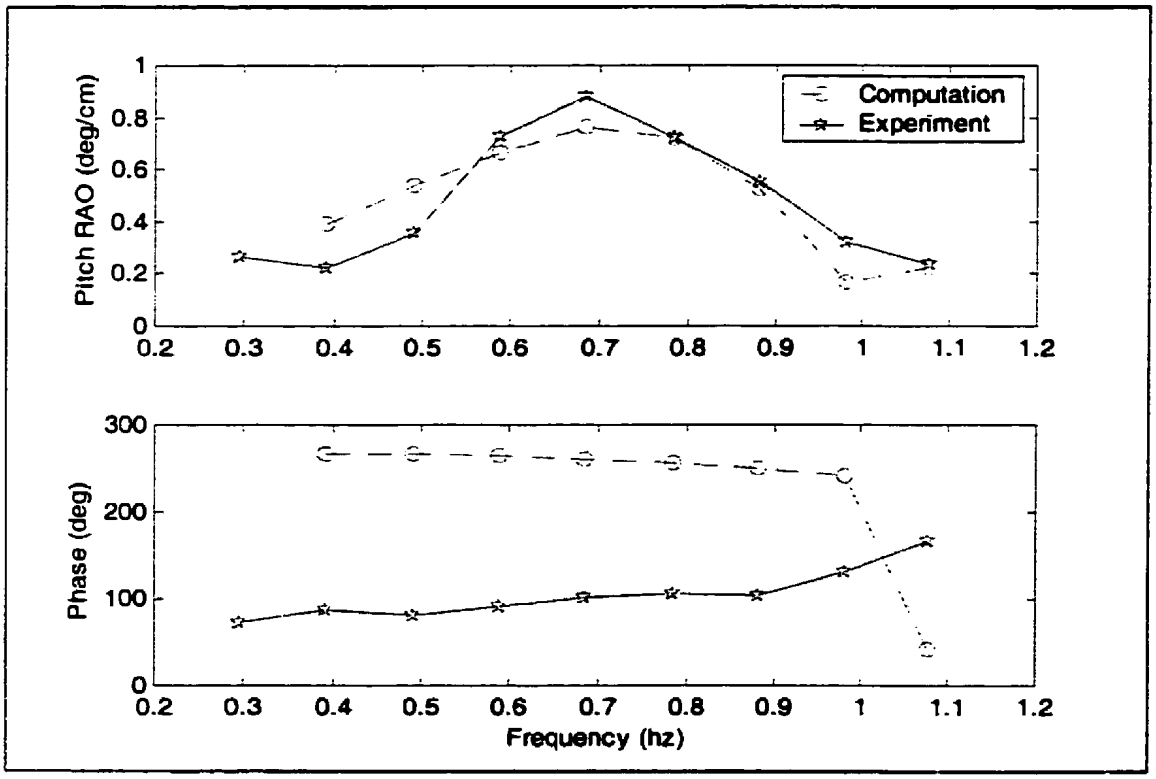

Figure 19: Frequency Response Functions for Pitch

The computed frequency response functions of heave and pitch motions agree well with the experimental results for the frequency range from 0.4Hz to 0.9Hz. There is a discrepancy for frequencies 1.0Hz and 1.1Hz. This is the frequency range where resonance occurs. The assumption of linearity may not be valid in this range.

For the frequency response functions of wave-induced bending moment, the agreement between theoretical and experimental values is not as good as in the case of motions. This is expected since errors in the motion computations produce larger errors in the bending moment computations.

Due to time and resource constraints, we used a strip theory based on Lewis-form method. It has limitations in computational accuracy. A more sophisticated theory will yield better results.

4.5 Frequency-domain Results

In the previous sections, the obtained frequency response functions or RAOs expressed the frequency-domain relationship between ship responses and wave elevation. Following linear-random theory, they can be used to estimate the statistical parameters of the ship responses from the wave spectrum.

In this work, the main objective is the relationship between wave-induced bending moment and ship motions. The input signal is the heave or pitch motion instead of the wave elevation. Therefore, the RAOs should be calculated as the ratios between the bending moment amplitudes and the motion amplitudes. These amplitude values are available from both the experimental results and the computational results presented in the previous sections.

Based on the regular wave results given in Table 13, Table 15, and Table 17, the RAOs of the heave-moment system are calculated and plotted in Figure 20. The RAOs of the pitch-moment system are calculated and plotted in Figure 21. The results are dependent on the forward speed and the heading angle.

Given the power spectra of the ship motions, the statistical parameters of the wave-induced bending moment can be estimated from the above RAOs.

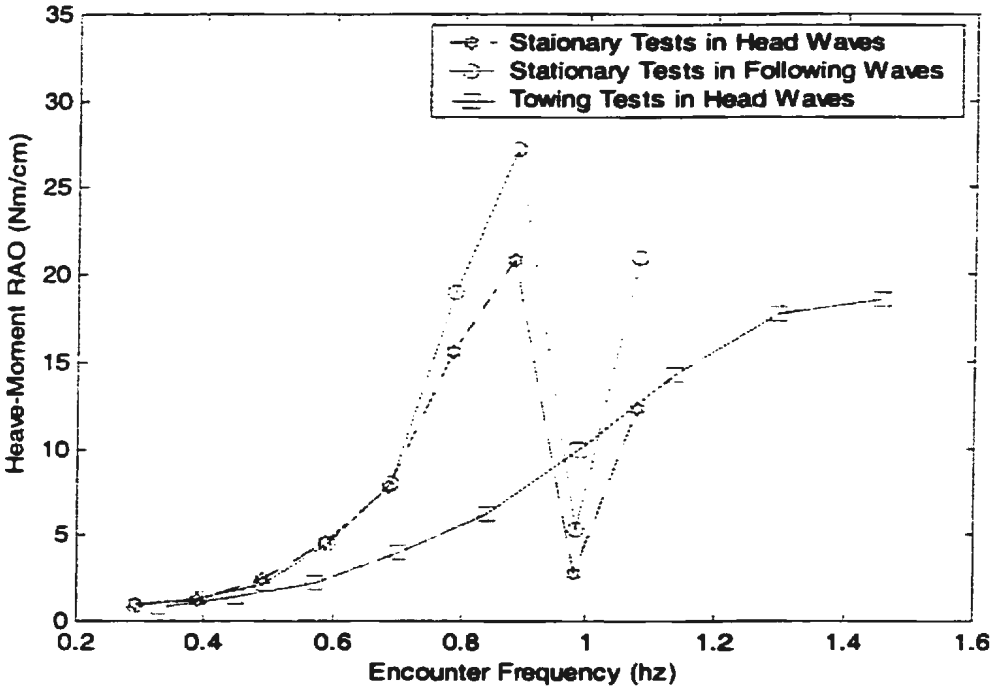

Figure 20: RAOs for Heave - Bending Moment System

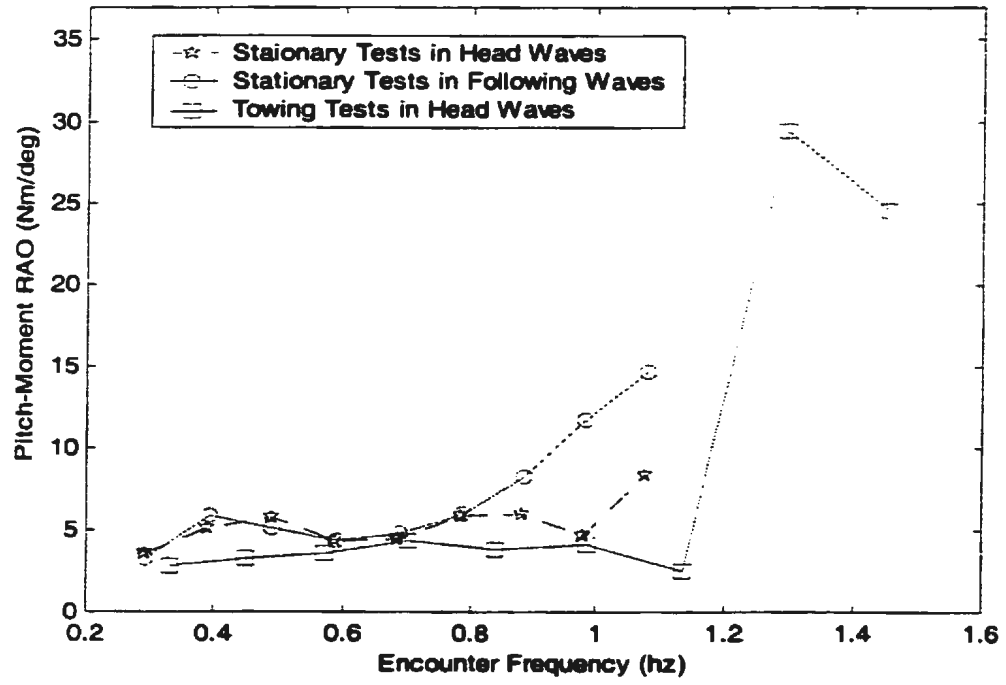

Figure 21: RAOs for Pitch - Bending Moment System

Although the frequency-domain relationships shown in Figure 20 and Figure 21 are suitable for the statistical estimation of the bending moment parameters, they are not sufficient for real-time estimation of the instantaneous values. A time-domain relationship is needed for this purpose.

5. Time-domain Analysis

5.1 Mathematical Formulation

In this work, the objective is to estimate the instantaneous bending moment from ship motion measurements. This real-time estimation procedure requires a time-domain relationship between the wave-induced bending moment and ship motions. It can be obtained by transforming the frequency-domain model into the time domain.

The frequency-domain model of ship vertical motions and wave-induced bending moments is expressed by equations (11) and (12). For steady-state solutions, both the motions and the bending moments are sinusoidal with a frequency ω equal to the encounter frequency. Therefore the equations can be written in the complex form as

$$\begin{aligned} A(i\omega)X_z(\omega) + B(i\omega)X_\theta(\omega) &= F_3(i\omega)U(\omega) \\ C(i\omega)X_z(\omega) + D(i\omega)X_\theta(\omega) &= F_5(i\omega)U(\omega) \end{aligned} \qquad (23)$$

and

$$Y(\omega) = \alpha(i\omega)X_z(\omega) + \beta(i\omega)X_\theta(\omega) + L(i\omega)U(\omega) \qquad (24)$$

where $Y(\omega)$, $U(\omega)$, $X_z(\omega)$ and $X_\theta(\omega)$ are complex amplitudes of the bending moment y(t), wave elevation $\zeta(t)$, heave displacement z(t) and pitch angle $\theta(t)$, respectively. Other complex coefficients in equation (23) and (24) can be expressed in terms of the coefficients in equations (11) and (12),

$$A(i\omega)=[C_{33}-\omega^2(M+A_{33})]+i(\omega B_{33})$$
$$B(i\omega)=(C_{35}-\omega^2 A_{35})+i(\omega B_{35})$$
$$C(i\omega)=(C_{53}-\omega^2 A_{53})+i(\omega B_{53})$$
$$D(i\omega)=[C_{55}-\omega^2(I+A_{55})]+i(\omega B_{55})$$
$$F_3(i\omega)=\frac{F_3}{U(\omega)}$$
$$F_5(i\omega)=\frac{F_5}{U(\omega)}$$

(25)

and

$$\alpha(i\omega)=(C_y-\omega^2 A_y)+i(\omega B_y)$$
$$\beta(i\omega)=(H_y-\omega^2 D_y)+i(\omega E_y)$$
$$L(i\omega)=\frac{y_\zeta}{U(\omega)}$$

(26)

The motion responses $X_z(\omega)$ and $X_\theta(\omega)$ can be obtained from equation (23) in terms of the wave complex amplitude $U(\omega)$ as

$$\begin{bmatrix} X_z(\omega) \\ X_\theta(\omega) \end{bmatrix} = \begin{bmatrix} A(i\omega) & B(i\omega) \\ C(i\omega) & D(i\omega) \end{bmatrix}^{-1} \begin{bmatrix} F_3(i\omega) \\ F_5(i\omega) \end{bmatrix} U(\omega)$$

(27)

Equation (27) can be rewritten in the following form

$$U(\omega)=\frac{A(i\omega)D(i\omega)-B(i\omega)C(i\omega)}{D(i\omega)F_3(i\omega)-B(i\omega)F_5(i\omega)}X_z(\omega)$$

(28)

or

$$U(\omega)=\frac{A(i\omega)D(i\omega)-B(i\omega)C(i\omega)}{A(i\omega)F_5(i\omega)-C(i\omega)F_3(i\omega)}X_\theta(\omega)$$

(29)

Substitution of equation (28) into equation (24) results in the following equation

$$Y(\omega) = a(i\omega)X_z(\omega) + b(i\omega)X_\theta(\omega) \qquad (30)$$

where

$$a(i\omega) = \alpha(i\omega) + \frac{A(i\omega)D(i\omega) - B(i\omega)C(i\omega)}{D(i\omega)F_3(i\omega) - B(i\omega)F_5(i\omega)}L(i\omega) \qquad (31)$$

$$b(i\omega) = \beta(i\omega)$$

Equations (30) and (31) express the frequency-domain relationship between the bending moment and ship motions. This relationship is independent of the wave excitation. The complex coefficients a(iω) and b(iω) are frequency-dependent for any combination of ship speed and heading angle. To get estimates for the instantaneous bending moment, we have to transform equation (30) to the time domain.

Tick (1959) has shown that frequency-dependent equations actually represent systems that are described in the time domain by equations involving convolution integrals. Under certain conditions they may be approximated by constant-coefficient differential equations. Following the approach of Tick (1959), we can first apply the inverse Fourier transform on both sides of equation (30) and obtain a convolution integral equation in the time domain as

$$y(t) = \int_0^{+\infty} h_a(\tau)z(t-\tau)d\tau + \int_0^{+\infty} h_b(\tau)\theta(t-\tau)d\tau \qquad (32)$$

where

$$h_a(\tau) = \frac{1}{2\pi}\int_{-\infty}^{+\infty} a(i\omega)e^{i\omega\tau}d\omega \qquad (33)$$
$$h_b(\tau) = \frac{1}{2\pi}\int_{-\infty}^{+\infty} b(i\omega)e^{i\omega\tau}d\omega$$

Since this is a real-valued system, the complex coefficients in equation (30) must have Hermitian symmetry as

$$a(-i\omega) = a^*(i\omega) \qquad (34)$$
$$b(-i\omega) = b^*(i\omega)$$

If a(iω) and b(iω) can be approximated by polynomials, their real parts must be even polynomials and the imaginary parts must be odd polynomials to satisfy the above Hermitian symmetry. The simplest approximation uses the second order polynomials as

$$a(i\omega) = (\overline{A}_1\omega^2 + \overline{A}_3) + i(\overline{A}_2\omega) \qquad (35)$$
$$b(i\omega) = (\overline{B}_1\omega^2 + \overline{B}_3) + i(\overline{B}_2\omega)$$
$$-\infty < \omega < +\infty$$

where $\overline{A}_i, \overline{B}_i$ are real-valued constants. Then,

$$h_a(\tau) = -\overline{A}_1\ddot{\delta}(\tau) + \overline{A}_2\dot{\delta}(\tau) + \overline{A}_3\delta(\tau) \qquad (36)$$
$$h_b(\tau) = -\overline{B}_1\ddot{\delta}(\tau) + \overline{B}_2\dot{\delta}(\tau) + \overline{B}_3\delta(\tau)$$

where δ(τ) is the Dirac delta-function. Substituting (36) into equation (32) and performing the integration, we get a 2nd order constant-coefficient differential equation

$$y(t) = -\overline{A}_1\ddot{z}(t) + \overline{A}_2\dot{z}(t) + \overline{A}_3 z(t) - \overline{B}_1\ddot{\theta}(t) + \overline{B}_2\theta(t) + \overline{B}_3\theta(t) \qquad (37)$$
$$-\infty < \omega < +\infty$$

In the above derivation, the approximation given in equation (35) is assumed to be valid for the full frequency range (-∞, +∞). Since the ship motions and the wave-induced bending moment are both narrow-band processes, we need only consider the approximation in a narrow-band frequency range. The approximation thus becomes

$$a(i\omega) = (\overline{C}_1\omega^2 + \overline{C}_3) + i(\overline{C}_2\omega)$$
$$b(i\omega) = (\overline{D}_1\omega^2 + \overline{D}_3) + i(\overline{D}_2\omega) \qquad (38)$$
$$\omega_1 < |\omega| < \omega_2$$

Substitution of (38) into equation (30) results in

$$Y(\omega) = [(\overline{C}_1\omega^2 + \overline{C}_3) + i(\overline{C}_2\omega)]X_z(\omega) + [(\overline{D}_1\omega^2 + \overline{D}_3) + i(\overline{D}_2\omega)]X_\theta(\omega) \qquad (39)$$
$$\omega_1 < |\omega| < \omega_2$$

Taking the inverse Fourier transform of both sides, we get

$$y(t) = \frac{1}{2\pi}\overline{C}_1\int_\omega \omega^2 X_z(\omega)e^{i\omega t}d\omega + \frac{1}{2\pi}\overline{C}_2\int_\omega i\omega X_z(\omega)e^{i\omega t}d\omega + \frac{1}{2\pi}\overline{C}_3\int_\omega X_z(\omega)e^{i\omega t}d\omega \qquad (40)$$
$$+\frac{1}{2\pi}\overline{D}_1\int_\omega \omega^2 X_\theta(\omega)e^{i\omega t}d\omega + \frac{1}{2\pi}\overline{D}_2\int_\omega i\omega X_\theta(\omega)e^{i\omega t}d\omega + \frac{1}{2\pi}\overline{D}_3\int_\omega X_\theta(\omega)e^{i\omega t}d\omega$$
$$\omega_1 < |\omega| < \omega_2$$

Using the following identities:

$$\int_\omega \omega^2 X(\omega)e^{i\omega t}d\omega = -\frac{d^2}{dt^2}[\int_\omega X(\omega)e^{i\omega t}d\omega] \qquad (41)$$
$$\int_\omega i\omega X(\omega)e^{i\omega t}d\omega = \frac{d}{dt}[\int_\omega X(\omega)e^{i\omega t}d\omega]$$

equation (40) reduces to a second order constant-coefficient differential equation in the following form:

$$y(t) = -\overline{C}_1\ddot{z}(t) + \overline{C}_2\dot{z}(t) + \overline{C}_3 z(t) - \overline{D}_1\ddot{\theta}(t) + \overline{D}_2\dot{\theta}(t) + \overline{D}_3\theta(t) \qquad (42)$$
$$\omega_1 < |\omega| < \omega_2$$

This is a time-domain approximation for a narrow-band process. For more complicated cases, the coefficients a(iω) and b(iω) may be approximated by higher-order polynomials, and the convolution integral equation (32) reduces to a constant-coefficient differential equation of a higher order.

5.2 Neural Networks Model

5.2.1 Structure and Algorithm

There are six unknown coefficients involved in the time-domain model given by equation (42). It is not easy to determine the individual values of these coefficients. Instead, we can express this parametric model in the following form:

$$y(t) = F_y[\ddot{z}(t), \dot{z}(t), z(t), \ddot{\theta}(t), \dot{\theta}(t), \theta(t)] \qquad (43)$$

A neural network model is employed in this work to approximate the function F_y in equation (43). This is achieved through a learning process using a set of known input-output data.

Artificial neural networks constitute a set of cellular computational structures that can be implemented in both hardware and software forms. The operation of neural networks can be viewed as that of nonlinear systems. Static networks are used to map the static input-output relationship, while recurrent networks are used to simulate dynamic systems. In the system given by equation (43), the output y(t) is a function only of the current six inputs. A typical static network, single-hidden-layer MLP network, is suitable to model this system. The network structure is illustrated in Figure 22.

This MLP network has six input neurons and one output neuron. A single bias neuron is added to each of the input and hidden layers. Data passing through the neurons in the hidden layer undergo a nonlinear transformation using a sigmoid function. Linear neurons are used in both the input and the output layers. All three layers are fully

connected as shown in Figure 22, and the weight values between the layers can be adjusted to map any input-output relationship.

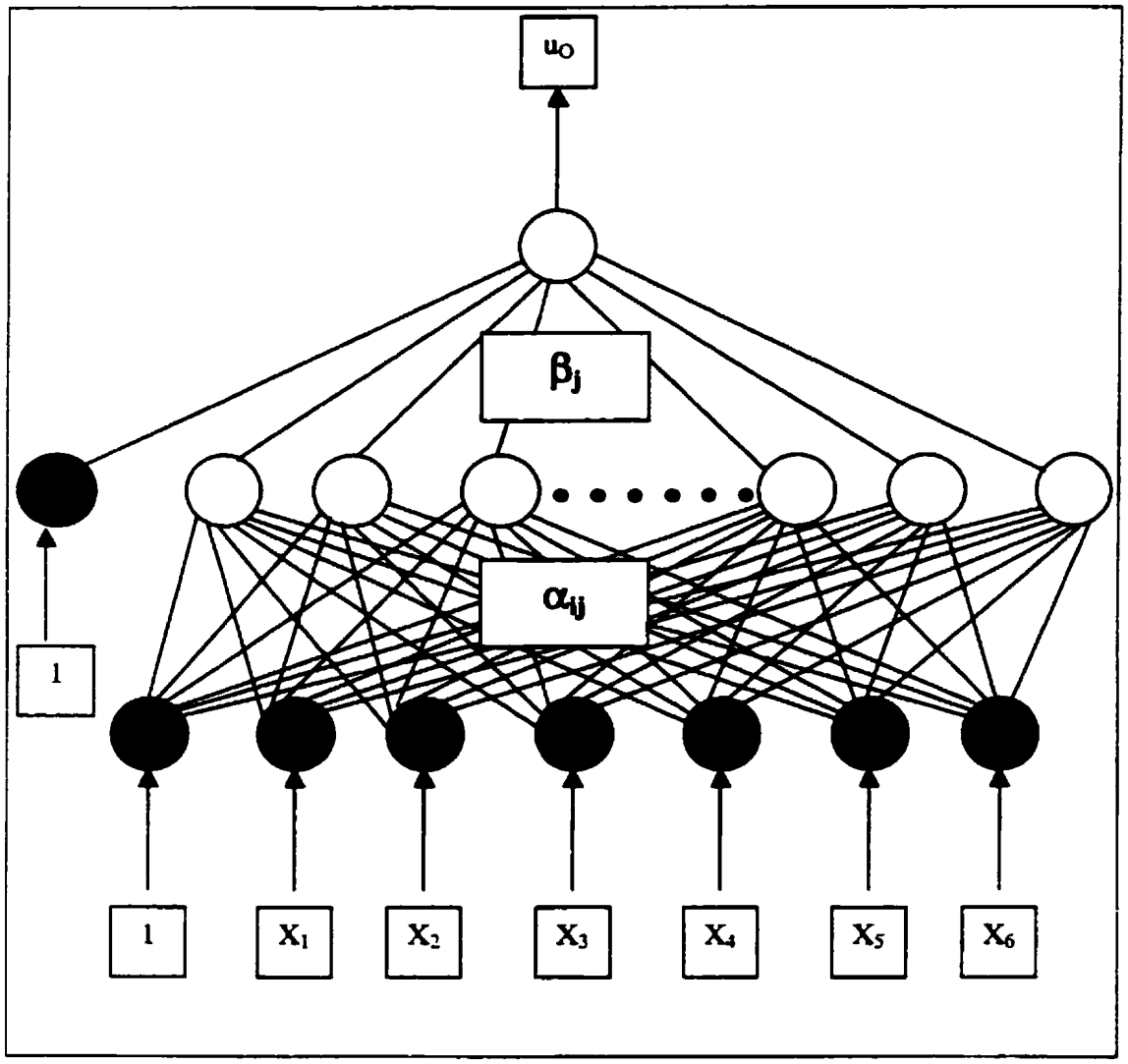

Figure 22: Structure of Single-hidden-layer MLP Neural Network

If the first layer weights are denoted as α_{ij}, the output of the j^{th} hidden neuron is given as

$$u_{Hj} = [1+\exp(-\sum_{i=0}^{6} \alpha_{ij} x_i)]^{-1} \qquad (44)$$

where the 0^{th} component of the input vector, $x_0=1$, is the bias input, and α_{0j} are the bias weights. Similarly, the second layer weights are denoted as β_j, and the neural network output is given as

$$u_o = \sum_{j=1}^{N_H} u_{Hj}\beta_j \qquad (45)$$

where N_H is the number of the neurons in the hidden layer. It has to be chosen carefully to model the system properly.

The important feature of neural networks is their ability to approximate arbitrary functions through on-line and off-line learning processes. During the learning process, the neural network is presented with a set of input-output points and trained to implement a mapping that matches the sample points as closely as possible. The most popular learning method for the MLP is the backpropagation algorithm. It uses a gradient search technique to find the optimum weight values that minimize a criterion function. In this work the criterion function is the SUM-of-Squared-Error function defined as follows,

$$J = \sum_{p=1}^{N} J_p \qquad (46)$$
$$J_p = \frac{1}{2}[u_0(p) - y(p)]^2$$

where $u_O(p)$ is the network output for the p^{th} training points, y(p) is the corresponding actual value, J_p is the squared error of the p^{th} training points, and J is the total squared error for all training points. The weights of the network are adjusted iteratively according to the following algorithm,

$$\alpha_{ij}(k+1)=\alpha_{ij}(k)-\mu\frac{\partial J}{\partial \alpha_{ij}}|_{(k)}=\alpha_{ij}(k)-\mu\sum_{p=1}^{N}\frac{\partial J_p}{\partial \alpha_{ij}}|_{(k)} \qquad (47)$$

$$\beta_j(k+1)=\beta_j(k)-\mu\frac{\partial J}{\partial \beta_j}|_{(k)}=\beta_j(k)-\mu\sum_{p=1}^{N}\frac{\partial J_p}{\partial \beta_j}|_{(k)}$$

where μ is a positive constant called the learning rate. To implement this algorithm we must have an expression for the partial derivative of J_p with respect to each weight in the network. This can be derived from the output layer backwards (Hush and Horne, 1993), and the final results are given as

$$\frac{\partial J_p}{\partial \beta_j}=\frac{\partial J_p}{\partial u_O(p)}\frac{\partial u_O(p)}{\partial \beta_j}=[u_O(p)-y(p)]u_{Hj} \qquad (48)$$

$$\frac{\partial J_p}{\partial \alpha_{ij}}=\frac{\partial J_p}{\partial u_O(p)}\frac{\partial u_O(p)}{\partial u_{Hj}}\frac{\partial u_{Hj}}{\partial \alpha_{ij}}=[u_O(p)-y(p)]\beta_j u_{Hj}(1-u_{Hj})x_i$$

The results of equation (48) are substituted into equation (47) to implement the gradient search. The weights are typically initialized to small random values. The process of computing the gradient and adjusting the weights is repeated until a minimum value of J is found,

$$\frac{\partial J}{\partial \alpha_{ij}}=\sum_{p=1}^{N}\frac{\partial J_p}{\partial \alpha_{ij}}=0 \qquad (49)$$

$$\frac{\partial J}{\partial \beta_j}=\sum_{p=1}^{N}\frac{\partial J_p}{\partial \beta_j}=0$$

A cross-validation technique can be used to monitor the generalization performance during the learning process.

5.2.2 Training Data Selection

Generalization performance is a measure of how well the network performs on the actual data outside the training set. It represents the quality of the training results. From Hush and Horne (1993), generalization performance is heavily influenced by the selection of the training data samples.

In this work, the following criteria are used for the training data selection:

1. Representative — The training data must satisfy the mathematical model of the underlying system.
2. Informative — The training data should include information covering the whole frequency range of the frequency-dependent system.
3. Efficient — The ratio of the information amount to training data number should be high enough to reduce the computational time.
4. Noiseless — The training data should have minimum noise effects.

Conventionally, the time histories from the experiments are used as the training data. They are naturally representative of the underlying system. In this work there are two groups of test data available, the regular-wave test data and the random-wave test data. Since the system given by equation (43) is a frequency-dependent system, the regular-wave time histories with the discrete frequency values are not informative on the whole frequency range. Only the random time histories may have enough information and can possibly be used as training data. However, in this case a long time history is needed to retrieve the complete information. This requires a large amount of computational time. In

addition, the random data obtained from model experiments or full-scale tests are usually contaminated by noise. They are not efficient or noiseless as the training data.

As an alternative to the raw test data, the statistical data is another source for the training data selection. Previous experience from similar studies (Xu and Haddara, 2001) shows that one set of the auto- and cross-correlation functions provides good training results. These correlation functions are Fourier transforms of the auto- and cross-spectral of the ship motions and the hull bending moment. They are informative on the whole frequency range. Since all correlation functions are in decay form, the complete information is carried on a limited number of data points. This provides an efficient training scheme. In addition, the averaging process involved in the calculation of the correlation functions greatly reduces the effect of noise on the data. Therefore, the correlation functions meet the most requirements of the training data. The only concern is that the selected correlation functions must satisfy the system model expressed in equation (43). One set of the training data is derived as follows.

Multiplying both sides of equation (30) by the complex conjugate $X_z^*(\omega)$, one gets

$$X_z^*(\omega)Y(\omega) = a(i\omega)X_z^*(\omega)X_z(\omega) + b(i\omega)X_z^*(\omega)X_\theta(\omega) \qquad (50)$$

Thus the auto-spectral density $S_{zz}(\omega)$, cross-spectral density $S_{z\theta}(\omega)$ and $S_{zy}(\omega)$ are related as

$$S_{zy}(\omega) = a(i\omega)S_{zz}(\omega) + b(i\omega)S_{z\theta}(\omega) \qquad (51)$$

Taking the inverse Fourier transform of equation (51) gives the time-domain expression

$$R_{zy}(t) = \int_0 h_a(\tau) R_{zz}(t-\tau) d\tau + \int_0 h_b(\tau) R_{z\theta}(t-\tau) d\tau \qquad (52)$$

where $R_{zz}(\tau)$ is the auto-correlation function of the heave displacement z(t), $R_{zy}(\tau)$ is the cross-correlation function between the heave displacement z(t) and the bending moment y(t), and $R_{z\theta}(\tau)$ is the cross-correlation function between the heave displacement z(t) and the angular pitch displacement $\theta(t)$. They can be estimated from the random time histories in the following form

$$R_{zy}(\tau) = \lim_{T\to\infty} \frac{1}{T} \int_0^T z(t) y(t+\tau) dt \qquad (53)$$
$$R_{zz}(\tau) = \lim_{T\to\infty} \frac{1}{T} \int_0^T z(t) z(t+\tau) dt$$
$$R_{z\theta}(\tau) = \lim_{T\to\infty} \frac{1}{T} \int_0^T z(t) \theta(t+\tau) dt$$

Equation (52) is identical to equation (32). Therefore, an expression similar to equation (43) can be used to relate the auto- and cross-correlation functions of the motions and the bending moment. This relationship is given as

$$R_{zy}(\tau) = F_y[\ddot{R}_{zz}(\tau), \dot{R}_{zz}(\tau), R_{zz}(\tau), \ddot{R}_{z\theta}(\tau), \dot{R}_{z\theta}(\tau), R_{z\theta}(\tau)] \qquad (54)$$

Equation (54) is equivalent to the system model given in equation (43). Therefore, we can conclude that samples from the correlation functions can be used for the training of the neural network.

5.2.3 Training Procedure

In this work, a commercial software package "NeuroShell 2" is used to create and train the single-hidden-layer MLP network. There are six input variables and one output

variable. In the training process, the input variables are correlation functions $R_{zz}, R_{z\theta}$ and their derivatives, while the output variable is R_{zy}. The auto- and cross-correlation functions were estimated from the random time histories using equation (53). Their derivatives were obtained using the following algorithm:

$$\dot{R}(t) = \frac{R(t+\Delta t) - R(t-\Delta t)}{2(\Delta t)} \qquad (55)$$

$$\ddot{R}(t) = \frac{R(t+\Delta t) - 2R(t) + R(t-\Delta t)}{(\Delta t)^2}$$

Since "NeuroShell 2" requires all variables to be in the range [0,1] or [–1,1], we need to know the real value range of each input variable and scale the actual input data to the required range. In order to achieve the uniform value ranges for different test data, all correlation functions and their derivatives were divided by value $R_{zz}(0)$. In this work 10sec long correlation functions were calculated and normalized, and 480 sample points were selected for network training.

After the training points were imported into "NeuralShell 2" using the *File Import* module, the inputs/output variables and their real value ranges were specified in the *Define Inputs And Outputs* module. Generally, the real value ranges of the input and the output variables have to be specified close to those of the training data. Otherwise the network may lose its ability to spot small differences between the points. In this work, we specified the real value ranges of the variables to be 20% wider than those of the training data. This allows for some flexibility in future predictions.

The network architecture and the parameters were specified in the *Design* module. The single-hidden-layer MLP network was chosen in this work. There were six input neurons and one bias neuron in the input layer, and only one neuron in the output layer. The number of hidden neurons was set by default to 24 plus one bias neuron. In the MLP networks, the number of the hidden neurons determines how well a system can be modeled. If we use too many, the network will tend to memorize the training points instead of learning the relationship between the input and the output. This network will not generalize well. If we use too few, the network may not have enough "power" to learn the system well. Specifying the right number of the hidden neurons is a matter of trial and error, and the default number was calculated here with the following formula:

$$N_{neurons} \approx \frac{1}{2}(N_{input} + N_{output}) + \sqrt{N_{points}} \qquad (56)$$

where N_{input} is 6, N_{output} is 1, and N_{points} is 480.

After determining the neuron number, we have to specify the scaling functions for the input layer and the activation functions for the hidden and output layers, respectively. When the input variables are imported into the neural network, they must be scaled within the numerical range [0,1] or [-1,1] for the efficient operation of the network. In this work, the linear scaling functions were used for the input neurons

$$f_I(x) = 1 - \frac{2(X_{max} - x)}{X_{max} - X_{min}} \qquad (57)$$

where x denotes the actual input to the neuron, $f_I(x)$ is the output of the neuron, and X_{max} and X_{min} are maximum and minimum values of the corresponding variable, respectively.

The numerical range of $f_I(x)$ is [-1,1]. These outputs from the input layer neurons were weighted and then passed to the hidden layer, and the neurons in the hidden layer produced their outputs based upon the sum of the weighted values passed to them. The activation function between the hidden neurons input and output was specified as a sigmoid function

$$f_h(y) = \frac{1}{1+e^{-y}} \qquad (58)$$

The outputs $f_h(y)$ were weighted and passed to the output layer. Since the network output is a continuous variable, the activation function for the output neuron was specified as a linear function

$$f_o(z) = z \qquad (59)$$

The output $f_o(z)$ is the final output of the neural network. The learning rate and momentum for all links were set to 0.1 and 0.1, respectively. The initial weight values were randomly set within the range [-0.3, +0.3].

After the network architecture was decided, several parameters for the training process had to be specified in the *Training Criteria* module. The most important is the set-up of the NET-PERFECT function, which limits the over-training of the network and prevents the pure "memorization" of the training points. With the NET-PERFECT feature, the network is only trained to build the model that smoothly interpolates between close training points, thus the network could generalize well in later predictions. In the operation, a test set was created by randomly extracting 57 points from the 480 sample

points. The network was trained using the training set of 423 points, but at specified intervals it was tested by computing the average error on the 57 test points. The test interval was set as 200 training events. We also specified that the network be saved on the best test set, thus NET-PERFECT saved the network weight values every time the average error of the test set reached a new minimum value. The training process was stopped after the minimum test error did not change for 40,000 training events.

After the network training was completed, other sets of data could be processed through the trained neural network in the *Apply To File* module. The network outputs could be compared with the actual values for validation. The statistical indicator R^2 was calculated as

$$R^2 = 1 - \frac{\sum_n (y_n - \hat{y}_n)^2}{\sum_n (y_n - \mu_y)^2} \qquad (60)$$

where y_n is the actual value, $\hat{y}_n$ is the network output, and μ_y is the mean of the actual values. A perfect fit would result in an R^2 value of 1, a very good fit near 1, and a poor fit near 0. After the neural network has been validated, it can be used for prediction or real-time estimation.

5.3 Time-domain Results

The proposed technique was applied to the 'R-class Icebreaker' model test data. All test data was filtered using a low-pass filter with a cut-off frequency of 2.5Hz. The auto- and cross-correlation functions of each random test run were computed first. For every combination of forward speed and heading angle, one set of correlation functions was used for the network training. Other sets of correlation functions were imported into the trained network for validation. The validated network was then used for the real-time estimation of the midship bending moment in regular and random waves. The estimated values were compared with the actual values obtained from the experiments.

5.3.1 Stationary Tests in Head Waves

The correlation functions of the random test J6h75a were used for the network training. The training data sample consisted of 480 training points, which were selected from 10sec long correlation functions. The final R^2 value is 0.999. The training data and the results are plotted in Figure 23. The network weight values are presented in Table 20.

The correlation functions obtained from other test runs were used to validate the neural network model. The R^2 values are presented in Table 21. All correlation functions satisfied the trained neural network very well.

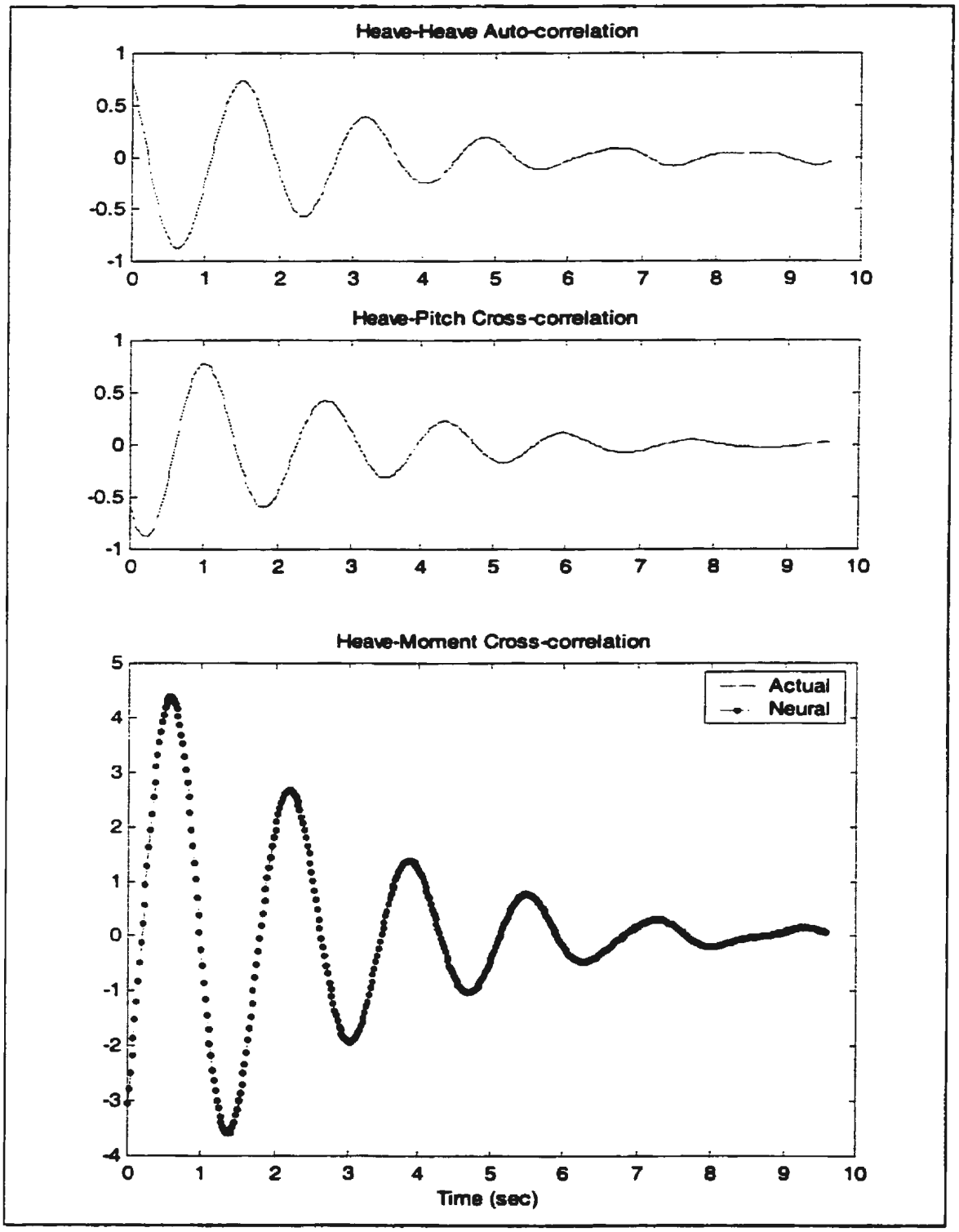

Figure 23: Training Results for Stationary Test in Head Waves

Table 20: Network Weight Values for Stationary Tests in Head Waves

Hidden	Input							Output
	bias	1	2	3	4	5	6	
bias	/	/	/	/	/	/	/	-0.20
1	-0.23	-0.16	0.28	0.00	-0.11	0.51	-0.15	0.58
2	0.10	-0.07	-0.17	-0.22	-0.22	-0.19	-0.11	-0.17
3	-0.07	0.02	0.15	0.25	0.01	0.27	0.22	0.36
4	0.21	0.02	0.18	-0.04	0.03	-0.15	-0.05	-0.19
5	0.11	0.08	0.31	-0.05	-0.20	0.03	0.15	-0.01
6	-0.02	0.08	0.33	0.19	0.35	-0.06	0.06	-0.22
7	0.31	0.03	0.02	0.12	-0.52	0.56	-0.16	0.82
8	0.31	0.06	-0.11	-0.14	0.15	0.23	0.15	0.17
9	0.28	-0.09	-0.21	0.15	0.03	-0.02	0.23	0.09
10	0.24	-0.11	-0.18	0.01	-0.22	0.13	-0.05	0.21
11	-0.01	0.00	0.28	0.06	-0.21	0.60	-0.12	0.75
12	0.25	0.05	-0.23	-0.01	-0.10	-0.52	0.22	-0.40
13	-0.15	0.13	-0.06	-0.04	0.43	-0.35	-0.24	-0.50
14	0.08	0.14	-0.22	-0.16	0.25	-0.28	0.35	-0.52
15	-0.23	-0.12	0.17	-0.24	0.05	-0.48	0.04	-0.65
16	-0.24	-0.17	-0.31	-0.10	0.19	-0.08	-0.26	-0.02
17	-0.05	0.39	-0.17	-0.03	0.08	0.74	-0.18	0.79
18	-0.02	0.18	0.28	0.14	0.06	0.17	-0.19	0.07
19	-0.15	0.24	-0.11	-0.04	-0.09	-0.26	0.25	-0.33
20	-0.08	0.27	-0.13	0.33	-0.24	0.07	0.04	0.20
21	0.30	-0.04	-0.03	0.09	0.24	-0.38	0.25	-0.56
22	-0.25	-0.23	0.18	-0.22	0.21	-0.48	-0.18	-0.61
23	-0.17	0.02	0.23	-0.19	-0.24	0.31	0.16	0.22
24	-0.26	-0.16	0.11	0.17	-0.09	0.17	-0.26	0.30

Table 21: Validation Results for Stationary Tests in Head Waves (Correlation Functions)

Test Data	Test Conditions	Peak Frequency	Significant Wave Height	Random Seed	R^2
Training (J6h75a)	JONSWAP Head Waves	0.6 Hz	0.75cm	1	**0.999**
B5a	Broad-band Head Waves	0.3 ~ 1.2 Hz	5.0 cm	1	**0.969**
B5b				2	**0.960**
B5c				3	**0.971**
B75a	Broad-band Head Waves	0.3 ~ 1.2 Hz	7.5 cm	1	**0.983**
B75b				2	**0.969**
B75c				3	**0.980**
J5h5a	JONSWAP Head Waves	0.5 Hz	5.0 cm	1	**0.963**
J5h5b				2	**0.982**
J5h5c				3	**0.984**
J5h75a	JONSWAP Head Waves	0.5 Hz	7.5 cm	1	**0.968**
J5h75b				2	**0.976**
J5h75c				3	**0.983**
J6h5a	JONSWAP Head Waves	0.6 Hz	5.0 cm	1	**0.996**
J6h5b				2	**0.998**
J6h5c				3	**0.996**
J6h75a	JONSWAP Head Waves	0.6 Hz	7.5 cm	1	**0.999**
J6h75b				2	**0.996**
J6h75c				3	**0.997**
J7h5c	JONSWAP Head Waves	0.7 Hz	5.0 cm	3	**0.992**
J7h75a	JONSWAP Head Waves	0.7 Hz	7.5 cm	1	**0.992**
J7h75b				2	**0.995**
J7h75c				3	**0.996**

For each regular wave test, 48 equally spaced points were selected from 10-second long time histories and imported into the neural network for validation. The results are shown in Table 22 and Figure 24. Excellent fits are obtained for the frequency range 0.4Hz to 0.9Hz. The agreement is not so good for frequencies in the range of 1.0Hz and 1.1Hz. This is expected since resonance occurs within this range.

Table 22: Validation Results for Stationary Tests in Regular Head Waves

Test Data	Test Conditions	Frequency	Wave Height	R^2
W4h6	Stationary Tests in Regular Head Waves	0.4 Hz	6.0 cm	**0.813**
W5h6		0.5 Hz		**0.829**
W6h6		0.6 Hz		**0.899**
W7h6		0.7 Hz		**0.975**
W8h6		0.8 Hz		**0.937**
W9h6		0.9 Hz		**0.931**
W10h6		1.0 Hz		**0.715**
W11h6		1.1 Hz		**0.718**

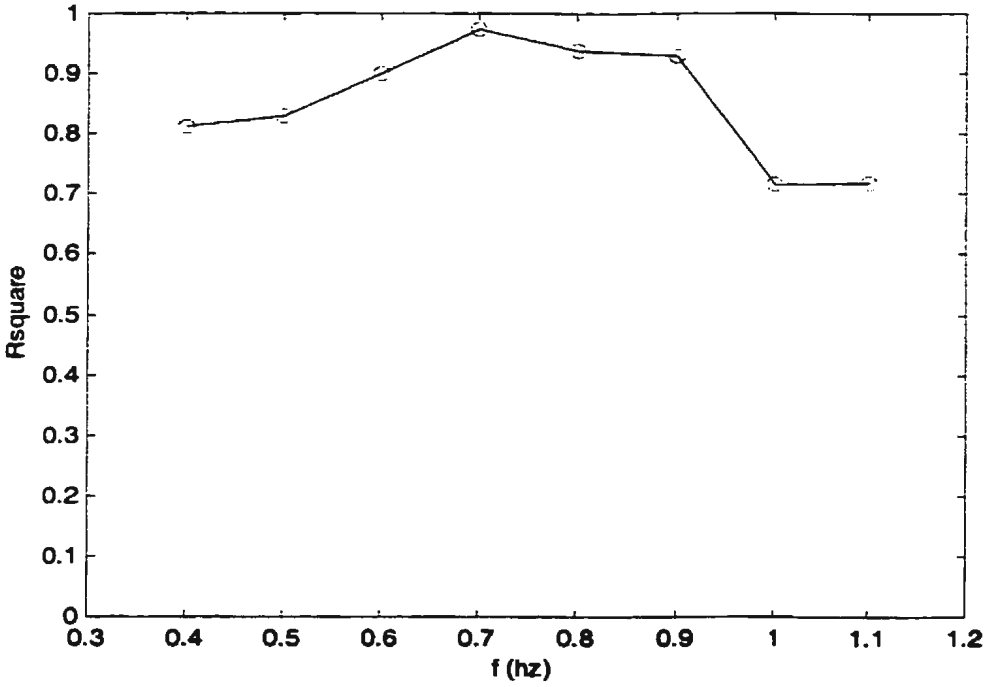

Figure 24: Validation Results for Stationary Tests in Regular Head Waves

This trained neural network could be used for the real-time estimation of instantaneous bending moment on the frequency range [0.4Hz, 1.1Hz]. A typical example for 10sec

long estimates of J6h75a random test is shown in Figure 25. There are 480 points estimated, and R^2 value is 0.943.

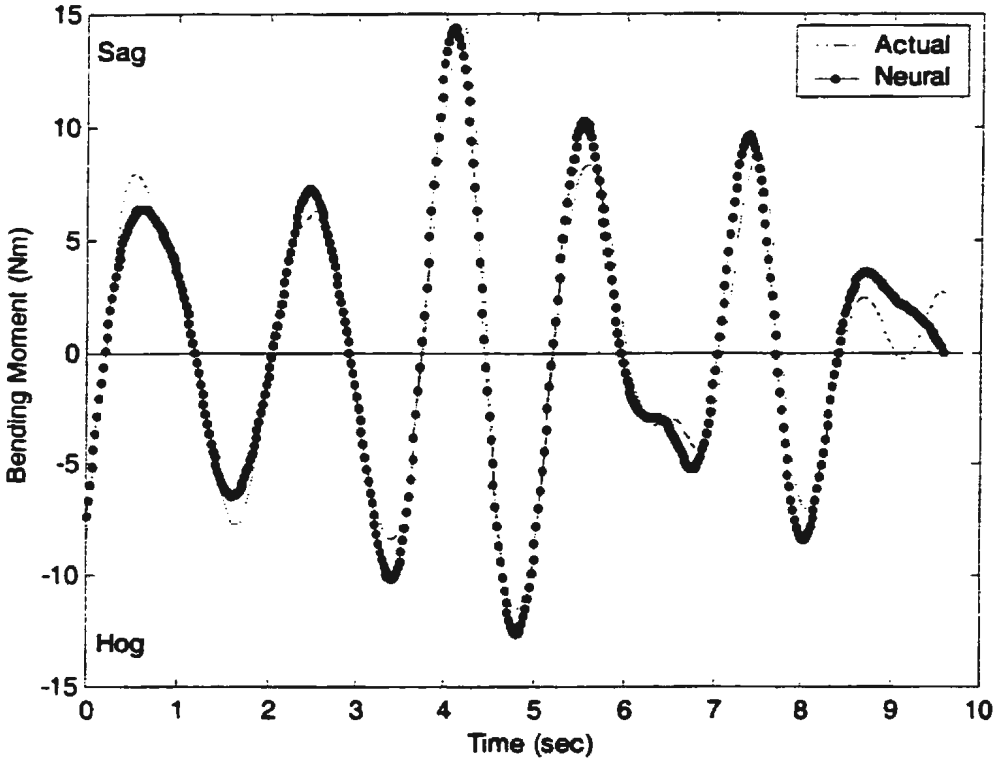

Figure 25: Estimation Example for Random Test J6h75a

5.3.2 Stationary Tests in Following Waves

The correlation functions of the random test Fj6h75a were used for the network training. The training data sample consisted of 480 training points, which were selected from 10sec long correlation functions. The final R^2 value is 0.998. The training data and results are plotted in Figure 26. The neural network weight values are presented in Table 23.

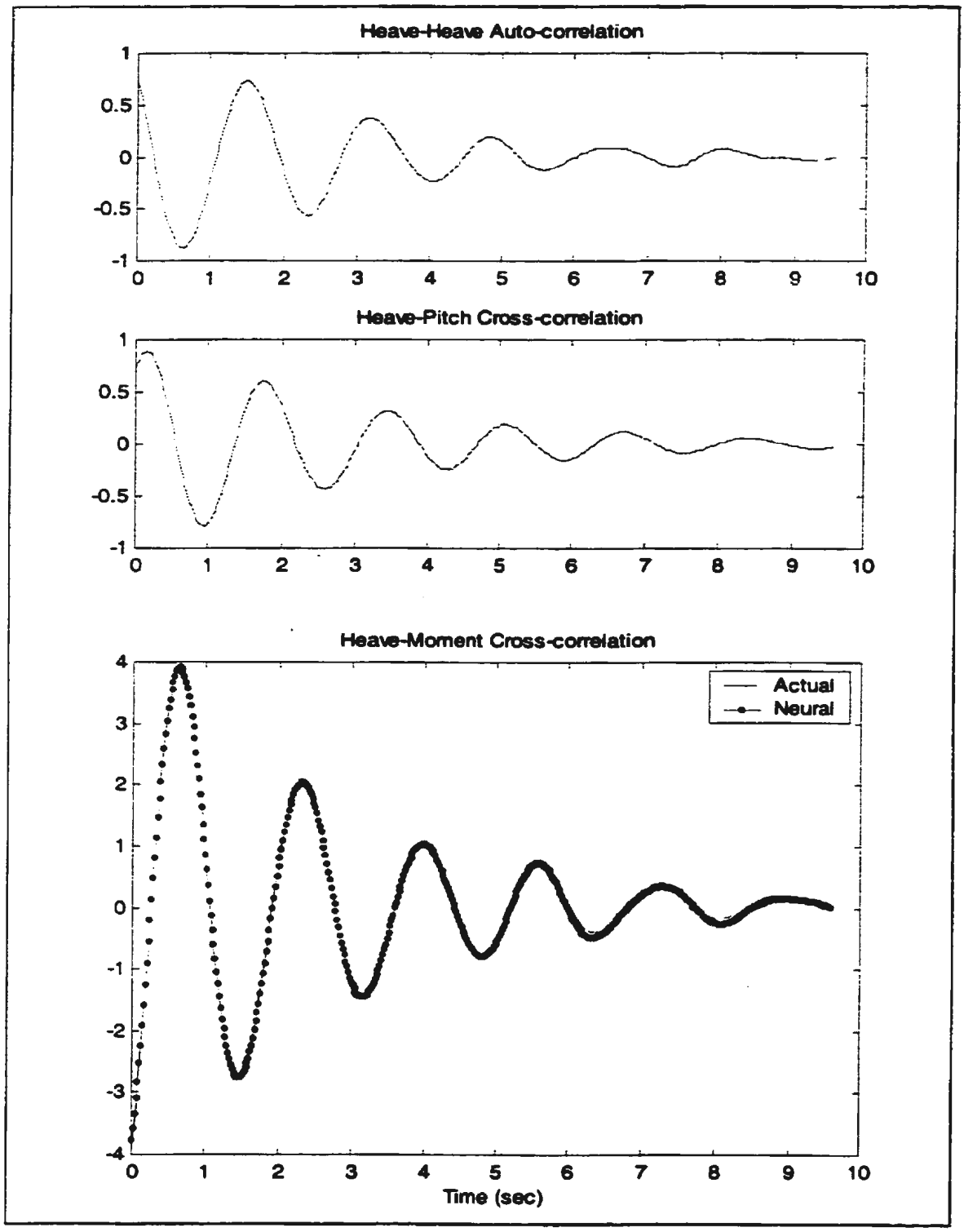

Figure 26: Training Results for Stationary Tests in Following Waves

Table 23: Network Weight Values for Stationary Tests in Following Waves

Hidden	Input							Output
	bias	1	2	3	4	5	6	
bias	/	/	/	/	/	/	/	-0.15
1	-0.17	-0.33	0.23	0.01	-0.01	-0.16	-0.22	0.40
2	0.14	-0.04	-0.23	-0.21	-0.22	0.06	-0.12	-0.07
3	0.01	0.11	0.27	0.02	0.08	-0.56	-0.07	0.72
4	0.31	0.11	0.15	-0.07	0.06	0.20	-0.11	-0.16
5	0.17	0.10	0.29	-0.05	-0.22	0.17	0.14	0.09
6	0.10	0.14	0.19	0.20	0.39	0.41	0.09	-0.42
7	0.06	-0.22	0.16	0.15	-0.30	-0.13	-0.31	0.47
8	0.36	0.04	0.01	-0.19	0.19	-0.23	0.11	0.17
9	0.38	0.03	0.19	-0.03	-0.14	-0.47	0.19	0.52
10	0.25	-0.10	0.00	-0.06	-0.23	-0.26	-0.10	0.33
11	-0.01	-0.29	0.25	0.14	-0.07	-0.08	-0.17	0.38
12	0.33	0.10	-0.23	0.03	-0.29	-0.32	0.21	0.17
13	-0.14	0.16	-0.17	0.09	0.35	0.26	-0.12	-0.47
14	0.03	0.11	-0.39	0.01	0.25	0.47	0.58	-0.87
15	0.03	0.07	-0.07	-0.25	-0.06	0.21	0.05	-0.29
16	-0.25	-0.21	0.02	-0.11	-0.04	-0.48	-0.21	0.42
17	-0.37	0.15	-0.46	0.03	0.38	0.22	0.00	-0.42
18	0.03	0.15	0.09	0.19	0.19	0.51	-0.09	-0.44
19	-0.10	0.27	-0.36	0.03	0.01	0.30	0.27	-0.50
20	-0.10	0.23	-0.10	0.31	-0.23	-0.27	0.00	0.28
21	0.38	0.12	0.01	0.06	0.26	0.29	0.21	-0.43
22	0.06	-0.13	0.04	-0.16	0.05	0.11	-0.19	-0.12
23	-0.15	-0.03	0.15	-0.18	-0.18	0.24	0.22	-0.07
24	-0.30	-0.17	0.24	0.08	-0.11	-0.45	-0.45	0.70

The correlation functions of other test runs were imported into the neural network for the validation. The R^2 values are presented in Table 24. The agreement is excellent for all sets of correlation functions with one exception. The broad-band following wave test Fb5b produced a poor fit. This is expected since the analysis is based on the narrow-band process assumption.

Table 24: Validation Results for Stationary Tests in Following Waves (Correlation Functions)

Test Data	Test Conditions	Peak Frequency	Significant Wave Height	Random Seed	R^2
Training (Fj6h75a)	JONSWAP Following Waves	0.6 Hz	0.75cm	1	**0.998**
Fb5a	Broad-band Following Waves	0.3 ~ 1.2 Hz	5.0 cm	1	**0.903**
Fb5b				2	**0.558**
Fb75a	Broad-band Following Waves	0.3 ~ 1.2 Hz	7.5 cm	1	**0.861**
Fb75b				2	**0.957**
Fj5h5a	JONSWAP Following Waves	0.5 Hz	5.0 cm	1	**0.981**
Fj5h5b				2	**0.976**
Fj5h75a	JONSWAP Following Waves	0.5 Hz	7.5 cm	1	**0.947**
Fj5h75b				2	**0.957**
Fj6h5a	JONSWAP Following Waves	0.6 Hz	5.0 cm	1	**0.995**
Fj6h5b				2	**0.988**
Fj6h75a	JONSWAP Following Waves	0.6 Hz	7.5 cm	1	**0.998**
Fj6h75b				2	**0.999**
Fj7h5a	JONSWAP Following Waves	0.7 Hz	5.0 cm	1	**0.971**
Fj7h5b				2	**0.975**
Fj7h75a	JONSWAP Following Waves	0.7 Hz	7.5 cm	1	**0.980**
Fj7h75b				2	**0.986**

For every regular wave test, 48 equally spaced points were selected from a 10-second long time history and imported into the neural network for validation. The results are shown in Table 25 and Figure 27. The neural network model is only valid on a narrow-band frequency range centered around the peak frequency of 0.6Hz. This agrees with the narrow-band process assumption.

Table 25: Validation Results for Stationary Tests in Regular Following Waves

Test Data	Test Conditions	Frequency	Wave Height	R^2
Fw3h6	Stationary Tests in Regular Following Waves	0.3 Hz	6.0 cm	**0.000**
Fw4h6		0.4 Hz		**0.650**
Fw5h6		0.5 Hz		**0.852**
Fw6h6		0.6 Hz		**0.982**
Fw7h6		0.7 Hz		**0.998**
Fw8h6		0.8 Hz		**0.874**
Fw9h6		0.9 Hz		**0.749**
Fw10h6		1.0 Hz		**0.947**
Fw11h6		1.1 Hz		**0.689**

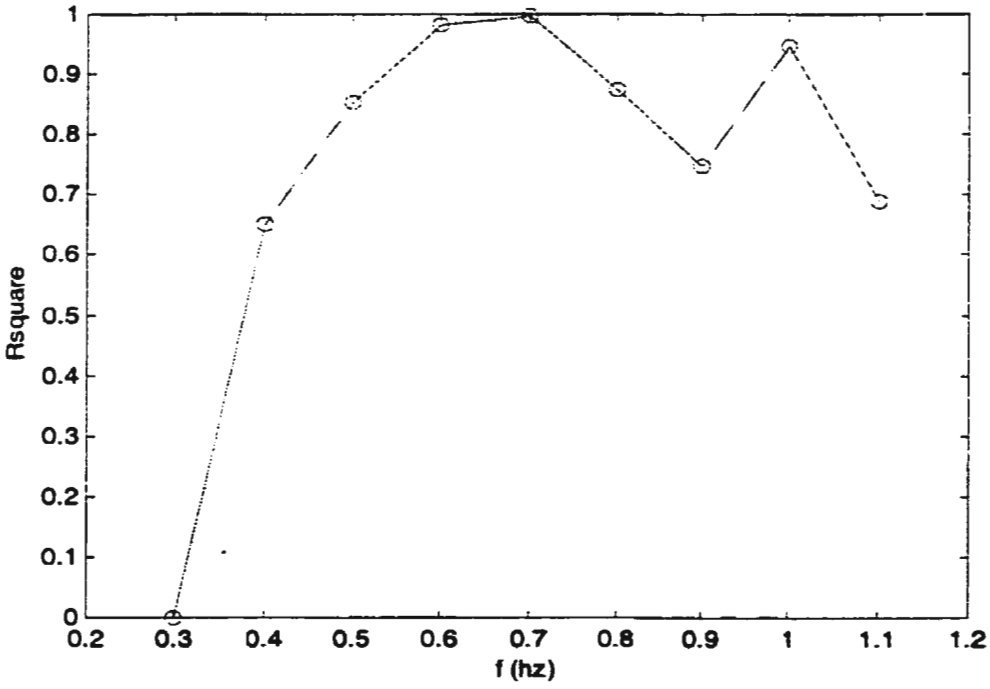

Figure 27: Validation Results for Stationary Tests in Regular Following Waves

The trained network could be used for the real-time estimation of instantaneous bending moment in narrow-band waves. A typical example for 10-second long estimates of Fj6h75a random test is shown in Figure 28. There are 480 points estimated, and R^2 value is 0.959.

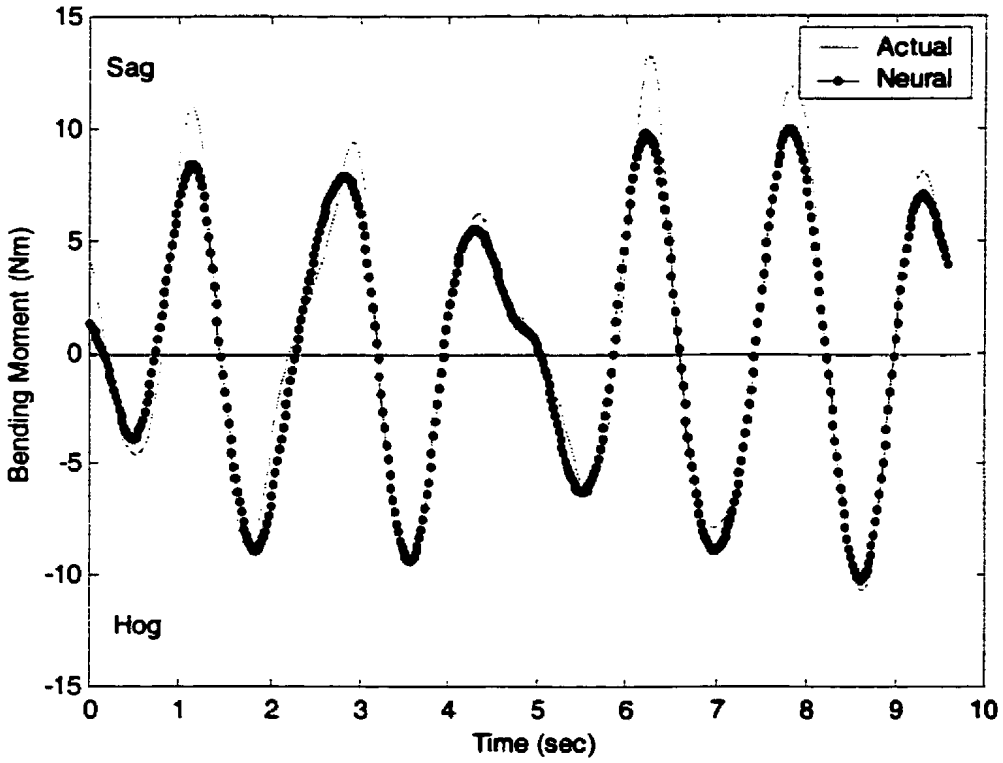

Figure 28: Estimation Example for Random Test Fj6h75a

5.3.3 Towing Tests in Head Waves

Due to the limited length of the tank, the time history from a single test run was not long enough for data analysis. Thus the data from seven test runs were joined together to form a single time history, and 10sec long correlation functions were computed for the network training. The training sample consisted of 480 points, and the final R^2 value is 0.995. The

training data and the results are plotted in Figure 29. The neural network weight values are presented in Table 26.

The training data shown in Figure 29 do not have good decay form. This is caused by discontinuity between different data segments. The accuracy of the neural network model may also be affected.

For each regular wave test, 48 equally spaced points were selected from a 10sec long time history and imported into the neural network for validation. The results are shown in Table 27 and Figure 30. The neural network model is valid only on a very narrow frequency range. This agrees with the narrow-band assumption adopted in the mathematical formulation. Another reason is the inaccuracies of the neural network model caused by discontinuity in joined time histories.

This network was also used for the real-time estimation of instantaneous bending moment in narrow-band waves. A typical example of 10sec long estimates of the JONSWAP random test is shown in Figure 31. There are 480 points estimated, and R^2 value is 0.819. The estimation result is not too bad even though the training data are not very good.

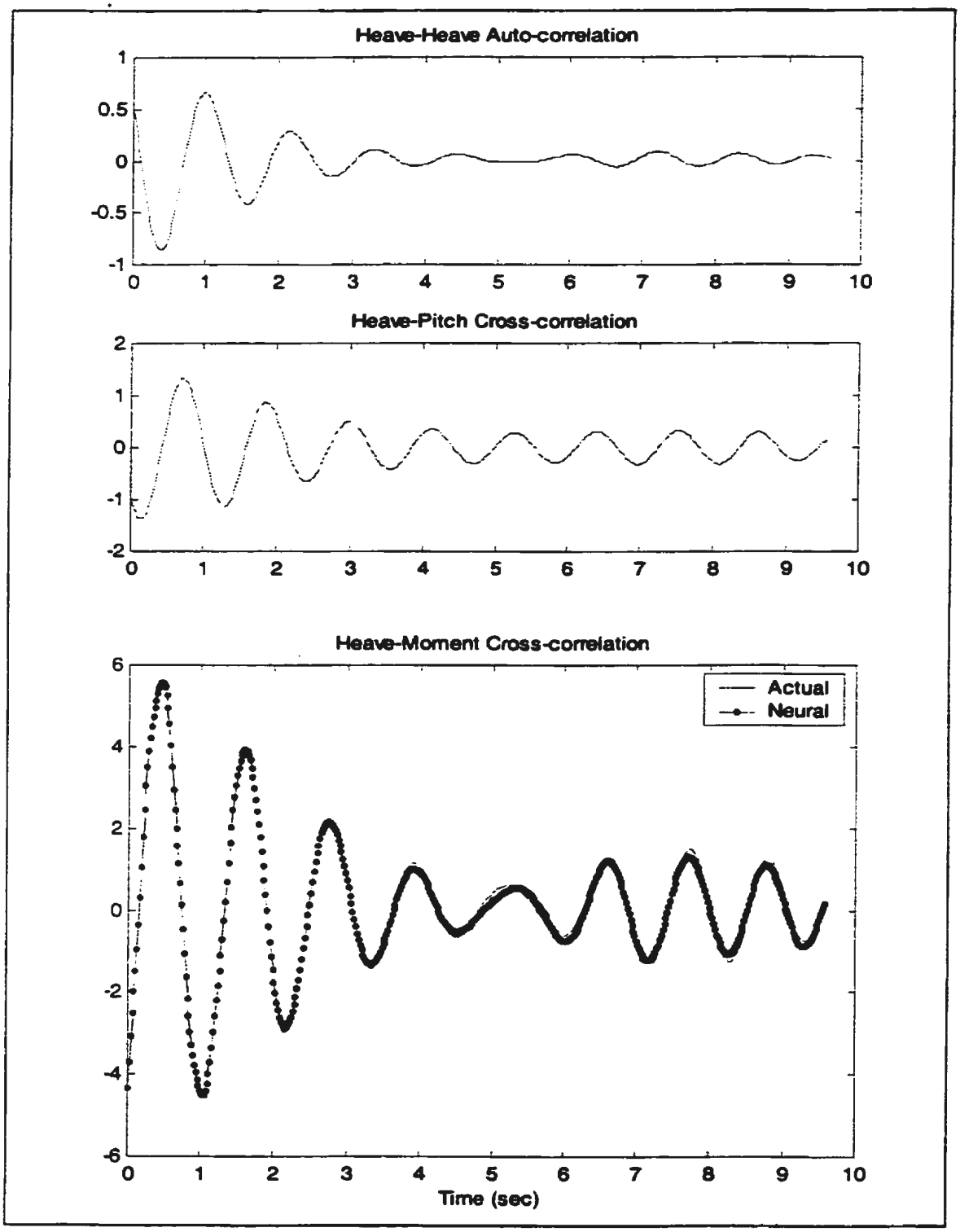

Figure 29: Training Results for Towing Tests in Head Waves

Table 26: Network Weight Values for Towing Tests in Head Waves

Hidden	Input							Output
	bias	1	2	3	4	5	6	
bias	/	/	/	/	/	/	/	-0.23
1	0.28	-0.20	0.32	0.44	0.04	-0.02	-0.23	0.13
2	0.52	-0.16	-0.18	-0.40	-0.35	0.17	-0.26	-0.48
3	0.33	0.29	0.29	0.61	0.26	-0.54	0.49	0.88
4	0.71	-0.03	0.19	-0.14	-0.06	0.18	-0.11	-0.19
5	0.60	-0.25	0.27	-0.11	-0.31	0.45	0.06	-0.41
6	0.49	0.06	0.30	0.21	0.26	0.17	0.11	0.10
7	0.42	-0.62	-0.84	2.00	-0.92	1.15	0.67	1.10
8	0.79	-0.02	-0.07	-0.12	0.22	0.08	0.11	0.00
9	0.72	0.10	-0.13	0.31	0.11	-0.42	0.38	0.52
10	0.68	0.03	-0.10	0.06	-0.15	-0.19	-0.05	0.09
11	0.31	-1.09	0.58	2.06	0.69	1.78	-0.85	0.92
12	0.67	0.11	-0.24	-0.25	-0.24	-0.20	0.34	0.00
13	0.62	0.19	-0.05	-0.19	0.26	0.11	-0.22	-0.14
14	0.19	-0.13	-0.43	-0.88	-0.09	0.54	0.22	-0.76
15	0.24	-0.23	-0.04	-0.93	-0.37	0.38	-0.04	-0.78
16	0.10	0.19	-0.22	0.08	0.26	-0.55	-0.18	0.388
17	0.22	0.34	-0.25	0.23	0.22	0.10	0.00	0.21
18	0.42	0.19	0.29	0.15	0.05	0.24	-0.15	-0.01
19	-0.05	0.41	-0.65	-0.85	-0.82	0.00	0.65	-0.78
20	0.25	0.57	0.04	0.48	-0.01	-0.40	0.31	0.67
21	0.85	-0.24	0.01	-0.04	0.08	0.30	0.11	-0.30
22	0.45	-0.40	0.05	-0.31	-0.17	0.21	-0.28	-0.52
23	0.37	-0.53	0.15	-0.24	-0.37	0.69	-0.06	-0.73
24	0.24	0.28	0.25	0.53	0.09	-0.61	-0.06	0.66

Table 27: Validation Results for Towing Tests (o.5m/sec)

Test Data	Test Conditions	Encounter Fre.	Wave Height	R^2
Training (JONSWAP)	Towing Tests (0.5m/s) in Regular Head Waves	Peak Fre. 0.840 Hz	Significant Height 7.5 cm	**0.995**
S5w3h6		0.333 Hz	6.0 cm	**0.000**
S5w4h6		0.450 Hz		**0.000**
S5w5h6		0.573 Hz		**0.000**
S5w6h6		0.702 Hz		**0.520**
S5w7h5		0.841 Hz	5.0 cm	**0.988**
S5w8h5		0.987 Hz		**0.724**
S5w9h5		0.135 Hz		**0.000**
S5w10h5		1.292 Hz		**0.977**
S5w11h5		1.454 Hz		**0.508**

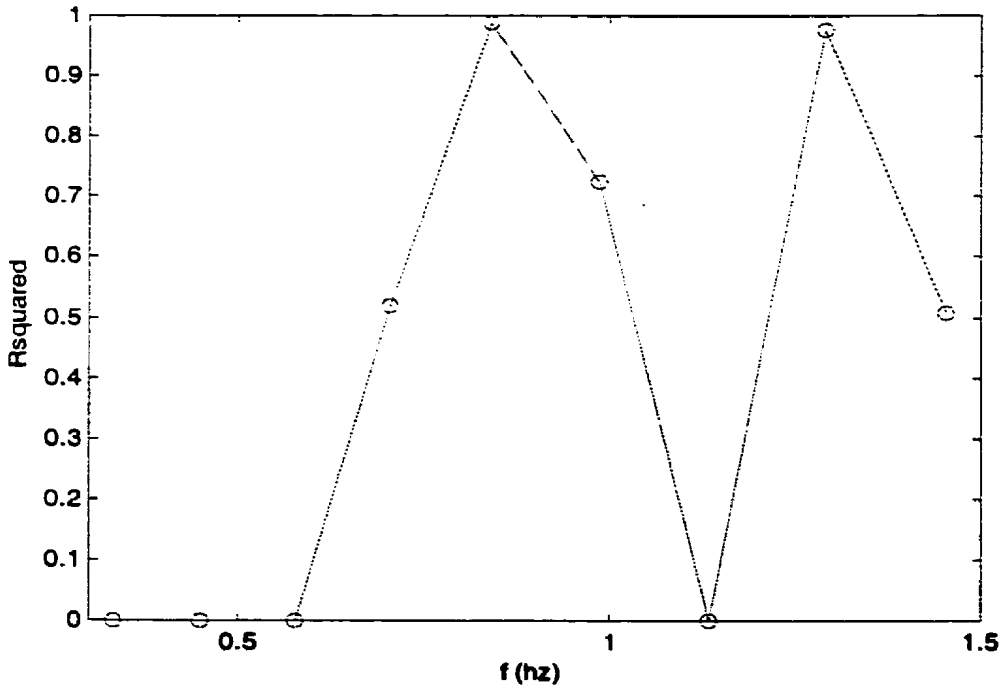

Figure 30: Validation Results for Regular Wave Towing Tests (0.5m/sec)

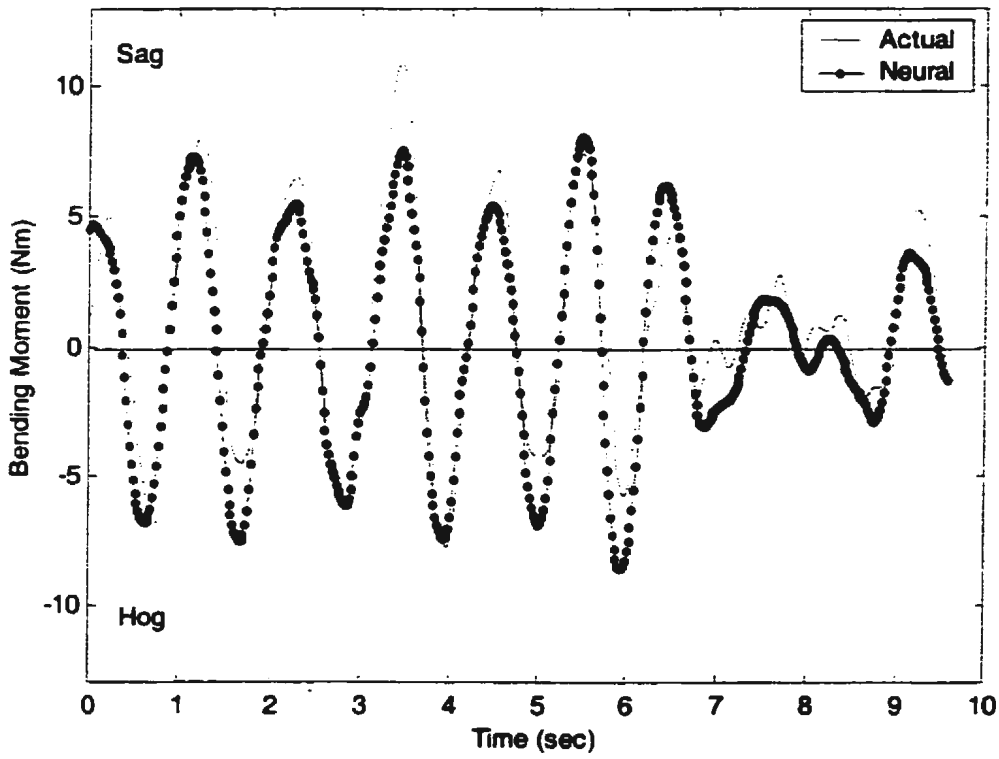

Figure 31: Estimation Example for JONSWAP Wave Towing Test (0.5m/sec)

6. Time-domain Simulations

6.1 Simulation Procedure

The single-hidden-layer MLP network is used in the present technique to learn the time-domain relationship between wave-induced bending moment and ship motions. In the previous sections, the auto- and cross-correlation functions were estimated from the experimental data for the training of neural networks. These correlation functions can also be estimated from the simulated time histories.

A time-domain simulation procedure based on frequency-domain solutions is used in this section. The frequency response functions are available from both theoretical computations and wave tank tests. The JONSWAP random waves were simulated using the following expression

$$S(f)=\frac{5H_s^{\,2}f_m^{\,4}}{16f^5\gamma^{\frac{1}{3}}}\exp(-\frac{5f_m^{\,4}}{4f^4})\gamma^{\exp\left[\frac{(f-f_m)^2}{2\sigma^2f_m^{\,2}}\right]} \qquad (61)$$

where the peak enhancement factor γ is 3.3, the shape parameter σ is 0.07 ($f<f_m$) or 0.09 ($f>f_m$), the significant height H_s is 7.5cm, and the peak frequency f_m is 0.6Hz. This is the wave spectrum used in the previous experiments. In the simulation process, the spectrum was divided into 51 equally spaced segments on a frequency range 0.4Hz to 0.9Hz. In each segment, the spectrum value was assumed to be constant over a frequency interval of 0.01Hz. This spectrum value was then used to generate one regular wave component. The elevation of each wave component is expressed as

$$\varsigma_i(t) = \sqrt{2S(f_i)\Delta f}\cos(2\pi f_i t + \varphi_i) \qquad (62)$$
$$\Delta f = 0.01hz$$

where the phase angle φ_i is a random variable with a uniform distribution.

Using the frequency response functions defined in equation (15), the harmonic heave, pitch and bending moment components were generated as

$$\begin{aligned} z_i(t) &= |H_z(\omega_i)|\varsigma_{ai}\cos[2\pi f_i t + \varphi_i + ang(H_z)] \\ \theta_i(t) &= |H_\theta(\omega_i)|\varsigma_{ai}\cos[2\pi f_i t + \varphi_i + ang(H_\theta)] \\ y_i(t) &= |H_y(\omega_i)|\varsigma_{ai}\cos[2\pi f_i t + \varphi_i + ang(H_y)] \end{aligned} \qquad (63)$$

The frequency response functions were computed and tested only at discrete frequency points 0.4Hz, 0.5Hz, 0.6Hz, 0.7Hz, 0.8Hz, 0.9Hz, 1.0Hz, and 1.1Hz. The values between these points were obtained using a linear interpolation method. The 450sec long random time histories of heave, pitch and bending moment were simulated by the superposition of 51 regular components,

$$\begin{aligned} z(t) &= \sum_{i=1}^{51} z_i(t) \\ \theta(t) &= \sum_{i=1}^{51} \theta_i(t) \\ y(t) &= \sum_{i=1}^{51} y_i(t) \end{aligned} \qquad (64)$$

The correlation functions were computed from the above simulated time histories using equation (53).

6.2 Simulation Results

For the stationary model in head waves, the frequency response functions were available from both strip theory computations and regular wave tests. The first simulation was based on the computed frequency response functions given in Table 19. The simulated correlation functions were compared with those estimated from the model test of J6h75a. This comparison is shown in Figure 32. There is a discrepancy in the heave-moment cross-correlation function. The second simulation was based on the experimental frequency response functions given in Table 14. The comparisons between the simulated correlation functions and the results of model test J6h75a are shown in Figure 33. There is an excellent agreement between the two sets of correlation functions.

Obviously, the discrepancy of the first simulation results shown in Figure 32 is caused by the inaccuracy of the computed frequency response functions. The second simulation results shown in Figure 33 have demonstrated the validity of this simulation method.

For the stationary model in following waves, the simulation was based on the experimental frequency response functions given in Table 16. The simulated correlation functions were compared with those estimated from the model test Fj6h75a. The comparison results are plotted in Figure 34. There is an excellent agreement between two sets of correlation functions.

For the towed model in head waves, the simulation was based on the experimental frequency response functions given in Table 18. The simulated correlation functions were compared with those estimated from the joined test data. The comparison results are plotted in Figure 35. There is a quite big discrepancy shown in the plot.

In Figure 35, both the experimental and the simulated correlation functions are not accurate enough. The experimental time history was formed by joining seven segments. Discontinuity between different segments must have some effects on the accuracy of the estimated correlation functions. In the simulation, the time history was generated using the frequency response functions. Since only values at 10 discrete frequency points were available, the values at other points were obtained by linear interpolations. For the towed model in head waves, the values of the frequency response functions have several big jumps between the 10 discrete points shown in Table 18. These jumps make it very difficult to obtain the accurate values from the linear interpolations. More values of the frequency response functions are needed, particularly within the range of jumps.

Generally, it is possible to obtain the correlation functions from the time-domain simulations. If the available frequency response functions are accurate and sufficient enough, the simulated correlation functions can be used for the training of neural networks. The calibrated neural network will provide a numerical estimation model.

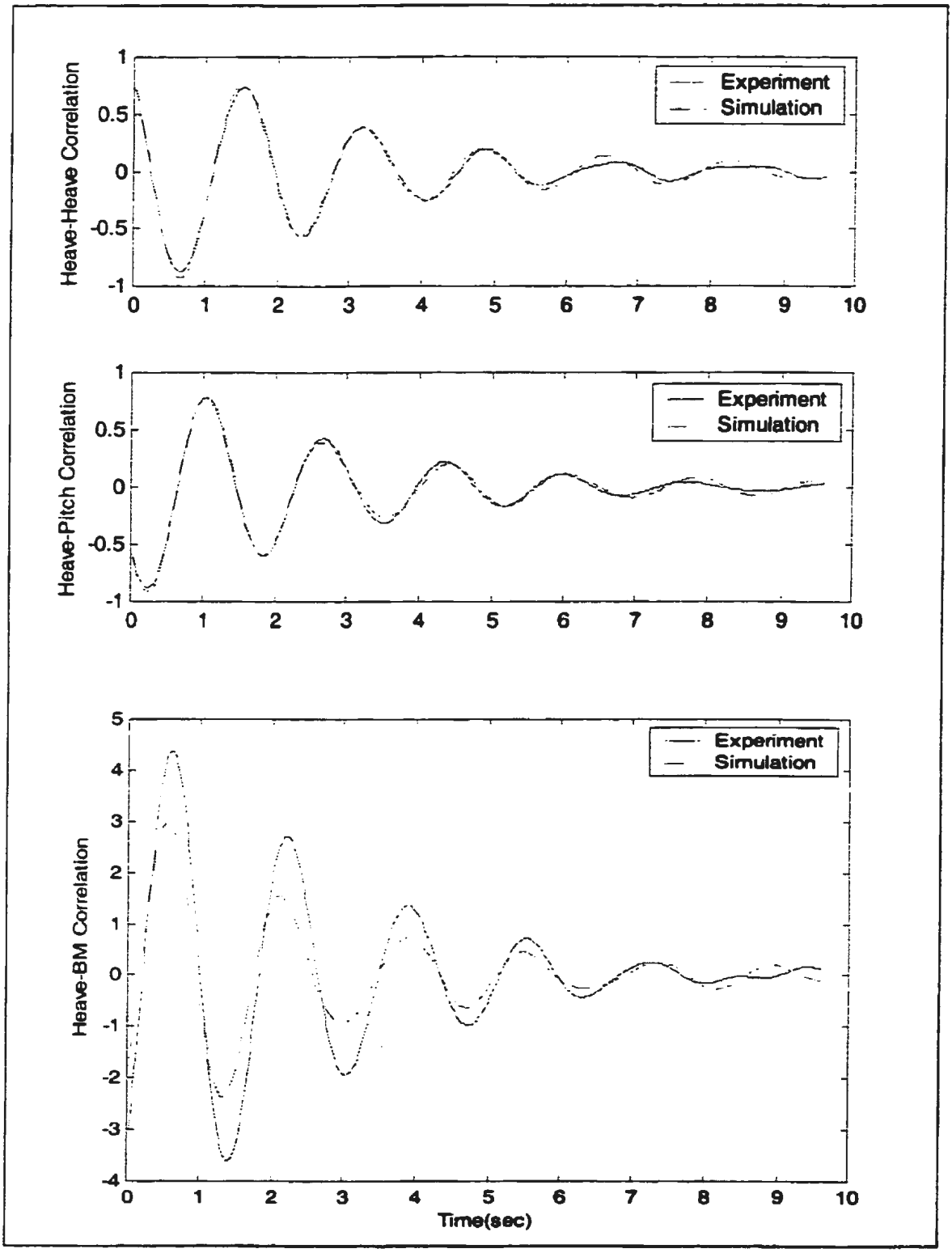

Figure 32: Simulation Results for Stationary Model in Head Waves (Computed Frequency Response Functions)

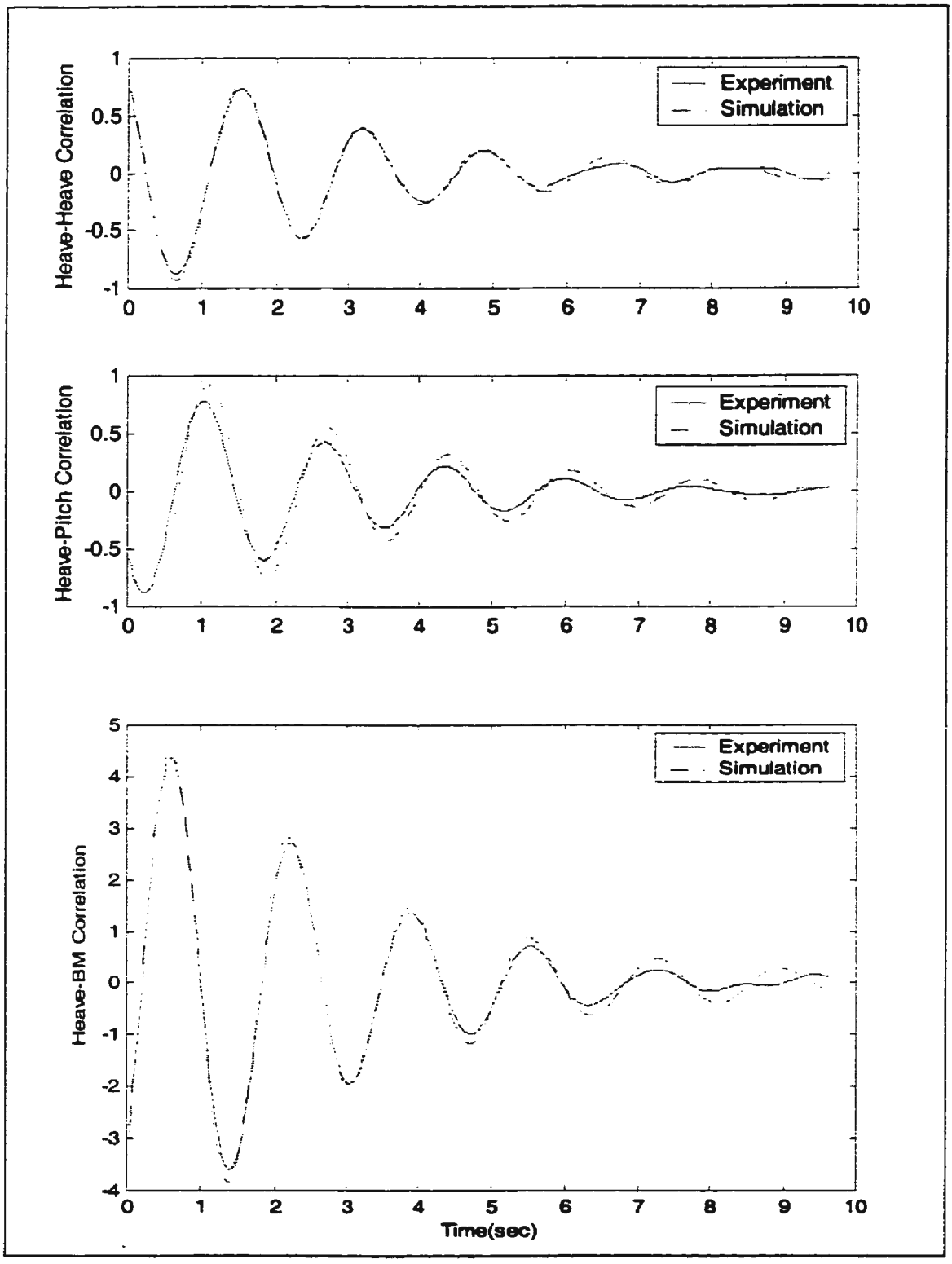

Figure 33: Simulation Results for Stationary Model in Head Waves (Experimental Frequency Response Functions)

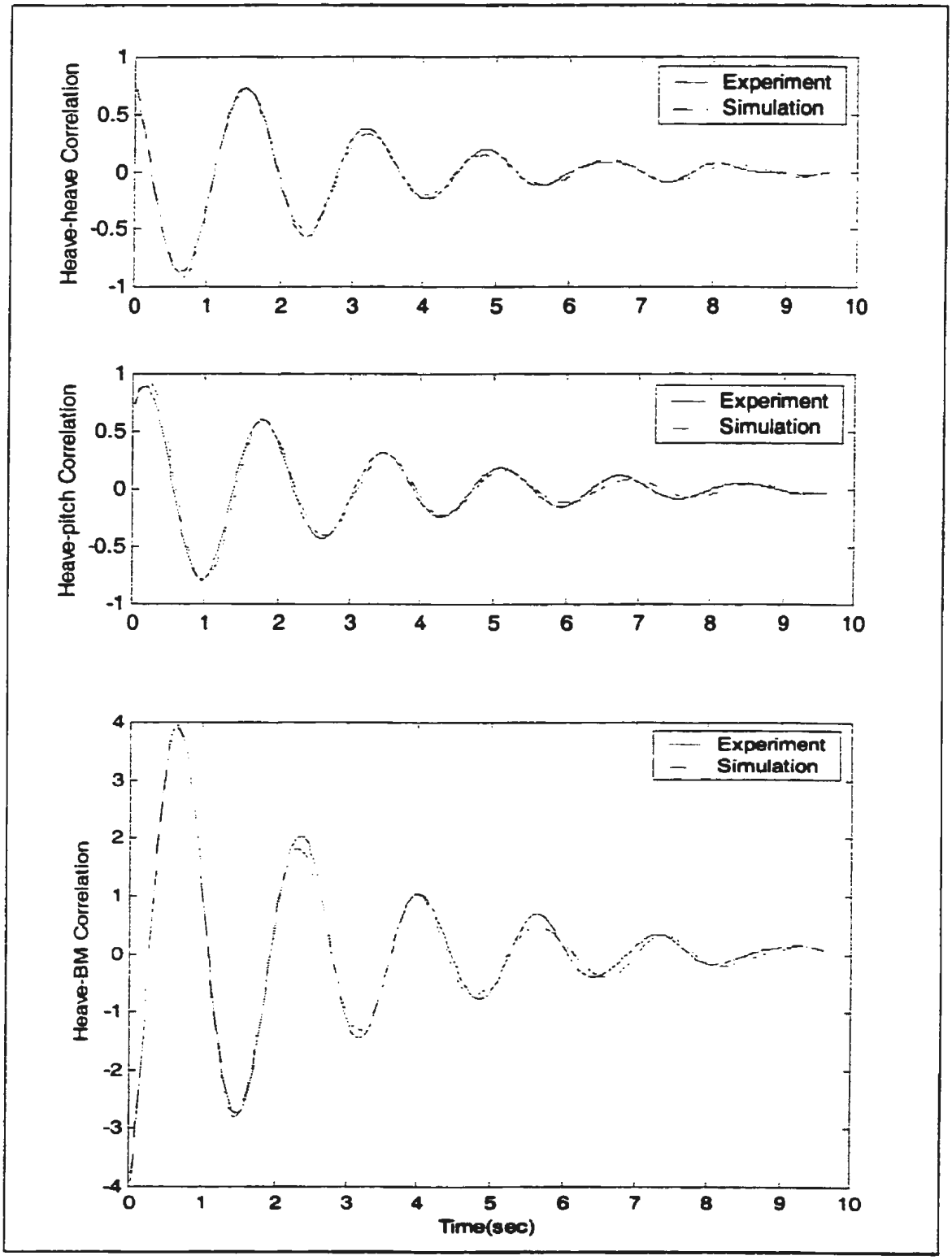

Figure 34: Simulation Results for Stationary Model in Following Waves

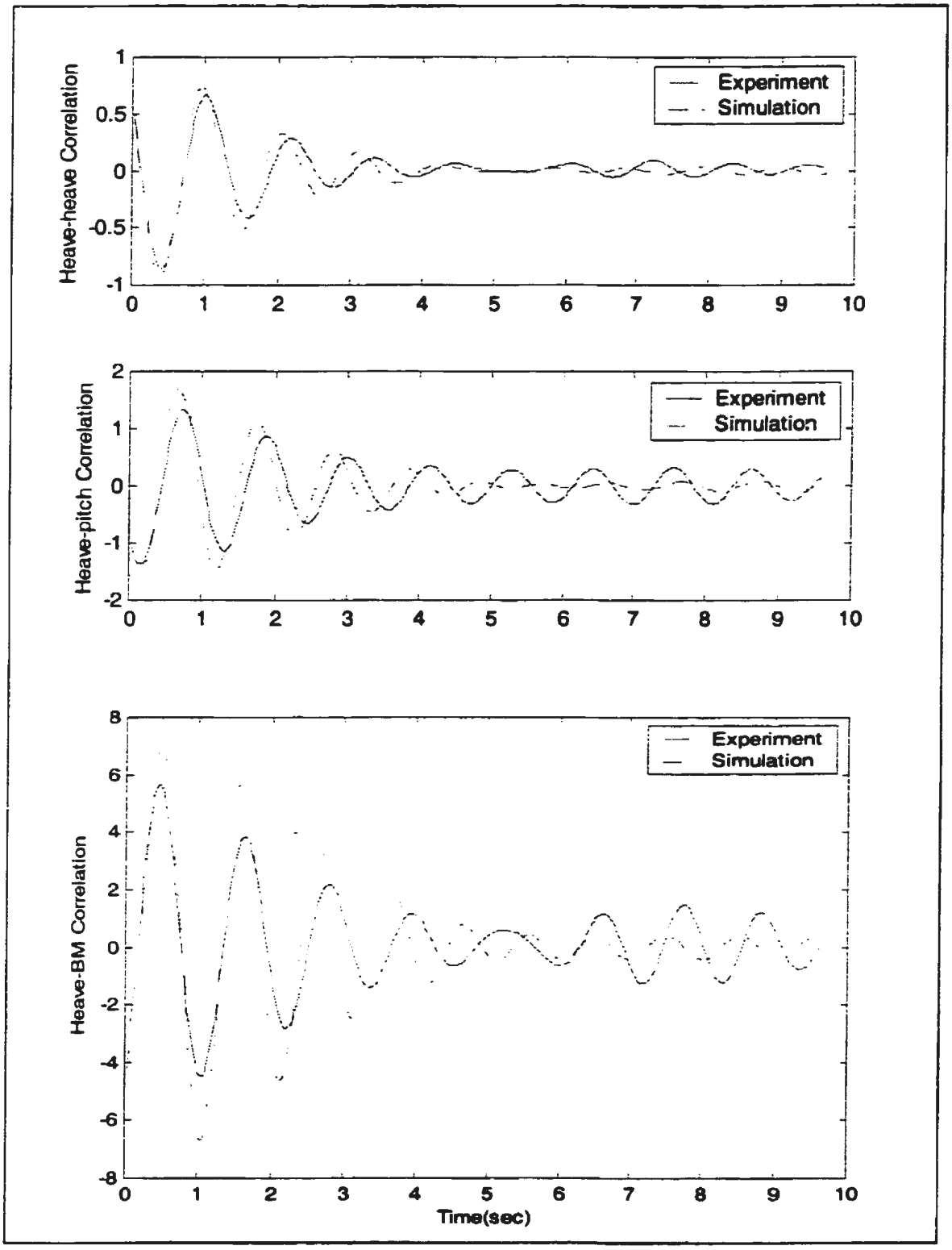

Figure 35: Simulation Results for Towed Model in Head Waves (0.5m/s)

7. Conclusions and Recommendations

In this work, a time-domain technique was developed for estimating the wave-induced vertical bending moment from coupled heave and pitch motions. The estimated values can be compared with those obtained from the strain measurements to ensure the validity of Hull Response Monitoring Systems (HRMS).

The frequency-domain analysis showed that the relationship between vertical bending moment and coupled heave and pitch motions can be expressed by their frequency response functions or Response Amplitude operators (RAOs). They could be obtained from both theoretical computations and ship model experiments. This frequency-domain relationship is suitable for the estimation of the statistical parameters of the bending moment, but not sufficient for the real-time estimation of the instantaneous values.

A time-domain relationship between the bending moment and the ship motions was formulated in this work through a Fourier transform of the frequency-domain model. It was shown that the wave-induced vertical bending moment can be approximated by a function of the heaving and pitching displacements, velocities, and accelerations in the time domain.

An efficient neural network technique was developed in this work to identify the time-domain model through a learning process. It was proved herein that one can use a set of auto- and cross-correlation functions of the bending moment and the ship motions to train the neural network. This should reduce the computational time significantly and improve

the accuracy of the training results. The calibrated neural network model is expected to produce accurate estimates of the instantaneous bending moment.

The experimental data of an "R-class Icebreaker" ship model were used to validate the methodology. For the stationary model in both head waves and following waves, the estimates from the neural networks had an excellent agreement with the bending moment values measured from the experiments. For the towing test in head waves, a single time history was formed by joining seven short segments. The accuracy of the estimated correlation functions was affected by discontinuity in joined time history. Even with this defect, the bending moment estimates from the neural network had a good agreement with the experimental values. A more sophisticated test facility should produce long enough time histories and better training data.

From the verification results shown in Figure 24, Figure 27, and Figure 30, the proposed technique has variable effective range for different test conditions. In the head sea stationary tests, the technique is effective across the range of the tested frequencies with a slight degeneration around the motion resonance frequency. In the following sea stationary tests, it is more effective in the narrow band around the spectral peak frequency with sharp declines in effectiveness outside this region. In the head sea towing tests, the verification results are not very good due to the inaccuracies of the training data. The above variation of the effective range is caused by the approximation given in equation (35) and (38). For the head sea stationary condition, this approximation is valid for a broad-band frequency range. For the following sea stationary condition, it is only valid in a narrow band around the spectral peak frequency. To get an accurate

estimation model effective over the whole frequency range, we have to develop a technique based on the general time-domain model given in equation (32). It is a dynamic model involving convolution integrals, and the recurrent neural networks are suitable tools.

Due to the limitations of the MUN test facility, the experimental data for other directional seas and multidirectional seas are not available in this work. More validations are needed in further research.

After the technique was validated by the experimental data, a simulation method was also investigated to produce the simulated correlation functions as the training data. This time-domain simulation was based on the frequency-domain solutions. The comparisons between the simulation results and the experimental results showed that the accuracy of the simulated correlation functions was greatly determined by the accuracy of the frequency-domain solutions. It is suggested that the proposed technique can be used in conjunction with a time-domain simulation package to provide a numerical estimation model.

The current work is based on a mathematical model for a rigid ship hull and a linear relationship between the wave-induced bending moment and the vertical ship motions. This poses certain limitations on the range of applicability. Since neural networks can easily model nonlinear systems, the present technique can be extended to include the nonlinear effects in the estimation. In this case the time-domain mathematical model needs to be reformulated.

In addition to rigid-body wave loads, both the springing and whipping bending moments are also related to ship motions. The whipping bending moment may be as large as the wave-induced bending moment, while the springing loads are found to be important for very long flexible ships. It is possible to estimate these vibratory loads from ship motion information. In this case, the mathematical formulation of the time-domain model involves consideration of the hull structural properties as well as the hydrodynamic forces.

References

Ashcroft, F.H. (1996). "Shipboard Monitoring", *SNAME Transactions*, Vol. 104, 1996, pp. 549-552.

Bendat, J.S. and Piersol, A.G. (1986). *Random Data Analysis and Measurement Procedures, 2nd Edition*, John Wiley & Sons, Inc.

Bhattacharyya, R. (1978). *Dynamics of Marine Vehicles*, John Wiley & Sons, Inc.

Broome, D.R. and Pittaras, A. (1990). "The Time Prediction of Ship Motions at Sea", *Offshore Technology Conference*, Houston, Texas, 6222, pp. 199-206.

Chung, J.C., Bien; Z.; Kim, Y.S. (1990). "A Note on Ship-Motion Prediction Based on Wave-Excitation Input Estimation", *IEEE Journal of Oceanic Engineering*, Vol. 15, pp. 244-250.

De Does, Ir.J.Ch. (1960). "Experimental Determination of Bending Moment for Three Models of Different Fullness in Regular Waves", *International Shipbuilding Progress*, Vol. 7, No. 68, April 1960, pp. 139-160.

Daidola, J.C. and Mishkevich, V. (1995). *Hydrodynamic Impact Loading on Displacement Ship Hulls*, Ship Structure Committee, Report SSC-385.

Frank, W. (1967). "Oscillation of Cylinders in or below the Free Surface of Deep Fluids", Report No. 2375, NSRDC, Washington, D.C.

Haddara, M.R. and Hinchey, M. (1995). "On the Use of Neural Network Techniques in the Analysis of Free Roll Decay Curves", *International Shipbuilding Progress*, Vol. 42, No. 430, pp. 166-178.

Haddara, M.R. and Xu, J. (1999). "Identification of Ship Coupled Heave-Pitch Motion Using Neural Networks", *Ocean Engineering*, Vol. 26, No.5, pp. 381-400.

Hardier, G. (1997). "Recurrent Neural Networks for Ship Modeling and Control", *Proceedings, Eleventh Ship Control Systems Symposium*, Southampton, United Kingdom, pp. 39-62.

Hermanski, G. (1993). *Model Experiments to Determine Wave Induced Bending Moment on a Great Lakes Bulk Carrier*, Institute for Marine Dynamics, National Research Council Canada, Report TR-1993-02.

Hua, J. and Palmquist, M. (1995). "Wave Estimation Through Ship Motion Measurement - A Practical Approach", *Proceedings, RINA International Conference on Seakeeping and Weather*, London, United Kingdom, Paper No. 6.

Hush, D.R. and Horne, B.G. (1993). "Progress in Supervised Neural Networks", *IEEE Signal Processing Magazine*, January 1993, pp.8-39.

Hutchison, B.L. (1990). "Seakeeping Studies: A Status Report", *SNAME Transactions*, Vol. 98, pp. 263-317.

Jacobs, W.R. (1958). "The Analytical Calculation of Ship Bending Moments in Regular Waves", *Journal of Ship Research*, June 1958, pp. 20-29.

Jensen, J.J. and Dogliani, M. (1996). "Wave-Induced Ship Hull Vibrations in Stochastic Seaways", *Marine Structure*, September 1996, pp. 353-387.

Kaplan, P. (1995). "Computer Simulation/Prediction of Ship Motions and Loads in a Seaway", *Proceedings, RINA International Conference on Seakeeping and Weather*, London, United Kingdom, Paper No. 17.

Korvin-Kroukovsky, B.V. and Jacobs, W.R. (1957). "Pitching and Heaving Motions of a Ship in Regular Waves", *SNAME Transactions*, Vol. 65, pp. 590-632.

Lacey, P. and Chen, H. (1995). "Improved Passage Planning Using Weather Forecasting, Maneuvering Guidance, and Instrumentation Feedback", *Marine Technology*, Vol. 32, No. 1, pp. 1-19.

Lewis, E.V. (1989). *Principles of Naval Architecture (Vol. III)*, SNAME.

Lewis, E.V. (1954). "Ship Model Tests to Determine Bending Moments in Waves", *SNAME Transactions*, Vol. 62, 1954, pp. 426-490.

Lewis, F.M. (1929). "The Inertia of the Water Surrounding a Vibrating Ship", *SNAME Transactions.*, Vol. 37, 1929.

Little, R.S. and Lewis, E.V. (1971). "A Statistical Study of Wave Induced Bending Moments on Large Oceangoing Tanker and Bulk Carriers", *SNAME Transactions*, Vol. 79, pp. 117-168.

Ljung, L. (1999). *System Identification Theory for the User, Second Edition*, Prentice Hall PTR.

McTaggart, K.; Datta, I., Stirling, A.; Gibson, S.; Glen, I. (1997). "Motions and Loads of a Hydroelastic Frigate Model in Severe Seas", *SNAME Transactons*, Vol. 105, 1997, pp. 427-453.

Mansour, A.E. (1990). *An Introduction to Structural Reliability Theory*, Ship Structure Committee, Report SSC-351.

Moan, T. and Berge, S. (1997). *Proceedings of the 13th International Ship and Offshore Structures Congress*, Trondheim, Norway.

Newman, J.N. and Sclavounos, P. (1980). "The Unified Theory of Ship Motions", *Proceedings, 13th Symposium on Naval Hydrodynamics*, Tokyo, Japan.

Ogilvie, T.F. (1964). "Recent Progress Toward the Understanding and Prediction of Ship Motions", *Proceedings, 5th Symposium on Naval Hydrodynamics*, ONR, Washington, D.C.

Oliver, J.C. (1990). *Advanced Methods for Ship Motion and Wave Load Prediction*, Ship Structure Committee, Report SSC-333.

Rice, S.O. (1944). "Mathematical Analysis of Random Noise", *Bell System Technical Journal*, Vol. 23 & Vol. 24.

Salvesen, N.; Tuck, E.O.; Faltinsen, O.M. (1970). "Ship Motions and Sea Loads", *SNAME Transactions*, Vol. 78, pp. 250-287.

Shi, W.B.; Thompson, P.A.; Hire, J.-C.L. (1996). "Thermal Stress and Hull Stress Monitoring", *SNAME Transactions*, Vol. 104, pp. 61-79.

Slaughter, S.B.; Cheung, M.C.; Sucharski, D.; Cowper, B. (1997). *State of the Art in Hull Response Monitoring Systems*, Ship Structure Committee, Report SSC-401.

St. Denis, M. and Pierson, W.J., Jr. (1953). "On the Motion of Ships in Confused Seas", *SNAME Transactions*, Vol. 61, 1953, pp. 280-357.

Tan, P.S.G.; Francescutto, A.; Cointe, R.; Hirayama, T.; Kishev, R.; McMreigh, K.; Naito, S.; Rutgersson, O.G.A.; Yum, D. (1996). *Seakeeping Committee Final Report and Recommendations to the 21st ITTC*, ITTC.

Tan, P.S.G.; McMreigh, K.; Bai, K.J.; Cointe, R.; Francescutto, A.; Kishev, R.; Lloyd, A.R.J.M.; Naito, S. (1993). *Seakeeping Committee Final Report and Recommendations to the 20th ITTC*, ITTC.

Thomson, W.T. (1981). *Theory of Vibration with Applications, 2nd Edition*, Prentice-Hall, Inc.

Tick, L.J. (1959). "Differential Equations With Frequency-Dependent Coefficients", *Journal of Ship Research*, Vol. 3, No. 2, pp. 45-46.

Troesch, A.W. (1984). "Wave-Induced Hull Vibrations: an Experimental and Theoretical Study", Journal of Ship Research, Vol. 28, No. 2, pp. 141-150.

Vulovich, R.; Hirayama, T.; Tohi, N.; Mizuno, H. (1989). "Characteristics of Hull Stresses Measured on a Large Containership in Rough Seas", *SNAME Transactions*, Vol. 97, 1989, pp. 397-428.

Wachnik, Z.G. and Schwartz, F.M. (1963). "Experimental Determination of Bending Moments and Shear Forces in a Multi-segmented Ship Model Moving in Waves", *International Shipbuilding Progress*, Vol. 10, No. 101, January, 1963.

Wilson, P.A. (1997). *Proceedings, Eleventh Ship Control Systems Symposium*, Southampton, United Kingdom.

Witmer, D.J. and Lewis, J.W. (1995). "The BP Oil Tanker Structural Monitoring System", *Marine Technology*, Vol. 32, No. 4, pp. 277-296.

Xu, J. and Haddara, M.R. (2001). "Estimation of Wave-Induced Ship Hull Bending Moment from Ship Motion Measurements", accepted for publication in *Marine Structures*.

Zhang, Y.; Hearn, G.E.; Sen, P. (1997). "Neural Network Approaches to a Class of Ship Control Problems", *Proceedings, Eleventh Ship Control Systems Symposium*, Southampton, United Kingdom, pp. 135-150.

Appendix I Strip Theory Computations

In this appendix, the coupled heave and pitch motions and the wave-induced midship bending moment of the rigid-body "R-class Icebreaker" ship model are solved in the frequency domain using a strip theory. The ship model is in head regular waves with zero forward speed.

From Lewis (1989) and Salvesen *et al.* (1970), the solution of the vertical ship motions in regular waves can be expressed by the complex amplitudes of the heave displacement z_a (positive upward) and the angular pitch displacement θ_a (positive bow downward) as

$$z_a = \frac{F_3 S - F_5 Q}{PS - QR} \qquad (65)$$
$$\theta_a = \frac{F_5 P - F_3 R}{PS - QR}$$

where

$$P = -\omega_e^2 (M + A_{33}) + C_{33} + i\omega_e B_{33} \qquad (66)$$
$$Q = -\omega_e^2 A_{35} + C_{35} + i\omega_e B_{35}$$
$$R = -\omega_e^2 A_{53} + C_{53} + i\omega_e B_{53}$$
$$S = -\omega_e^2 (I + A_{55}) + C_{55} + i\omega_e B_{55}$$

For zero forward speed and head sea conditions, the hydrodynamic coefficients in the above equations can be expressed in terms of the sectional coefficients in the following form:

$$A_{33} = \int_L a_{33} d\xi \qquad B_{33} = \int_L b_{33} d\xi \tag{67}$$

$$A_{35} = -\int_L \xi a_{33} d\xi \qquad B_{35} = -\int_L \xi b_{33} d\xi$$

$$A_{53} = -\int_L \xi a_{33} d\xi \qquad B_{53} = -\int_L \xi b_{33} d\xi$$

$$A_{55} = \int_L \xi^2 a_{33} d\xi \qquad B_{55} = \int_L \xi^2 b_{33} d\xi$$

$$C_{33} = \int_L c_{33} d\xi = \int_L \rho g B(\xi) d\xi$$

$$C_{35} = C_{53} = -\int_L \xi c_{33} d\xi = -\int_L \xi \rho g B(\xi) d\xi$$

$$C_{55} = \int_L \xi^2 c_{33} d\xi = \int_L \xi^2 \rho g B(\xi) d\xi$$

and the complex amplitudes of the wave excitation forces, F_3 and F_5, are simplified as

$$F_3 = \zeta_a \int_L e^{ik\xi} e^{-kT(\xi)} [c_{33} - \omega_0(\omega_e a_{33} - i b_{33})] d\xi \tag{68}$$

$$F_5 = \zeta_a \int_L e^{ik\xi} e^{-kT(\xi)} \{\xi [c_{33} - \omega_0(\omega_e a_{33} - i b_{33})]\} d\xi$$

For a rigid ship hull, the complex amplitude of the wave-induced midship bending moment (positive in sag direction) can be solved in terms of the resulting motions,

$$y_a(x_0) = (-A_y \omega_e^2 + C_y + i\omega_e B_y) z_a + (-D_y \omega_e^2 + H_y + i\omega_e E_y) \theta_a + y_\zeta \tag{69}$$

where

$$y_\zeta = \zeta_a \int_L e^{ik\xi} e^{-kT(\xi)} \{(\xi - x_0)[c_{33} - \omega_0(\omega_e a_{33} - i b_{33})]\} d\xi \tag{70}$$

and

$$A_y = -\int_{x_0}^{bow} (m_n + a_{33})(\xi - x_0)d\xi \qquad (71)$$

$$B_y = -\int_{x_0}^{bow} b_{33}(\xi - x_0)d\xi$$

$$C_y = -\int_{x_0}^{bow} c_{33}(\xi - x_0)d\xi$$

$$D_y = \int_{x_0}^{bow} (m_n + a_{33})\xi(\xi - x_0)d\xi$$

$$E_y = \int_{x_0}^{bow} b_{33}\xi(\xi - x_0)d\xi$$

$$H_y = \int_{x_0}^{bow} c_{33}\xi(\xi - x_0)d\xi$$

The two-dimensional sectional coefficients a_{33} and b_{33} can be determined using Lewis-form method. From Bhattacharyya (1978), the added mass coefficient a_{33} is calculated as

$$a_{33} = C\frac{\rho\pi B(\xi)^2}{8} \qquad (72)$$

where the coefficient C for Lewis-form sections is plotted in Figure 36 as a function of the draft/beam ratio (B/T), the area coefficient of the section (S/BT), as well as a function of the circular frequency of oscillation. Similarly, the sectional damping coefficient b_{33} is given by

$$b_{33} = \frac{\rho g^2 \overline{A}^2}{\omega_e^3} \qquad (73)$$

where the coefficient $\overline{A}$ for Lewis-form sections is plotted in Figure 37. It is assumed that the hydrodynamic coefficients for sections other than those of the mathematical Lewis form will not differ appreciably as long as the beam B, draft T, and the section area S are equal in both cases. The offsets of the full-scale "R-class Icebreaker" ship are presented in Table 28.

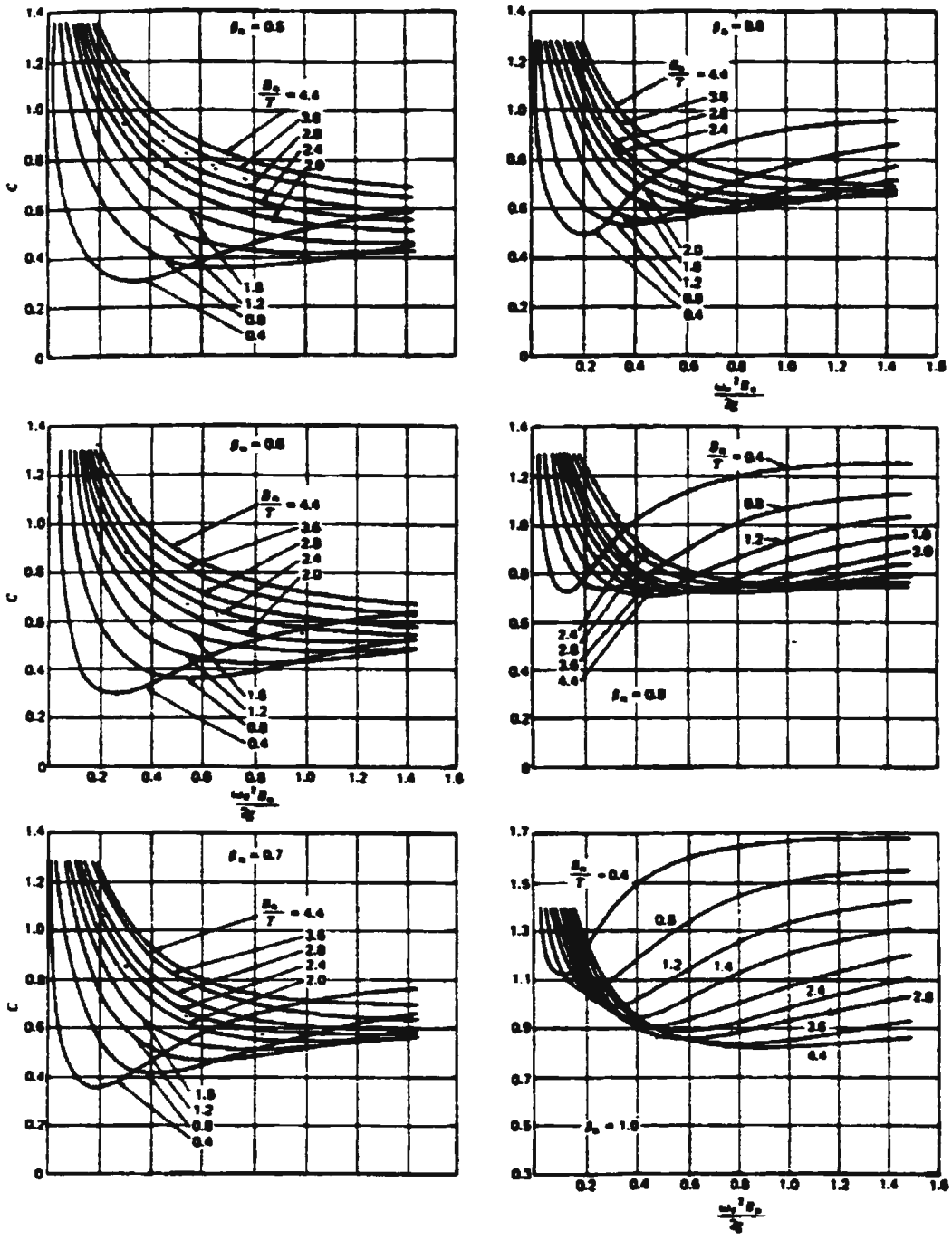

Figure 36: Coefficients C for Lewis-form Sections in Heaving Motion (Bhattacharyya, 1978)

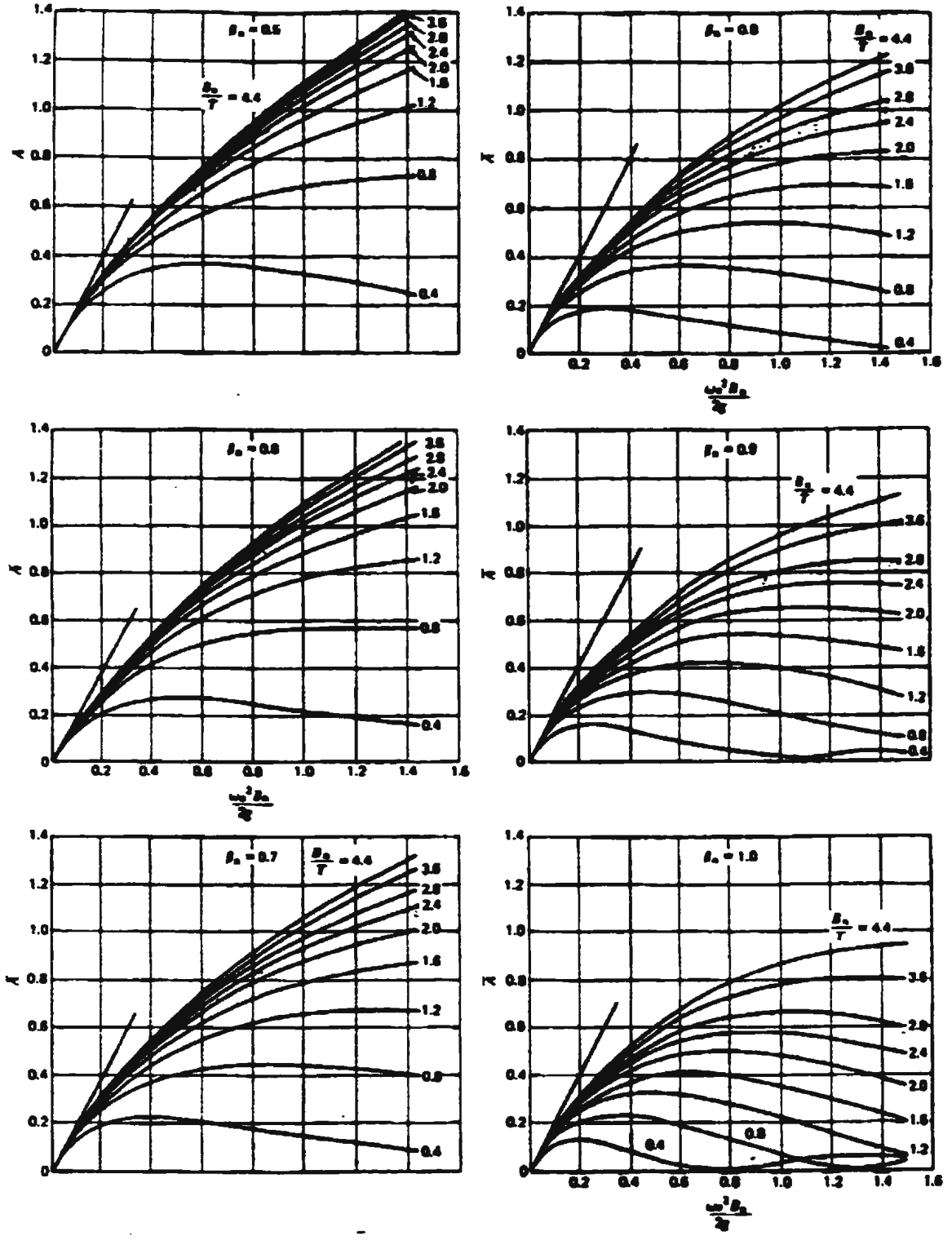

Figure 37: Coefficient $\overline{A}$ for Lewis-form Section in Heaving Motion (Bhattacharyya, 1978)

Table 28: Offsets Table of the Full-scale "R-class Icebreaker" Ship

	Offsets Table for Full-scale 'R-class Icebreaker'						
Z	Station 20	Station 19	Station 18	Station 17	Station 16	Station 15	Station 14
(m)	X=0.000m	4.326m	8.651m	12.977m	17.303m	21.629m	25.954m
0.250	0.000	0.000	0.000	0.000	0.000	0.000	0.000
0.250	0.000	0.255	0.510	1.008	2.569	4.159	4.392
0.500	0.000	0.255	0.583	1.364	3.392	5.121	6.218
0.750	0.000	0.255	0.664	1.708	3.960	5.710	6.797
1.000	0.000	0.255	0.755	2.045	4.407	6.157	7.194
1.250	0.000	0.255	0.853	2.377	4.783	6.498	7.496
1.500	0.000	0.255	0.957	2.703	5.112	6.775	7.737
1.750	0.000	0.255	1.067	3.024	5.408	7.008	7.930
2.000	0.000	0.255	1.186	3.342	5.682	7.207	8.087
2.250	0.000	0.255	1.317	3.659	5.937	7.384	8.220
2.500	0.000	0.255	1.462	3.973	6.179	7.544	8.339
2.750	0.000	0.255	1.621	4.282	6.408	7.692	8.443
3.000	0.000	0.255	1.795	4.583	6.626	7.831	8.535
3.250	0.000	0.259	1.991	4.873	6.832	7.960	8.615
3.500	0.000	0.267	2.215	5.154	7.028	8.082	8.687
3.750	0.000	0.278	2.476	5.425	7.209	8.194	8.753
4.000	0.000	0.295	2.787	5.687	7.376	8.298	8.813
4.250	0.000	0.312	3.154	5.941	7.528	8.393	8.870
4.500	0.000	0.366	3.567	6.184	7.668	8.479	8.924
4.750	0.000	0.747	3.994	6.414	7.796	8.557	8.977
5.000	0.000	1.308	4.414	6.632	7.915	8.629	9.028
5.250	0.000	1.849	4.808	6.838	8.027	8.695	9.076
5.500	0.000	2.372	5.172	7.033	8.131	8.756	9.122
5.750	0.000	2.888	5.506	7.216	8.228	8.813	9.166
6.000	0.000	3.379	5.812	7.387	8.319	8.866	9.209
6.250	0.794	3.828	6.090	7.542	8.403	8.916	9.248
6.500	1.322	4.232	6.339	7.682	8.482	8.963	9.285
6.750	1.814	4.591	6.562	7.805	8.555	9.007	9.321
7.000	2.264	4.910	6.757	7.916	8.623	9.048	9.356
7.250	2.665	5.191	6.928	8.015	8.686	9.088	9.390
7.500	3.025	5.436	7.076	8.104	8.743	9.127	9.423
7.750	3.350	5.648	7.203	8.185	8.794	9.164	9.442
8.000	3.640	5.832	7.313	8.258	8.843	9.185	9.442
8.250	3.897	5.990	7.410	8.324	8.887	9.205	9.439
8.500	4.121	6.126	7.497	8.382	8.924	9.222	9.430
8.750	4.312	6.243	7.575	8.435	8.960	9.236	9.422
9.000	4.472	6.345	7.644	8.482	8.991	9.248	9.413
9.250	4.603	6.431	7.704	8.525	9.017	9.256	9.404
9.500	4.709	6.504	7.756	8.565	9.036	9.261	9.395
9.750	4.793	6.566	7.802	8.600	9.051	9.264	9.386
10.000	4.860	6.619	7.841	8.626	9.061	9.267	9.377
10.250	4.913	6.666	7.876	8.642	9.070	9.270	9.369
10.500	4.960	6.709	7.909	8.654	9.077	9.273	9.360

	Offsets Table for Full-scale 'R-class Icebreaker'						
Z	Station 13	Station 12	Station 11	Station 10	Station 9	Station 8	Station 7
(m)	30.280m	34.606m	38.931m	43.257m	47.513m	51.750m	55.988m
0.250	0.000	0.000	0.000	0.000	0.000	0.000	0.000
0.250	4.392	4.392	4.392	4.392	4.392	4.392	4.392
0.500	6.937	7.262	7.292	7.292	7.309	7.155	6.666
0.750	7.472	7.797	7.843	7.843	7.851	7.711	7.297
1.000	7.822	8.125	8.188	8.188	8.175	8.048	7.701
1.250	8.078	8.370	8.450	8.450	8.420	8.295	7.982
1.500	8.286	8.563	8.654	8.654	8.606	8.479	8.195
1.750	8.456	8.723	8.812	8.812	8.752	8.629	8.375
2.000	8.595	8.854	8.933	8.933	8.870	8.754	8.526
2.250	8.711	8.957	9.025	9.025	8.964	8.858	8.655
2.500	8.812	9.034	9.091	9.091	9.038	8.945	8.761
2.750	8.899	9.092	9.123	9.123	9.104	9.015	8.846
3.000	8.971	9.135	9.148	9.148	9.148	9.075	8.924
3.250	9.028	9.171	9.172	9.172	9.172	9.131	8.999
3.500	9.073	9.197	9.197	9.197	9.197	9.181	9.056
3.750	9.111	9.222	9.222	9.222	9.222	9.219	9.106
4.000	9.145	9.247	9.247	9.247	9.247	9.248	9.151
4.250	9.178	9.271	9.271	9.271	9.271	9.269	9.187
4.500	9.212	9.296	9.296	9.296	9.296	9.296	9.224
4.750	9.248	9.321	9.321	9.321	9.321	9.321	9.261
5.000	9.284	9.346	9.346	9.346	9.346	9.346	9.302
5.250	9.318	9.370	9.370	9.370	9.370	9.370	9.334
5.500	9.351	9.395	9.395	9.395	9.395	9.395	9.362
5.750	9.383	9.420	9.420	9.420	9.420	9.420	9.396
6.000	9.412	9.445	9.445	9.445	9.445	9.445	9.429
6.250	9.440	9.469	9.469	9.469	9.469	9.469	9.458
6.500	9.468	9.494	9.494	9.494	9.494	9.494	9.480
6.750	9.495	9.519	9.519	9.519	9.519	9.519	9.506
7.000	9.522	9.544	9.544	9.544	9.544	9.544	9.535
7.250	9.549	9.568	9.568	9.568	9.568	9.568	9.563
7.500	9.576	9.593	9.593	9.593	9.593	9.593	9.591
7.750	9.585	9.600	9.600	9.600	9.600	9.600	9.599
8.000	9.585	9.600	9.600	9.600	9.600	9.600	9.599
8.250	9.579	9.594	9.594	9.594	9.594	9.594	9.594
8.500	9.562	9.576	9.576	9.576	9.576	9.576	9.576
8.750	9.545	9.558	9.558	9.558	9.558	9.558	9.558
9.000	9.528	9.541	9.541	9.541	9.541	9.541	9.539
9.250	9.511	9.523	9.523	9.523	9.523	9.523	9.521
9.500	9.494	9.505	9.505	9.505	9.505	9.505	9.503
9.750	9.477	9.487	9.487	9.487	9.487	9.487	9.485
10.000	9.460	9.469	9.469	9.469	9.469	9.469	9.467
10.250	9.443	9.451	9.451	9.451	9.451	9.451	9.449
10.500	9.426	9.433	9.433	9.433	9.433	9.433	9.431

	Offsets Table for Full-scale 'R-class Icebreaker'						
Z	Station 6	Station 5	Station 4	Station 3	Station 2	Station 1	Station 0
(m)	60.255m	64.463m	68.700m	72.938m	77.175m	81.413m	85.650m
0.250	0.000	0.000	0.000	0.000	0.000	0.000	0.000
0.250	4.371	3.677	2.664	1.576	0.508	0.000	0.000
0.500	5.826	4.748	3.526	2.160	0.694	0.000	0.000
0.750	6.565	5.508	4.187	2.638	0.911	0.000	0.000
1.000	7.059	6.053	4.712	3.048	1.135	0.000	0.000
1.250	7.405	6.462	5.144	3.412	1.360	0.000	0.000
1.500	7.672	6.791	5.510	3.745	1.587	0.000	0.000
1.750	7.895	7.070	5.828	4.060	1.819	0.000	0.000
2.000	8.087	7.311	6.111	4.353	2.051	0.000	0.000
2.250	8.252	7.520	6.365	4.639	2.288	0.000	0.000
2.500	8.391	7.705	6.596	4.908	2.527	0.000	0.000
2.750	8.509	7.873	6.813	5.153	2.775	0.000	0.000
3.000	8.615	8.019	7.009	5.398	3.017	0.095	0.000
3.250	8.708	8.149	7.190	5.632	3.257	0.289	0.000
3.500	8.793	8.267	7.358	5.853	3.505	0.508	0.000
3.750	8.870	8.379	7.514	6.061	3.759	0.750	0.000
4.000	8.939	8.485	7.661	6.258	4.018	1.031	0.000
4.250	9.000	8.582	7.798	6.444	4.281	1.351	0.000
4.500	9.056	8.671	7.926	6.620	4.543	1.691	0.000
4.750	9.107	8.753	8.044	6.787	4.800	2.035	0.000
5.000	9.156	8.828	8.154	6.946	5.046	2.380	0.000
5.250	9.202	8.895	8.256	7.098	5.278	2.717	0.000
5.500	9.247	8.958	8.350	7.243	5.494	3.035	0.104
5.750	9.288	9.019	8.438	7.379	5.693	3.337	0.297
6.000	9.327	9.072	8.518	7.509	5.879	3.623	0.748
6.250	9.364	9.119	8.592	7.630	6.055	3.889	1.155
6.500	9.399	9.164	8.661	7.744	6.227	4.145	1.602
6.750	9.431	9.205	8.724	7.849	6.396	4.385	1.957
7.000	9.462	9.240	8.782	7.948	6.559	4.614	2.267
7.250	9.491	9.270	8.835	8.041	6.716	4.832	2.546
7.500	9.518	9.297	8.883	8.129	6.863	5.041	2.804
7.750	9.548	9.320	8.928	8.212	7.003	5.242	3.041
8.000	9.551	9.339	8.970	8.290	7.135	5.433	3.259
8.250	9.551	9.353	9.007	8.364	7.261	5.614	3.461
8.500	9.536	9.363	9.042	8.433	7.381	5.787	3.651
8.750	9.520	9.368	9.074	8.497	7.496	5.950	3.830
9.000	9.504	9.369	9.102	8.557	7.606	6.104	3.998
9.250	9.488	9.370	9.128	8.611	7.710	6.248	4.158
9.500	9.473	9.368	9.149	8.662	7.806	6.383	4.309
9.750	9.457	9.364	9.166	8.709	7.893	6.510	4.450
10.000	9.441	9.360	9.180	8.754	7.974	6.627	4.583
10.250	9.426	9.355	9.191	8.797	8.049	6.735	4.711
10.500	9.410	9.351	9.202	8.840	8.123	6.837	4.835

The sectional geometric data of the full-scale "R-class Icebreaker" ship are calculated from the offset values and listed in Table 29. The strip theory computations for a 1:40 scale ship model in head wave conditions are performed using the scaled geometric data. The computational details at the frequency point 0.685Hz are presented in Table 30.

Table 29: Sectional Data of the Full-scale "R-class Icebreaker" Ship

Full Scale Ship Data							
LBP(m)=	87.93		Midship(m)	43.965		LCB(m)=	43.635
FP Draft(m)	6.71		Mid Draft(m)	6.93		AP Draft(m)	7.16
Station	From AP	Beam	Draft	Area	From LCB		
	X(m)	Bn(m)	Tn(m)	Sn(m)	Xc(m)	dX(m)	
FP	85.650	4.520	1.562	3.244	42.015		
1	81.413	9.200	4.003	18.514	37.778	4.237	
2	77.175	13.120	6.746	48.912	33.540	4.238	
3	72.938	15.900	6.769	75.992	29.303	4.237	
4	68.700	17.600	6.792	95.128	25.065	4.238	
5	64.463	18.500	6.815	107.790	20.828	4.237	
6	60.225	18.940	6.838	115.790	16.590	4.238	
7	55.988	19.100	6.861	120.344	12.353	4.237	
8	51.750	19.100	6.884	122.788	8.115	4.238	
9	47.513	19.100	6.907	123.908	3.878	4.237	
10	43.257	19.120	6.930	124.506	-0.378	4.256	
11	38.931	19.120	6.953	124.946	-4.704	4.326	
12	34.606	19.120	6.976	125.060	-9.029	4.325	
13	30.280	19.100	6.999	123.504	-13.355	4.326	
14	25.954	18.800	7.022	118.704	-17.681	4.326	
15	21.629	18.200	7.045	110.472	-22.006	4.325	
16	17.303	17.400	7.068	96.042	-26.332	4.326	
17	12.977	16.100	7.091	73.124	-30.658	4.326	
18	8.651	14.000	7.114	45.396	-34.984	4.326	
19	4.326	10.620	3.387	18.228	-39.309	4.325	
AP	0.000	6.000	1.381	4.654	-43.635	4.326	

Table 30: Strip Theory Computations for 1:40 "R-class Icebreaker" Model

		Ship Model Calculation				Wave Frequency (hz)			0.685	(rad/sec)	4.304
		Model Speed (m/sec)		0		Encounter Frequency (hz)			0.685	(rad/sec)	4.304
Station	xc(m)	Bn(m)	Tn(m)	Sn(m^2)		Sn/(Bn*Tn)	Bn/Tn	F(f,Bn)	C	A	Simpson
FP	1.050	0.113	0.039	0.002		0.459	2.894	0.107	1.4	0.2	1
1	0.944	0.230	0.100	0.012		0.503	2.298	0.217	1	0.32	4
2	0.839	0.328	0.169	0.031		0.553	1.945	0.310	0.88	0.43	2
3	0.733	0.398	0.169	0.047		0.706	2.349	0.376	0.77	0.5	4
4	0.627	0.440	0.170	0.059		0.796	2.591	0.416	0.76	0.58	2
5	0.521	0.463	0.170	0.067		0.855	2.715	0.437	0.82	0.59	4
6	0.415	0.474	.0.171	0.072		0.894	2.770	0.447	0.86	0.53	2
7	0.309	0.478	0.172	0.075		0.918	2.784	0.451	0.86	0.52	4
8	0.203	0.478	0.172	0.077		0.934	2.775	0.451	0.86	0.5	2
9	0.097	0.478	0.173	0.077		0.939	2.765	0.451	0.86	0.5	4
10	-0.009	0.478	0.173	0.078		0.940	2.759	0.452	0.86	0.5	2
11	-0.118	0.478	0.174	0.078		0.940	2.750	0.452	0.86	0.5	4
12	-0.226	0.478	0.174	0.078		0.938	2.741	0.452	0.86	0.5	2
13	-0.334	0.478	0.175	0.077		0.924	2.729	0.451	0.86	0.5	4
14	-0.442	0.470	0.176	0.074		0.899	2.677	0.444	0.86	0.52	2
15	-0.550	0.455	0.176	0.069		0.862	2.583	0.430	0.79	0.56	4
16	-0.658	0.435	0.177	0.060		0.781	2.462	0.411	0.73	0.53	2
17	-0.766	0.403	0.177	0.046		0.641	2.270	0.380	0.73	0.51	4
18	-0.875	0.350	0.178	0.028		0.456	1.968	0.331	0.9	0.45	2
19	-0.983	0.266	0.085	0.011		0.507	3.136	0.251	1.15	0.41	4
AP	-1.091	0.150	0.035	0.003		0.562	4.345	0.142	1.4	0.24	1

$F(f, B_n) = \frac{\omega_e^2 B_n}{2g}$; C is from Figure 36; A is from Figure 37.

Station	a33(kg/m)	M1(a33)	M2(a33)	b33(kg/ms)	M1(b33)	M2(b33)	cn(kg/mss)	M1(cn)	M2(cn)	mn(kg/m)	M2(mn)
FP	7.020	7.374	7.745	48.188	50.616	53.165	1107.4	1163.2	1221.78	11.449	12.631
1	20.773	19.619	18.529	123.361	116.509	110.037	2254	2128.8	2010.54	11.449	10.212
2	37.177	31.173	26.139	222.749	186.775	156.611	3214.4	2695.3	2259.99	11.449	8.049
3	47.776	35.000	25.640	301.175	220.633	161.631	3895.5	2853.7	2090.58	11.449	6.144
4	57.778	36.205	22.687	405.261	253.947	159.129	4312	2702.0	1693.15	96.376	37.843
5	68.879	35.865	18.675	419.356	218.359	113.699	4532.5	2360.1	1228.89	145.603	39.477
6	75.716	31.403	13.024	338.401	140.352	58.211	4640.3	1924.6	798.21	107.465	18.486
7	77.000	23.780	7.344	325.751	100.600	31.068	4679.5	1445.1	446.30	49.444	4.716
8	77.000	15.621	3.169	301.175	61.101	12.396	4679.5	949.4	192.60	60.049	2.471
9	77.000	7.465	0.724	301.175	29.199	2.831	4679.5	453.7	43.98	48.916	0.460
10	77.162	-0.729	0.007	301.175	-2.846	0.027	4684.4	-44.3	0.42	47.628	0.004
11	77.162	-9.074	1.067	301.175	-35.418	4.165	4684.4	-550.9	64.78	116.959	1.618
12	77.162	-17.417	3.932	301.175	-67.983	15.345	4684.4	-1057.4	238.68	64.393	3.281
13	77.000	-25.708	8.583	301.175	-100.555	33.573	4679.5	-1562.4	521.64	81.693	9.107
14	74.600	-32.975	14.576	325.751	-143.990	63.647	4606	-2036.0	899.95	82.893	16.196
15	64.224	-35.333	19.438	377.794	-207.843	114.345	4459	-2453.1	1349.58	82.893	25.089
16	54.244	-35.709	23.507	338.401	-222.769	146.649	4263	-2806.3	1847.41	28.278	12.255
17	46.441	-35.595	27.282	313.343	-240.162	184.072	3944.5	-3023.3	2317.18	31.037	18.233
18	43.294	-37.865	33.117	243.952	-213.360	186.605	3430	-2999.9	2623.69	11.449	8.757
19	31.833	-31.283	30.742	202.510	-199.012	195.574	2601.9	-2557.0	2512.78	11.449	11.056
AP	12.370	-13.494	14.720	69.391	-75.697	82.576	1470	-1603.6	1749.31	11.449	13.624
										m(kg)	Iyy(kgmm
SUM	125.547	-3.130	33.344	625.626	-15.458	197.485	8604.462	-192.824	2654.466	121.496	26.585
	A33	B33	A35	B35	A53	B53	A55	B55	C33	C35(C53)	C55
	125.547	625.626	3.130	15.458	3.130	15.458	33.344	197.485	8604.462	192.824	2654.466

$a_{33} = C\frac{\rho\pi B_n^{\ 2}}{8}$; $b_{33} = \frac{\rho g^2 \overline{A}^2}{\omega_e^{\ 3}}$; $c_n = \rho g B_n$; m_n is weight distribution;

M_1 and M_2 are first and second moments, respectively.

Station	T*(x)	exp(-k*T)	k*xc	cos(k*xc)	sin(k*xc)	f3(R)	f3(I)	h3(R)	h3(I)	f3+h3(R)	f3+h3(I)
FP	0.018	0.967	1.985	-0.403	0.915	-431.151	979.808	-132.873	-195.795	-564.024	784.01
1	0.050	0.909	1.785	-0.213	0.977	-435.916	2002.645	-397.307	-444.556	-833.223	1558.09
2	0.093	0.838	1.585	-0.014	1.000	-37.917	2694.952	-795.634	-588.665	-833.551	2106.29
3	0.119	0.798	1.385	0.185	0.983	575.197	3054.320	-1146.99	-502.476	-571.789	2551.84
4	0.135	0.775	1.184	0.377	0.926	1258.737	3093.836	-1563.86	-258.737	-305.126	2835.10
5	0.146	0.759	0.984	0.554	0.833	1905.105	2866.290	-1677.63	-48.214	227.477	2818.08
6	0.153	0.749	0.784	0.708	0.706	2461.553	2454.321	-1514.31	30.796	947.244	2485.12
7	0.158	0.743	0.584	0.834	0.551	2899.229	1914.919	-1457.38	284.956	1441.845	2199.87
8	0.161	0.738	0.383	0.927	0.374	3202.785	1292.093	-1334.1	493.343	1868.684	1785.44
9	0.162	0.736	0.183	0.983	0.182	3386.378	627.584	-1205.99	746.737	2180.387	1374.32
10	0.163	0.735	-0.018	1.000	-0.018	3443.111	-61.506	-1033.52	971.505	2409.588	910.00
11	0.163	0.734	-0.222	0.975	-0.220	3355.288	-758.337	-813.908	1159.817	2541.380	401.48
12	0.164	0.734	-0.427	0.910	-0.414	3130.676	-1423.109	-561.427	1300.496	2569.248	-122.61
13	0.162	0.737	-0.631	0.807	-0.590	2783.501	-2034.029	-284.975	1390.988	2498.527	-643.04
14	0.158	0.742	-0.835	0.671	-0.742	2292.747	-2534.718	83.6815	1458.307	2376.429	-1076.41
15	0.152	0.751	-1.040	0.506	-0.862	1694.822	-2886.326	600.33	1388.068	2295.152	-1498.26
16	0.138	0.770	-1.244	0.321	-0.947	1053.469	-3110.758	814.475	1093.098	1867.943	-2017.66
17	0.114	0.807	-1.449	0.122	-0.993	387.679	-3158.923	995.454	821.456	1383.134	-2337.47
18	0.081	0.858	-1.653	-0.082	-0.997	-241.919	-2932.773	954.292	611.634	712.373	-2321.14
19	0.043	0.922	-1.857	-0.283	-0.959	-678.401	-2301.295	924.619	294.272	246.218	-2007.02
AP	0.019	0.964	-2.062	-0.472	-0.882	-668.281	-1249.625	358.039	59.007	-310.242	-1190.62
										F3(R)	F3(I)
										2424.899	942.785

$$T^*(x) = \frac{S_n}{B_n}; \qquad K = \frac{\omega_0^{\,2}}{g}; \qquad f_3(R) = e^{-KT^*(x)}\cos(Kx_c)c_n; \qquad f_3(I) = e^{-KT^*(x)}\sin(Kx_c)c_n;$$

$$h_3(R) = e^{-KT^*(x)}[-\cos(Kx_c)\omega_e\omega_0 a_{33} - \sin(Kx_c)\omega_0 b_{33}]; \qquad h_3(I) = e^{-KT^*(x)}[-\sin(Kx_c)\omega_e\omega_0 a_{33} + \cos(Kx_c)\omega_0 b_{33}]$$

Station	xc(f3+h3)r	xc(f3+h3)I	f(U)r	f(U)I	Momen(R)	Momen(I)					
FP	-592.437	823.51	0	0	-592.437	823.51					
1	-786.937	1471.54	0	0	-786.937	1471.54					
2	-698.932	1766.12	0	0	-698.932	1766.12					
3	-418.879	1869.42	0	0	-418.879	1869.42					
4	-191.199	1776.54	0	0	-191.199	1776.54					
5	118.447	1467.37	0	0	118.447	1467.37					
6	392.869	1030.70	0	0	392.869	1030.70					
7	445.278	679.38	0	0	445.278	679.38					
8	379.109	362.22	0	0	379.109	362.22		P(R)	4028.452		
9	211.388	133.24	0	0	211.388	133.24		P(I)	2692.605		
10	-22.771	-8.60	0	0	-22.771	-8.60		Q(R)	134.844		
11	-298.866	-47.21	0	0	-298.866	-47.21		Q(I)	66.527		
12	-579.944	27.68	0	0	-579.944	27.68		R(R)	134.844		
13	-834.196	214.70	0	0	-834.196	214.70		R(I)	66.527		
14	-1050.441	475.80	0	0	-1050.441	475.80		S(R)	1544.386		
15	-1262.678	824.27	0	0	-1262.678	824.27		S(I)	849.9461		
16	-1229.667	1328.23	0	0	-1229.667	1328.23		F3(R)	2424.899		
17	-1060.103	1791.55	0	0	-1060.103	1791.55		F3(I)	942.785		
18	-623.041	2030.07	0	0	-623.041	2030.07		F5(R)	856.573		
19	-241.964	1972.35	0	0	-241.964	1972.35		F5(I)	-2183.022		
AP	338.435	1298.82	0	0	338.435	1298.82					
					F5(R)	F5(I)					
					856.573	-2183.022					

$P(R) = C_{33} - \omega_e^2(m + A_{33})$; $Q(R) = C_{35} - \omega_e^2 A_{35}$; $R(R) = C_{53} - \omega_e^2 A_{53}$; $S(R) = C_{55} - \omega_e^2(I_{yy} + A_{55})$

$P(I) = \omega_e B_{33}$ $Q(I) = \omega_e B_{35}$ $R(I) = \omega_e B_{53}$ $S(I) = \omega_e B_{55}$

Station	xc-X0 (m)	mn+a33	Product	f(U)	0	An	Simpson	b33(xc-X0)	U*a33	Bn	c33(xc-X0)	Cn	
FP	1.050	18.469	19.399	0		-19.399	1	50.616	0	-50.616	1163.19	-1163.185	
1	0.944	32.222	30.432	0		-30.432	4	116.509	0	-116.509	2128.79	-2128.79	
2	0.839	48.626	40.773	0		-40.773	2	186.775	0	-186.775	2695.27	-2695.274	
3	0.733	59.225	43.387	0		-43.387	4	220.633	0	-220.633	2853.75	-2853.746	
4	0.627	154.155	96.597	0		-96.597	2	253.947	0	-253.947	2702.01	-2702.007	
5	0.521	214.481	111.680	0		-111.680	4	218.359	0	-218.359	2360.07	-2360.073	
6	0.415	183.181	75.974	0		-75.974	2	140.352	0	-140.352	1924.56	-1924.564	
7	0.309	126.444	39.049	0		-39.049	4	100.600	0	-100.600	1445.15	-1445.147	
8	0.203	137.049	27.804	0		-27.804	2	61.101	0	-61.101	949.35	-949.3536	
9	0.097	125.916	12.208	0		-12.208	4	29.199	0	-29.199	453.68	-453.6775	
X0(mid)	0	124.789	0.000	0		0.000	1	0.000	0	0.000	0.00	0	
						A				**B**		**C**	
						-51.188				**-144.0245**		**-1931.72**	
Station	xc(m)	xc(mn+a33	Product	f(U)		Dn	xc*b33	Product	f(U)	En	xc*c33	Hn	
FP	1.050	19.399	20.376	0		20.376	50.616	53.165	0	53.165	1163.19	1221.78	
1	0.944	30.432	28.741	0		28.741	116.509	110.037	0	110.037	2128.79	2010.54	
2	0.839	40.773	34.188	0		34.188	186.775	156.611	0	156.611	2695.27	2259.99	
3	0.733	43.387	31.784	0		31.784	220.633	161.631	0	161.631	2853.75	2090.58	
4	0.627	96.597	60.530	0		60.530	253.947	159.129	0	159.129	2702.01	1693.15	
5	0.521	111.680	58.152	0		58.152	218.359	113.699	0	113.699	2360.07	1228.89	
6	0.415	75.974	31.510	0		31.510	140.352	58.211	0	58.211	1924.56	798.21	
7	0.309	39.049	12.059	0		12.059	100.600	31.068	0	31.068	1445.15	446.30	
8	0.203	27.804	5.641	0		5.641	61.101	12.396	0	12.396	949.35	192.60	
9	0.097	12.208	1.184	0		1.184	29.199	2.831	0	2.831	453.68	43.98	
X0(mid)	0	0.000	0.000	0		0.000	0.000	0.000	0	0.000	0.00	0.00	
						D				**E**		**H**	
						28.683				**88.437**		**1215.143**	

$A_n = -(m_n + a_{33})(x_c - x_0)$; $B_n = -b_{33}(x_c - x_0)$; $C_n = -c_n(x_c - x_0)$;

$D_n = (m_n + a_{33})x_c(x_c - x_0)$; $E_n = b_{33}x_c(x_c - x_0)$; $H_n = c_n x_c(x_c - x_0)$.

Station	f3+h3(R)	Product	f(U)r	Addition		f3+h3(I)	Product	f(U)I	Addition		
FP	-564.024	-592.437	0	-592.437		784.012	823.507	0	823.51		
1	-833.223	-786.937	0	-786.937		1558.090	1471.538	0	1471.54	**A**	**-51.188**
2	-833.551	-698.932	0	-698.932		2106.287	1766.122	0	1766.12	**B**	**-144.0245**
3	-571.789	-418.879	0	-418.879		2551.844	1869.417	0	1869.42	**C**	**-1931.72**
4	-305.126	-191.199	0	-191.199		2835.099	1776.544	0	1776.54	**D**	**28.683**
5	227.477	118.447	0	118.447		2818.076	1467.372	0	1467.37	**E**	**88.437**
6	947.244	392.869	0	392.869		2485.117	1030.702	0	1030.70	**H**	**1215.143**
7	1441.845	445.278	0	445.278		2199.875	679.376	0	679.38	**Mw(R)**	**-90.155**
8	1868.684	379.109	0	379.109		1785.436	362.220	0	362.22	**Mw(I)**	**1172.306**
9	2180.387	211.388	0	211.388		1374.321	133.240	0	133.24	**Fre(rad/s)**	**4.304**
X0(mid)	2409.588	0.000	0	0.000		909.999	0.000	0	0.00		
				Mw(R)					**Mw(I)**		
				-90.155					**1172.306**		

$$M_w(R) = \int_{x_0}^{bow} [f_3(R) + h_3(R)](x_r - x_0)dx_r$$

$$M_w(I) = \int_{x_0}^{bow} [f_3(I) + h_3(I)](x_r - x_0)dx_r$$

The above computations are performed at each frequency value of the regular wave tests, and the resulting coefficients and excitation forces are presented in Table 31.

Table 31: Computed Hydrodynamic Coefficients and Exciting Forces

f (hz)	0.392	0.490	0.588	0.685	0.784	0.882	0.980	1.077
P(R)	6674.607	5887.607	4978.069	4028.452	2845.297	1462.324	-127.046	-1964.160
P(I)	1716.990	2168.582	2597.614	2692.605	3034.788	3075.315	3174.711	2967.506
Q(R)	162.694	154.762	149.977	134.844	133.010	112.021	94.004	79.093
Q(I)	47.056	38.091	60.629	66.527	43.043	69.732	102.196	120.656
R(R)	162.694	154.762	149.977	134.844	133.010	112.021	94.004	79.093
R(I)	47.056	38.091	60.629	66.527	43.043	69.732	102.196	120.656
S(R)	2181.033	1982.103	1770.019	1544.386	1290.567	986.514	643.872	262.540
S(I)	466.014	607.099	754.714	849.946	939.412	1022.667	1110.795	1106.427
F3(R)	6203.765	5092.730	3931.362	2424.899	839.657	-381.029	-955.902	-849.701
F3(I)	1341.580	1468.128	1440.556	942.785	488.463	-92.221	-454.565	-415.557
F5(R)	407.117	575.957	761.983	856.573	809.860	541.038	151.208	-237.863
F5(I)	-1453.112	-1864.272	-2090.322	-2183.022	-1846.876	-1174.525	-303.360	417.912
Ay	-65.505	-59.679	-55.220	-51.188	-48.871	-47.422	-46.621	-46.340
By	-144.561	-151.604	-153.101	-144.024	-142.879	-131.485	-123.969	-108.073
Cy	-1931.720	-1931.720	-1931.720	-1931.720	-1931.720	-1931.720	-1931.720	-1931.720
Dy	36.890	33.757	31.094	28.683	27.207	26.276	25.638	25.313
Ey	84.475	91.492	93.081	88.437	89.155	83.687	80.498	71.596
Hy	1215.143	1215.143	1215.143	1215.143	1215.143	1215.143	1215.143	1215.143
Mw(R)	1236.769	833.036	408.406	-90.155	-540.361	-727.826	-615.086	-255.997
Mw(I)	975.096	1185.071	1265.253	1172.306	844.491	350.465	-145.257	-409.219

From the above calculations, we can get the following complex coefficients:

$$
\begin{aligned}
P &= P(R) + iP(I) \\
Q &= Q(R) + iQ(I) \\
R &= R(R) + iR(I) \\
S &= S(R) + iS(I) \\
F_3 &= F_3(R) + iF_3(I) \\
F_5 &= F_5(R) + iF_5(I) \\
y_\varsigma &= M_w(R) + iM_w(I)
\end{aligned}
\qquad (74)
$$

Substitution of P, Q, R, S, F_3, and F_5 into equation (65) results in the complex amplitudes of the heave displacement z_a and the angular pitch displacement θ_a. Subsequent substitution of z_a, θ_a, A_y, B_y, C_y, D_y, E_y, H_y, and y_ς into equation (69) gives

the complex amplitude of the wave-induced midship bending moment. The modulus and phase shift could be determined from the complex amplitude. The final results are listed in Table 19. The MATLAB M-file for the complex solutions is presented below.

solution.m

```
%M-file for Solution Of Regular Wave Motion
P=motion(1)+i*motion(2);
Q=motion(3)+i*motion(4);
R=motion(5)+i*motion(6);
S=motion(7)+i*motion(8);
F3=motion(9)+i*motion(10);
F5=motion(11)+i*motion(12);
x3=(F3*S-F5*Q)/(P*S-Q*R);
x5=(F5*P-F3*R)/(P*S-Q*R);
%Computation of Midship Bending Moment
A=motion(13);
B=motion(14);
C=motion(15);
D=motion(16);
E=motion(17);
H=motion(18);
Mw=motion(19)+i*motion(20);
omega=motion(21);
BM=(C-A*omega^2+i*B*omega)*x3+(H-D*omega^2+i*E*omega)*x5+Mw;
%Magnitude and Phase
mag3=abs(x3);
mag5=abs(x5);
magBM=abs(BM);
if real(x3)>=0
   phase3=atan(imag(x3)/real(x3))*180/pi;
else
   phase3=(pi+atan(imag(x3)/real(x3)))*180/pi;
end
if real(x5)>=0
   phase5=atan(imag(x5)/real(x5))*180/pi;
else
   phase5=(pi+atan(imag(x5)/real(x5)))*180/pi;
end
if real(BM)>=0
   phaseBM=atan(imag(BM)/real(BM))*180/pi;
else
   phaseBM=(pi+atan(imag(BM)/real(BM)))*180/pi;
end
result=[mag3,phase3;mag5,phase5;magBM,phaseBM]
```

Appendix II Data Analysis Programs

The computer programs used for the data analysis and numerical simulations are summarized in Table 32. All programs in this work are written as MATLAB M-files.

Table 32: Summary of the Computer Programs

Stationary Tests in Head Waves	
hregu.m	Frequency Analysis of Regular Wave Tests
hspec.m	Spectral Analysis of Random Wave Tests
hneural.m	Estimation of Correlation Functions for Neural Network Training
htest1.m	Regular Wave Data Processing for Neural Network Validation
htest3.m	Random Wave Data Processing for Neural Network Validation
hsimu.m	Estimation of Correlation Functions using Time-domain Simulations
Stationary Tests in Following Waves	
fregu.m	Frequency Analysis of Regular Wave Tests
fspec.m	Spectral Analysis of Random Wave Tests
fneural.m	Estimation of Correlation Functions for Neural Network Training
ftest1.m	Regular Wave Data Processing for Neural Network Validation
ftest3.m	Random Wave Data Processing for Neural Network Validation
fsimu.m	Estimation of Correlation Functions using Time-domain Simulations
Towing Tests in Head Waves (0.5m/sec)	
s5regu.m	Frequency Analysis of Regular Wave Tests
s5sample.m	Data Processing of Random Wave Tests
s5spec.m	Spectral Analysis of Joined Random Time History
s5neural.m	Estimation of Correlation Functions for Neural Network Training
s5test1.m	Regular Wave Data Processing for Neural Network Validation
s5test3.m	Random Wave Data Processing for Neural Network Validation
s5simu.m	Estimation of Correlation Functions using Time-domain Simulations

hregu.m

```
% Frequency Analysis of Regular Test (Head Wave Stationary Tests)
heave=-0.00140*data(:,1)+87.5966;
pitch=-0.00232*data(:,2)+70.5666;
speed=0.00015*data(:,3)-5.0490;
wave=0.00050*data(:,4)-17.3866;
bend=0.00580*data(:,5)-212.5687;
heave=heave(3001:6000)-mean(heave(1:100));
pitch=pitch(3001:6000)-mean(pitch(1:100));
wave=wave(3001:6000)-mean(wave(1:100));
bend=bend(3001:6000)-mean(bend(1:100));
t=[0:2999]'/50;
f
Icw=wave'*cos(2*pi*f*t)/3000;
Isw=wave'*sin(2*pi*f*t)/3000;
Ich=heave'*cos(2*pi*f*t)/3000;
Ish=heave'*sin(2*pi*f*t)/3000;
Icp=pitch'*cos(2*pi*f*t)/3000;
Isp=pitch'*sin(2*pi*f*t)/3000;
Icb=bend'*cos(2*pi*f*t)/3000;
Isb=bend'*sin(2*pi*f*t)/3000;
W=2*sqrt(Icw^2+Isw^2);
H=2*sqrt(Ich^2+Ish^2);
P=2*sqrt(Icp^2+Isp^2);
B=2*sqrt(Icb^2+Isb^2);
if Icw>=0
      phasew=(-atan(Isw/Icw))*180/pi;
else
      phasew=(pi-atan(Isw/Icw))*180/pi;
end
if Ich>=0
        phaseh=(-atan(Ish/Ich))*180/pi;
else
        phaseh=(pi-atan(Ish/Ich))*180/pi;
end
if Icp>=0
        phasep=(-atan(Isp/Icp))*180/pi;
else
        phasep=(pi-atan(Isp/Icp))*180/pi;
end
if Icb>=0
        phaseb=(-atan(Isb/Icb))*180/pi;
else
        phaseb=(pi-atan(Isb/Icb))*180/pi;
end
result=[f,W,H,phaseh-phasew,P,phasep-phasew,B,phaseb-phasew]
```

hspec.m

```
% Spectral Analysis of Random Test (Head Wave Stationary Tests)
heave=-0.00140*data(:,1)+87.5966;
pitch=-0.00232*data(:,2)+70.5666;
speed=0.00015*data(:,3)-5.0490;
wave=0.00050*data(:,4)-17.3866;
bend=0.00580*data(:,5)-212.5687;
heave=heave(2501:25000)-mean(heave(1:100));
pitch=pitch(2501:25000)-mean(pitch(1:100));
wave=wave(2501:25000)-mean(wave(1:100));
bend=bend(2501:25000)-mean(bend(1:100));
% Spectrum Estimation
fwave=fft(wave);
swave=fwave.*conj(fwave)/1125000;
fheave=fft(heave);
sheave=fheave.*conj(fheave)/1125000;
fpitch=fft(pitch);
spitch=fpitch.*conj(fpitch)/1125000;
fbend=fft(bend);
sbend=fbend.*conj(fbend)/1125000;
swave=swave(1:11250)*2;
sbend=sbend(1:11250)*2;
sheave=sheave(1:11250)*2;
spitch=spitch(1:11250)*2;
f=[0:11249]'/450;
raoh=sqrt(sheave./swave);
raop=sqrt(spitch./swave);
raob=sqrt(sbend./swave);
%Regular Wave Test Results
F=[0.294,0.392,0.490,0.588,0.685,0.784,0.882,0.980,1.077]';
AW=[3.40,3.31,3.56,2.82,2.70,3.28,3.30,4.13,3.32]';
AB=[3.27,3.83,7.39,8.89,10.48,13.75,10.82,6.14,6.63]';
AH=[3.29,3.05,3.02,1.94,1.35,0.88,0.52,2.22,0.54]';
AP=[0.91,0.75,1.28,2.06,2.37,2.36,1.82,1.32,0.79]';
RAOH=AH./AW; RAOP=AP./AW; RAOB=AB./AW;
%Plotting
subplot(2,1,1)
plot(f(100:600),swave(100:600),'r')
title ('Wave Spectrum'); ylabel ('S(f)')
subplot(2,1,2)
plot(f(100:600),raob(100:600),'-r',F,RAOB,'ob')
legend('Random Test','Regular Test')
title ('BM RAOs'); ylabel ('RAO')
figure
subplot(2,1,1)
plot(f(100:600),raoh(100:600),'-r',F,RAOH,'ob')
title ('Heave RAOs'); ylabel ('RAO')
subplot(2,1,2)
plot(f(100:600),raop(100:600),'-r',F,RAOP,'ob')
title ('Pitch RAOs')
ylabel ('RAO'); xlabel ('f(Hz)')
```

hneural.m

```
% Estimation of Correlation Functions for Training (Head Wave
Stationary Tests)
heave=-0.00140*data(:,1)+87.5966;
pitch=-0.00232*data(:,2)+70.5666;
speed=0.00015*data(:,3)-5.0490;
wave=0.00050*data(:,4)-17.3866;
bend=0.00580*data(:,5)-212.5687;
heave=heave(2501:25000)-mean(heave(1:100));
pitch=pitch(2501:25000)-mean(pitch(1:100));
wave=wave(2501:25000)-mean(wave(1:100));
bend=bend(2501:25000)-mean(bend(1:100));
% Estimation of Auto- and Cross-correlation Functions
for J=1:500
crosshh(J)=heave(1+(J-1):22500)'*heave(1:22500-(J-1))/(22500-(J-1));
crosshp(J)=pitch(1+(J-1):22500)'*heave(1:22500-(J-1))/(22500-(J-1));
crosshb(J)=bend(1+(J-1):22500)'*heave(1:22500-(J-1))/(22500-(J-1));
end
MX=max(crosshh);
crosshh=crosshh/MX;
crosshp=crosshp/MX;
crosshb=crosshb/MX;
% Calculation of Velocity & Acceleration
for K=1:480
      I=K+10;
      dhh(K)=crosshh(I);
      vhh(K)=(crosshh(I+10)-crosshh(I-10))/(2*0.2);
      ahh(K)=(crosshh(I+10)-2*crosshh(I)+crosshh(I-10))/(0.2)^2;
      dhp(K)=crosshp(I);
      vhp(K)=(crosshp(I+10)-crosshp(I-10))/(2*0.2);
      ahp(K)=(crosshp(I+10)-2*crosshp(I)+crosshp(I-10))/(0.2)^2;
      dhb(K)=crosshb(I);
end
t=[1:480]/50;
result=[dhh' vhh' ahh' dhp' vhp' ahp' dhb'];
```

htest1.m

```
% An M-file for Regular Test Verification (Head Wave Stationary Tests)
heave=-0.00140*data(:,1)+87.5966;
pitch=-0.00232*data(:,2)+70.5666;
speed=0.00015*data(:,3)-5.0490;
wave=0.00050*data(:,4)-17.3866;
bend=0.00580*data(:,5)-212.5687;
heave=heave(3001:6001)-mean(heave(1:100));
pitch=pitch(3001:6001)-mean(pitch(1:100));
wave=wave(3001:6001)-mean(wave(1:100));
bend=bend(3001:6001)-mean(bend(1:100));
% Resampling Data
for J=1:50
crosshh(J)=heave(1+(J-1)*10:3001)'*heave(1:3001-(J-1)*10)/(3001-(J-
1)*10);
crosshp(J)=pitch(1+(J-1)*10:3001)'*heave(1:3001-(J-1)*10)/(3001-(J-
1)*10);
crosshb(J)=bend(1+(J-1)*10:3001)'*heave(1:3001-(J-1)*10)/(3001-(J-
1)*10);
end
MX=max(crosshh);
crosshh=crosshh/MX;
crosshp=crosshp/MX;
crosshb=crosshb/MX;
% Calculation of Velocity & Acceleration
for K=1:48
      I=K+1;
      dhh(K)=crosshh(I);
      vhh(K)=(crosshh(I+1)-crosshh(I-1))/(2*0.2);
      ahh(K)=(crosshh(I+1)-2*crosshh(I)+crosshh(I-1))/(0.2)^2;
      dhp(K)=crosshp(I);
      vhp(K)=(crosshp(I+1)-crosshp(I-1))/(2*0.2);
      ahp(K)=(crosshp(I+1)-2*crosshp(I)+crosshp(I-1))/(0.2)^2;
      dhb(K)=crosshb(I);
      vhb(K)=(crosshb(I+1)-crosshb(I-1))/(2*0.2);
      ahb(K)=(crosshb(I+1)-2*crosshb(I)+crosshb(I-1))/(0.2)^2;
end
t=[1:48]/5;
result=[dhh' vhh' ahh' dhp' vhp' ahp' dhb'];
```

htest3.m

```
% An M-file for Random Test Verification (Head Wave Stationary Tests)
heave=-0.00140*data(:,1)+87.5966;
pitch=-0.00232*data(:,2)+70.5666;
speed=0.00015*data(:,3)-5.0490;
wave=0.00050*data(:,4)-17.3866;
bend=0.00580*data(:,5)-212.5687;
heave=heave(2501:25000)-mean(heave(1:100));
pitch=pitch(2501:25000)-mean(pitch(1:100));
wave=wave(2501:25000)-mean(wave(1:100));
bend=bend(2501:25000)-mean(bend(1:100));
% Resampling
N
crosshh=heave(N+1:N+500);
crosshp=pitch(N+1:N+500);
crosshb=bend(N+1:N+500);
MX=max(crosshh);
crosshh=crosshh/MX;
crosshp=crosshp/MX;
crosshb=crosshb/MX;
% Calculation of Velocity & Acceleration
for K=1:480
      I=K+10;
      dhh(K)=crosshh(I);
      vhh(K)=(crosshh(I+10)-crosshh(I-10))/(2*0.2);
      ahh(K)=(crosshh(I+10)-2*crosshh(I)+crosshh(I-10))/(0.2)^2;
      dhp(K)=crosshp(I);
      vhp(K)=(crosshp(I+10)-crosshp(I-10))/(2*0.2);
      ahp(K)=(crosshp(I+10)-2*crosshp(I)+crosshp(I-10))/(0.2)^2;
      dhb(K)=crosshb(I);
end
t=[1:480]/50;
%Frequency-domain Filter Implementation
fbend=fft(bend);
nfbend=zeros(size(fbend));
nfbend(1:1000)=fbend(1:1000);
nfbend(21502:22500)=fbend(21502:22500);
nbend=ifft(nfbend);
nbend=real(nbend);
fheave=fft(heave);
nfheave=zeros(size(fheave));
nfheave(1:1000)=fheave(1:1000);
nfheave(21502:22500)=fheave(21502:22500);
nheave=ifft(nfheave);
nheave=real(nheave);
fpitch=fft(pitch);
nfpitch=zeros(size(fpitch));
nfpitch(1:1000)=fpitch(1:1000);
nfpitch(21502:22500)=fpitch(21502:22500);
npitch=ifft(nfpitch);
npitch=real(npitch);
% Calculation for Filtered Values
```

```
for J=1:500
      ncrosshh(J)=nheave(1+N+(J-1));
      ncrosshp(J)=npitch(1+N+(J-1));
      ncrosshb(J)=nbend(1+N+(J-1));
end
ncrosshh=ncrosshh/MX;
ncrosshp=ncrosshp/MX;
ncrosshb=ncrosshb/MX;
% Calculation of Velocity & Acceleration
for K=1:480
      I=K+10;
      ndhh(K)=ncrosshh(I);
      nvhh(K)=(ncrosshh(I+10)-ncrosshh(I-10))/(2*0.2);
      nahh(K)=(ncrosshh(I+10)-2*ncrosshh(I)+ncrosshh(I-10))/(0.2)^2;
      ndhp(K)=ncrosshp(I);
      nvhp(K)=(ncrosshp(I+10)-ncrosshp(I-10))/(2*0.2);
      nahp(K)=(ncrosshp(I+10)-2*ncrosshp(I)+ncrosshp(I-10))/(0.2)^2;
      ndhb(K)=ncrosshb(I);
end
result=[ndhh' nvhh' nahh' ndhp' nvhp' nahp' ndhb'];
```

hsimu.m

```
%Simulation of Ship Motions and Bending Moment (Head Wave Stationary
Condition)
%JONSWAP Wave Spectrum
f1=0.4:0.01:0.6;
s1=0.21*7.5^2*0.6^4./f1.^5.*exp(-1.25*0.6^4./f1.^4).*3.3.^exp(-(f1-
0.6).^2/2/(0.07*0.6)^2);
f2=0.61:0.01:0.9;
s2=0.21*7.5^2*0.6^4./f2.^5.*exp(-1.25*0.6^4./f2.^4).*3.3.^exp(-(f2-
0.6).^2/2/(0.09*0.6)^2);
f=[f1,f2]';
s=[s1,s2]';
%Wave Simulation
phasew=rand(size(f))*2*pi;
ampliw=sqrt(2*s*0.01);
%Computed Frequency Transfer Functions
%F=[0.4:0.1:0.9]';
%Magh=[0.921,0.848,0.749,0.542,0.255,0.119]';
%Angleh=[-1.18,-2.54,-4.89,-8.16,-8.05,111.62]';
%Magp=[0.389,0.537,0.662,0.761,0.721,0.527]';
%Anglep=[267.7,266.2,263.8,260.6,256.6,249.0]';
%Magb=[0.683,1.345,2.130,3.208,3.939,4.017]';
%Angleb=[181.8,185.6,188.7,191.4,196.7,205.6]';
%Experimental Frequency Response Functions
F=[0.4:0.1:0.9]';
Magh=[0.921,0.848,0.688,0.5,0.268,0.158]';
Angleh=[5.8,9,8.5,16.6,23.8,83.3]';
Magp=[0.226,0.36,0.731,0.878,0.72,0.552]';
Anglep=[267.5,261.1,272.1,281.7,286.2,284.1]';
Magb=[1.1571,2.0758,3.1525,3.8815,4.1921,3.2788]';
Angleb=[205,203,205,196,188,194]';
%Heave Simulation
raoh=interp1(F,Magh,f);
phaseh=interp1(F,Angleh,f)*pi/180;
t=[0.02:0.02:450]';
heave=zeros(size(t));
for k=1:size(f)
   heave=heave+ampliw(k)*raoh(k)*cos(2*pi*f(k)*t+phasew(k)+phaseh(k));
end
%Pitch Simulation
raop=interp1(F,Magp,f);
phasep=interp1(F,Anglep,f)*pi/180;
pitch=zeros(size(t));
for k=1:size(f)
   pitch=pitch+ampliw(k)*raop(k)*cos(2*pi*f(k)*t+phasew(k)+phasep(k));
end
%Bending Moment Simulation
raob=interp1(F,Magb,f);
phaseb=interp1(F,Angleb,f)*pi/180;
bend=zeros(size(t));
for k=1:size(f)
   bend=bend+ampliw(k)*raob(k)*cos(2*pi*f(k)*t+phasew(k)+phaseb(k));
```

```
end
% Estimation of Correlation Functions
for J=1:500
crosshh(J)=heave(1+(J-1):22500)'*heave(1:22500-(J-1))/(22500-(J-1));
crosshp(J)=pitch(1+(J-1):22500)'*heave(1:22500-(J-1))/(22500-(J-1));
crosshb(J)=bend(1+(J-1):22500)'*heave(1:22500-(J-1))/(22500-(J-1));
end
MX=max(crosshh);
crosshh=crosshh/MX;
crosshp=crosshp/MX;
crosshb=crosshb/MX;
% Calculation of Velocity & Acceleration
for K=1:480
      I=K+10;
      dhh(K)=crosshh(I);
      vhh(K)=(crosshh(I+10)-crosshh(I-10))/(2*0.2);
      ahh(K)=(crosshh(I+10)-2*crosshh(I)+crosshh(I-10))/(0.2)^2;
      dhp(K)=crosshp(I);
      vhp(K)=(crosshp(I+10)-crosshp(I-10))/(2*0.2);
      ahp(K)=(crosshp(I+10)-2*crosshp(I)+crosshp(I-10))/(0.2)^2;
      dhb(K)=crosshb(I);
end
T=[1:480]/50;
result=[dhh' vhh' ahh' dhp' vhp' ahp' dhb'];
```

fregu.m

```
% Frequency Analysis of Regular Test (Following Wave Stationary Test)
heave=-0.0013967*data(:,1)+88.866;
pitch=-(-0.00090696*data(:,2)+30.743);
wave=0.00103865*data(:,4)-34.1906;
bend=0.00705158*data(:,3)-249.699;
heave=heave(3001:6000)-mean(heave(1:100));
pitch=pitch(3001:6000)-mean(pitch(1:100));
wave=wave(3001:6000)-mean(wave(1:100));
bend=bend(3001:6000)-mean(bend(1:100));
t=[0:2999]'/50;
f
Icw=wave'*cos(2*pi*f*t)/3000;
Isw=wave'*sin(2*pi*f*t)/3000;
Ich=heave'*cos(2*pi*f*t)/3000;
Ish=heave'*sin(2*pi*f*t)/3000;
Icp=pitch'*cos(2*pi*f*t)/3000;
Isp=pitch'*sin(2*pi*f*t)/3000;
Icb=bend'*cos(2*pi*f*t)/3000;
Isb=bend'*sin(2*pi*f*t)/3000;
W=2*sqrt(Icw^2+Isw^2);
H=2*sqrt(Ich^2+Ish^2);
P=2*sqrt(Icp^2+Isp^2);
B=2*sqrt(Icb^2+Isb^2);
if Icw>=0
      phasew=(-atan(Isw/Icw))*180/pi;
else
      phasew=(pi-atan(Isw/Icw))*180/pi;
end
if Ich>=0
        phaseh=(-atan(Ish/Ich))*180/pi;
else
        phaseh=(pi-atan(Ish/Ich))*180/pi;
end
if Icp>=0
        phasep=(-atan(Isp/Icp))*180/pi;
else
        phasep=(pi-atan(Isp/Icp))*180/pi;
end
if Icb>=0
        phaseb=(-atan(Isb/Icb))*180/pi;
else
        phaseb=(pi-atan(Isb/Icb))*180/pi;
end
result=[f,W,H,phaseh-phasew,P,phasep-phasew,B,phaseb-phasew]
```

fspec.m

```
% Spectral Analysis of Random Test (Following Wave Stationary Tests)
heave=-0.0013967*data(:,1)+88.866;
pitch=-(-0.00090696*data(:,2)+30.743);
wave=0.00103865*data(:,4)-34.1906;
bend=0.00705158*data(:,3)-249.699;
heave=heave(2501:25000)-mean(heave(1:100));
pitch=pitch(2501:25000)-mean(pitch(1:100));
wave=wave(2501:25000)-mean(wave(1:100));
bend=bend(2501:25000)-mean(bend(1:100));
% Spectrum Estimation
fwave=fft(wave);
swave=fwave.*conj(fwave)/1125000;
fheave=fft(heave);
sheave=fheave.*conj(fheave)/1125000;
fpitch=fft(pitch);
spitch=fpitch.*conj(fpitch)/1125000;
fbend=fft(bend);
sbend=fbend.*conj(fbend)/1125000;
f=[0:22499]'/450;
swave=swave(1:11250)*2;
sbend=sbend(1:11250)*2;
sheave=sheave(1:11250)*2;
spitch=spitch(1:11250)*2;
f=f(1:11250);
raoh=sqrt(sheave./swave);
raop=sqrt(spitch./swave);
raob=sqrt(sbend./swave);
%Regular Wave Test Results
F=[0.295,0.393,0.491,0.590,0.689,0.787,0.886,0.983,1.081]';
RAOB=[0.834,1.198,1.781,2.678,3.652,4.027,4.778,6.723,3.595]';
RAOH=[0.920,0.884,0.812,0.589,0.456,0.212,0.176,1.261,0.172]';
RAOP=[0.254,0.203,0.347,0.620,0.760,0.676,0.576,0.576,0.246]';
%Plotting
figure
subplot(2,1,1)
plot(f(100:600),swave(100:600),'r')
title ('Wave Spectrum'); ylabel ('S(f)')
subplot(2,1,2)
plot(f(100:600),raob(100:600),'-r',F,RAOB,'ob')
legend('Random Test','Regular Test')
title ('BM RAOs'); ylabel ('RAO')
figure
subplot(2,1,1)
plot(f(100:600),raoh(100:600),'-r',F,RAOH,'ob')
title ('Heave RAOs'); ylabel ('RAO')
subplot(2,1,2)
plot(f(100:600),raop(100:600),'-r',F,RAOP,'ob')
title ('Pitch RAOs')
ylabel ('RAO'); xlabel ('f(Hz)')
```

fneural.m

```
% Estimation of Correlation Functions for Training (Following Wave
Stationary Test)
heave=-0.0013967*data(:,1)+88.866;
pitch=-(-0.00090696*data(:,2)+30.743);
wave=0.00103865*data(:,4)-34.1906;
bend=0.00705158*data(:,3)-249.699;
heave=heave(2501:25000)-mean(heave(1:100));
pitch=pitch(2501:25000)-mean(pitch(1:100));
wave=wave(2501:25000)-mean(wave(1:100));
bend=bend(2501:25000)-mean(bend(1:100));
% Estimation of Correlation Functions
for J=1:500
crosshh(J)=heave(1+(J-1):22500)'*heave(1:22500-(J-1));
crosshh(J)=crosshh(J)/(22500-(J-1));
crosshp(J)=pitch(1+(J-1):22500)'*heave(1:22500-(J-1));
crosshp(J)=crosshp(J)/(22500-(J-1));
crosshb(J)=bend(1+(J-1):22500)'*heave(1:22500-(J-1));
crosshb(J)=crosshb(J)/(22500-(J-1));
end
MX=max(crosshh);
crosshh=crosshh/MX;
crosshp=crosshp/MX;
crosshb=crosshb/MX;
% Calculation of Velocity & Acceleration
for K=1:480
      I=K+10;
      dhh(K)=crosshh(I);
      vhh(K)=(crosshh(I+10)-crosshh(I-10))/(2*0.2);
      ahh(K)=(crosshh(I+10)-2*crosshh(I)+crosshh(I-10))/(0.2)^2;
      dhp(K)=crosshp(I);
      vhp(K)=(crosshp(I+10)-crosshp(I-10))/(2*0.2);
      ahp(K)=(crosshp(I+10)-2*crosshp(I)+crosshp(I-10))/(0.2)^2;
      dhb(K)=crosshb(I);
end
t=[1:480]/50;
result=[dhh' vhh' ahh' dhp' vhp' ahp' dhb'];
```

ftest1.m

```
% An M-file for Regular Test Verification (Head Wave Stationary Tests)
heave=-0.00140*data(:,1)+87.5966;
pitch=-0.00232*data(:,2)+70.5666;
speed=0.00015*data(:,3)-5.0490;
wave=0.00050*data(:,4)-17.3866;
bend=0.00580*data(:,5)-212.5687;
heave=heave(3001:6001)-mean(heave(1:100));
pitch=pitch(3001:6001)-mean(pitch(1:100));
wave=wave(3001:6001)-mean(wave(1:100));
bend=bend(3001:6001)-mean(bend(1:100));
% Resampling Data
for J=1:50
crosshh(J)=heave(1+(J-1)*10:3001)'*heave(1:3001-(J-1)*10)/(3001-(J-
1)*10);
crosshp(J)=pitch(1+(J-1)*10:3001)'*heave(1:3001-(J-1)*10)/(3001-(J-
1)*10);
crosshb(J)=bend(1+(J-1)*10:3001)'*heave(1:3001-(J-1)*10)/(3001-(J-
1)*10);
end
MX=max(crosshh);
crosshh=crosshh/MX;
crosshp=crosshp/MX;
crosshb=crosshb/MX;
% Calculation of Velocity & Acceleration
for K=1:48
      I=K+1;
      dhh(K)=crosshh(I);
      vhh(K)=(crosshh(I+1)-crosshh(I-1))/(2*0.2);
      ahh(K)=(crosshh(I+1)-2*crosshh(I)+crosshh(I-1))/(0.2)^2;
      dhp(K)=crosshp(I);
      vhp(K)=(crosshp(I+1)-crosshp(I-1))/(2*0.2);
      ahp(K)=(crosshp(I+1)-2*crosshp(I)+crosshp(I-1))/(0.2)^2;
      dhb(K)=crosshb(I);
      vhb(K)=(crosshb(I+1)-crosshb(I-1))/(2*0.2);
      ahb(K)=(crosshb(I+1)-2*crosshb(I)+crosshb(I-1))/(0.2)^2;
end
t=[1:48]/5;
result=[dhh' vhh' ahh' dhp' vhp' ahp' dhb'];
```

ftest3.m

```
% An M-file for Random Data Verification (Following Wave Stationary
Test)
heave=-0.0013967*data(:,1)+88.866;
pitch=-(-0.00090696*data(:,2)+30.743);
wave=0.00103865*data(:,4)-34.1906;
bend=0.00705158*data(:,3)-249.699;
heave=heave(2501:25000)-mean(heave(1:100));
pitch=pitch(2501:25000)-mean(pitch(1:100));
wave=wave(2501:25000)-mean(wave(1:100));
bend=bend(2501:25000)-mean(bend(1:100));
% Resampling
N
crosshh=heave(N+1:N+500);
crosshp=pitch(N+1:N+500);
crosshb=bend(N+1:N+500);
MX=max(crosshh);
crosshh=crosshh/MX;
crosshp=crosshp/MX;
crosshb=crosshb/MX;
% Calculation of Velocity & Acceleration
for K=1:480
      I=K+10;
      dhh(K)=crosshh(I);
      vhh(K)=(crosshh(I+10)-crosshh(I-10))/(2*0.2);
      ahh(K)=(crosshh(I+10)-2*crosshh(I)+crosshh(I-10))/(0.2)^2;
      dhp(K)=crosshp(I);
      vhp(K)=(crosshp(I+10)-crosshp(I-10))/(2*0.2);
      ahp(K)=(crosshp(I+10)-2*crosshp(I)+crosshp(I-10))/(0.2)^2;
      dhb(K)=crosshb(I);
end
t=[1:480]/50;
%Frequency-domain Filter Implementation
fbend=fft(bend);
nfbend=zeros(size(fbend));
nfbend(1:1000)=fbend(1:1000);
nfbend(21502:22500)=fbend(21502:22500);
nbend=ifft(nfbend);
nbend=real(nbend);
fheave=fft(heave);
nfheave=zeros(size(fheave));
nfheave(1:1000)=fheave(1:1000);
nfheave(21502:22500)=fheave(21502:22500);
nheave=ifft(nfheave);
nheave=real(nheave);
fpitch=fft(pitch);
nfpitch=zeros(size(fpitch));
nfpitch(1:1000)=fpitch(1:1000);
nfpitch(21502:22500)=fpitch(21502:22500);
npitch=ifft(nfpitch);
npitch=real(npitch);
% Calculation for Filtered Values
```

```
for J=1:500
      ncrosshh(J)=nheave(1+N+(J-1));
      ncrosshp(J)=npitch(1+N+(J-1));
      ncrosshb(J)=nbend(1+N+(J-1));
end
ncrosshh=ncrosshh/MX;
ncrosshp=ncrosshp/MX;
ncrosshb=ncrosshb/MX;
% Calculation of Filtered Velocity & Acceleration
for K=1:480
      I=K+10;
      ndhh(K)=ncrosshh(I);
      nvhh(K)=(ncrosshh(I+10)-ncrosshh(I-10))/(2*0.2);
      nahh(K)=(ncrosshh(I+10)-2*ncrosshh(I)+ncrosshh(I-10))/(0.2)^2;
      ndhp(K)=ncrosshp(I);
      nvhp(K)=(ncrosshp(I+10)-ncrosshp(I-10))/(2*0.2);
      nahp(K)=(ncrosshp(I+10)-2*ncrosshp(I)+ncrosshp(I-10))/(0.2)^2;
      ndhb(K)=ncrosshb(I);
end
result=[ndhh' nvhh' nahh' ndhp' nvhp' nahp' ndhb'];
```

fsimu.m

```
%Simulation of Ship Motions and Bending Moment (Following Wave
Stationary Test)
%JONSWAP Wave Spectrum
f1=0.4:0.01:0.6;
s1=0.21*7.5^2*0.6^4./f1.^5.*exp(-1.25*0.6^4./f1.^4).*3.3.^exp(-(f1-
0.6).^2/2/(0.07*0.6)^2);
f2=0.61:0.01:0.9;
s2=0.21*7.5^2*0.6^4./f2.^5.*exp(-1.25*0.6^4./f2.^4).*3.3.^exp(-(f2-
0.6).^2/2/(0.09*0.6)^2);
f=[f1,f2]';
s=[s1,s2]';
%Wave Simulation
phasew=rand(size(f))*2*pi;
ampliw=sqrt(2*s*0.01);
%Tested Frequency Transfer Functions
F=[0.4:0.1:0.9]';
Magh=[0.884,0.812,0.589,0.456,0.212,0.176]';
Angleh=[2.51,3.3,-2.01,2.066,-0.412,72.74]';
Magp=[0.203,0.347,0.62,0.76,0.676,0.576]';
Anglep=[279.3,271.6,271.2,277.7,285.4,287.1]';
Magb=[1.198,1.781,2.678,3.652,4.027,4.778]';
Angleb=[149.42,159,163.2,176.5,190.3,218.4]';
%Heave Simulation
raoh=interp1(F,Magh,f);
phaseh=interp1(F,Angleh,f)*pi/180;
t=[0.02:0.02:450]';
heave=zeros(size(t));
for k=1:size(f)
   heave=heave+ampliw(k)*raoh(k)*cos(2*pi*f(k)*t+phasew(k)+phaseh(k));
end
%Pitch Simulation
raop=interp1(F,Magp,f);
phasep=interp1(F,Anglep,f)*pi/180;
pitch=zeros(size(t));
for k=1:size(f)
   pitch=pitch+ampliw(k)*raop(k)*cos(2*pi*f(k)*t+phasew(k)+phasep(k));
end
%Bending Moment Simulation
raob=interp1(F,Magb,f);
phaseb=interp1(F,Angleb,f)*pi/180;
bend=zeros(size(t));
for k=1:size(f)
   bend=bend+ampliw(k)*raob(k)*cos(2*pi*f(k)*t+phasew(k)+phaseb(k));
end
% Estimation of Correlation Functions
for J=1:500
crosshh(J)=heave(1+(J-1):22500)'*heave(1:22500-(J-1))/(22500-(J-1));
crosshp(J)=pitch(1+(J-1):22500)'*heave(1:22500-(J-1))/(22500-(J-1));
crosshb(J)=bend(1+(J-1):22500)'*heave(1:22500-(J-1))/(22500-(J-1));
end
MX=max(crosshh);
```

```
crosshh=crosshh/MX;
crosshp=crosshp/MX;
crosshb=crosshb/MX;
% Calculation of Velocity & Acceleration
for K=1:480
      I=K+10;
      dhh(K)=crosshh(I);
      vhh(K)=(crosshh(I+10)-crosshh(I-10))/(2*0.2);
      ahh(K)=(crosshh(I+10)-2*crosshh(I)+crosshh(I-10))/(0.2)^2;
      dhp(K)=crosshp(I);
      vhp(K)=(crosshp(I+10)-crosshp(I-10))/(2*0.2);
      ahp(K)=(crosshp(I+10)-2*crosshp(I)+crosshp(I-10))/(0.2)^2;
      dhb(K)=crosshb(I);
end
T=[1:480]/50;
result=[dhh' vhh' ahh' dhp' vhp' ahp' dhb'];
```

s5regu.m

```
%Frequency Analysis of Regular Wave Towing Test(0.5m/sec)
cheave=-0.00140*calm(:,1)+87.5966;
cpitch=-0.00232*calm(:,2)+70.5666;
cspeed=0.00015*calm(:,3)-5.0490;
cwave=0.00050*calm(:,4)-17.3866;
cbend=0.00580*calm(:,5)-212.5687;
cheave=cheave-mean(cheave(1:100));
cpitch=cpitch-mean(cpitch(1:100));
cspeed=cspeed-mean(cspeed(1:100));
cwave=cwave-mean(cwave(1:100));
cbend=cbend-mean(cbend(1:100));
sheave=-0.00140*data(:,1)+87.5966;
spitch=-0.00232*data(:,2)+70.5666;
sspeed=0.00015*data(:,3)-5.0490;
swave=0.00050*data(:,4)-17.3866;
sbend=0.00580*data(:,5)-212.5687;
sheave=sheave-mean(sheave(1:100));
spitch=spitch-mean(spitch(1:100));
sspeed=sspeed-mean(sspeed(1:100));
swave=swave-mean(swave(1:100));
sbend=sbend-mean(sbend(1:100));
% Find the Speed Segment for Analysis
[mxi,I]=max(cspeed);
cheave=cheave(I+150:I+2649);
cpitch=cpitch(I+150:I+2649);
cspeed=cspeed(I+150:I+2649);
cwave=cwave(I+150:I+2649);
cbend=cbend(I+150:I+2649);
[mxj,J]=max(sspeed);
sheave=sheave(J+150:J+2649);
spitch=spitch(J+150:J+2649);
sspeed=sspeed(J+150:J+2649);
swave=swave(J+150:J+2649);
sbend=sbend(J+150:J+2649);
t=[0:2499]'/50;
% Find the Wave-induced Response
heave=sheave-mean(cheave);
pitch=spitch-mean(cpitch);
wave=swave-mean(cwave);
bend=sbend-mean(cbend);
speed=sspeed;
% Correlation Analysis for Amplitudes and Phase
f
Icw=wave'*cos(2*pi*f*t)/2500;
Isw=wave'*sin(2*pi*f*t)/2500;
Ich=heave'*cos(2*pi*f*t)/2500;
Ish=heave'*sin(2*pi*f*t)/2500;
Icp=pitch'*cos(2*pi*f*t)/2500;
Isp=pitch'*sin(2*pi*f*t)/2500;
Icb=bend'*cos(2*pi*f*t)/2500;
Isb=bend'*sin(2*pi*f*t)/2500;
```

```
Aw=2*sqrt(Icw^2+Isw^2);
Ah=2*sqrt(Ich^2+Ish^2);
Ap=2*sqrt(Icp^2+Isp^2);
Ab=2*sqrt(Icb^2+Isb^2);
if Icw>=0
      phasew=(-atan(Isw/Icw))*180/pi;
else
      phasew=(pi-atan(Isw/Icw))*180/pi;
end
if Ich>=0
        phaseh=(-atan(Ish/Ich))*180/pi;
else
        phaseh=(pi-atan(Ish/Ich))*180/pi;
end
if Icp>=0
        phasep=(-atan(Isp/Icp))*180/pi;
else
        phasep=(pi-atan(Isp/Icp))*180/pi;
end
if Icb>=0
        phaseb=(-atan(Isb/Icb))*180/pi;
else
        phaseb=(pi-atan(Isb/Icb))*180/pi;
end
result=[f,Aw,Ah,phaseh-phasew,Ap,phasep-phasew,Ab,phaseb-phasew]
```

s5sample.m

```
% An M-file for Data Preparation of Towing Tests (0.5m/sec)
cheave=-0.00140*calm(:,1)+87.5966;
cpitch=-0.00232*calm(:,2)+70.5666;
cspeed=0.00015*calm(:,3)-5.0490;
cwave=0.00050*calm(:,4)-17.3866;
cbend=0.00580*calm(:,5)-212.5687;
cheave=cheave-mean(cheave(1:100));
cpitch=cpitch-mean(cpitch(1:100));
cspeed=cspeed-mean(cspeed(1:100));
cwave=cwave-mean(cwave(1:100));
cbend=cbend-mean(cbend(1:100));
sheave=-0.00140*data(:,1)+87.5966;
spitch=-0.00232*data(:,2)+70.5666;
sspeed=0.00015*data(:,3)-5.0490;
swave=0.00050*data(:,4)-17.3866;
sbend=0.00580*data(:,5)-212.5687;
sheave=sheave-mean(sheave(1:100));
spitch=spitch-mean(spitch(1:100));
sspeed=sspeed-mean(sspeed(1:100));
swave=swave-mean(swave(1:100));
sbend=sbend-mean(sbend(1:100));
% Find the Speed Segment for Analysis
[mxi,I]=max(cspeed);cheave=cheave(I+150:I+2649);
cpitch=cpitch(I+150:I+2649);
cspeed=cspeed(I+150:I+2649);
cwave=cwave(I+150:I+2649);
cbend=cbend(I+150:I+2649);
[mxj,J]=max(sspeed);sheave=sheave(J+150:J+2649);
spitch=spitch(J+150:J+2649);
sspeed=sspeed(J+150:J+2649);
swave=swave(J+150:J+2649);
sbend=sbend(J+150:J+2649);
% Find the Wave-induced Response
heave=sheave-mean(cheave);
pitch=spitch-mean(cpitch);
wave=swave-mean(cwave);
bend=sbend-mean(cbend);
speed=sspeed;
sample=[wave heave pitch bend];
```

s5spec.m

```
% Spectral Analysis of Random Test (Head Wave Towing Test 0.5m/sec)
series=[];
calm=c05c;
data=s5j7r1;
s5sample
series=[series;sample];
data=s5j7r2;
s5sample
series=[series;sample];
data=s5j7r3;
s5sample
series=[series;sample];
data=s5j7r4;
s5sample
series=[series;sample];
calm=c05d;
data=s5j7r5;
s5sample
series=[series;sample];
data=s5j7r6;
s5sample
series=[series;sample];
data=s5j7r7;
s5sample
series=[series;sample];
%Read Data from Joined Time Series
wave=series(:,1);
heave=series(:,2);
pitch=series(:,3);
bend=series(:,4);
%Spectrum Estimation from Joined Time Series
fwave=fft(wave);
specw=fwave.*conj(fwave)/(17500*50);
fheave=fft(heave);
spech=fheave.*conj(fheave)/(17500*50);
fpitch=fft(pitch);
specp=fpitch.*conj(fpitch)/(17500*50);
fbend=fft(bend);
specb=fbend.*conj(fbend)/(17500*50);
specw=2*specw(1:8750);
spech=2*spech(1:8750);
specp=2*specp(1:8750);
specb=2*specb(1:8750);
f=[0:8749]'/350;
raoh=sqrt(spech./specw);
raop=sqrt(specp./specw);
raob=sqrt(specb./specw);
%Regular Wave Test Results
F=[0.333,0.450,0.573,0.702,0.840,0.841,0.987,1.135,1.292,1.454]';
AW=[2.82,2.23,2.61,3.02,2.95,2.57,1.37,2.90,3.23,3.12]';
AH=[2.90,2.24,2.53,2.41,1.99,1.68,1.31,0.34,0.43,0.25]';
```

```
AP=[0.81,0.96,1.64,2.22,3.26,2.77,3.20,1.98,0.26,0.19]';
AB=[2.30,3.12,5.84,9.71,12.39,11.73,13.09,4.86,7.65,4.65]';
RAOH=AH./AW;
RAOP=AP./AW;
RAOB=AB./AW;
%Plotting
figure
subplot(2,1,1)
plot(f(100:600),specw(100:600),'r')
title ('Wave Spectrum')
ylabel ('S(f)')
subplot(2,1,2)
plot(f(100:600),raob(100:600),'-r',F,RAOB,'ob')
legend('Random Test','Regular Test')
title ('BM RAOs')
ylabel ('RAO')
figure
subplot(2,1,1)
plot(f(100:600),raoh(100:600),'-r',F,RAOH,'ob')
title ('Heave RAOs')
ylabel ('RAO')
subplot(2,1,2)
plot(f(100:600),raop(100:600),'-r',F,RAOP,'ob')
title ('Pitch RAOs')
ylabel ('RAO')
xlabel ('f(Hz)')
```

s5neural.m

```
% Estimation of Correlation Functions for Training (Towing Test 0.5m/s)
series=[];
calm=c05c; data=s5j7r1;
s5sample
series=[series;sample];
data=s5j7r2;
s5sample
series=[series;sample];
data=s5j7r3;
s5sample
series=[series;sample];
data=s5j7r4;
s5sample
series=[series;sample];
calm=c05d; data=s5j7r5;
s5sample
series=[series;sample];
data=s5j7r6;
s5sample
series=[series;sample];
data=s5j7r7;
s5sample
series=[series;sample];
%Read Data from Joined Time Series
wave=series(:,1);
heave=series(:,2);
pitch=series(:,3);
bend=series(:,4);
% Estimation of Correlation Functions
for J=1:500
crosshh(J)=heave(1+(J-1):17500)'*heave(1:17500-(J-1))/(17500-(J-1));
crosshp(J)=pitch(1+(J-1):17500)'*heave(1:17500-(J-1))/(17500-(J-1));
crosshb(J)=bend(1+(J-1):17500)'*heave(1:17500-(J-1))/(17500-(J-1));
end
MX=max(crosshh);
crosshh=crosshh/MX;
crosshp=crosshp/MX;
crosshb=crosshb/MX;
% Calculation of Velocity & Acceleration
for K=1:480
      I=K+10;
      dhh(K)=crosshh(I);
      vhh(K)=(crosshh(I+10)-crosshh(I-10))/(2*0.2);
      ahh(K)=(crosshh(I+10)-2*crosshh(I)+crosshh(I-10))/(0.2)^2;
      dhp(K)=crosshp(I);
      vhp(K)=(crosshp(I+10)-crosshp(I-10))/(2*0.2);
      ahp(K)=(crosshp(I+10)-2*crosshp(I)+crosshp(I-10))/(0.2)^2;
      dhb(K)=crosshb(I);
end
t=[1:480]/50;
result=[dhh' vhh' ahh' dhp' vhp' ahp' dhb'];
```

s5test1.m

```
% An M-file of Regular Test Verification (Towing Tests 0.5m/sec)
s5sample
% Resampling Data
for J=1:50
crosshh(J)=heave(1+(J-1)*10:2500)'*heave(1:2500-(J-1)*10)/(2500-(J-
1)*10);
crosshp(J)=pitch(1+(J-1)*10:2500)'*heave(1:2500-(J-1)*10)/(2500-(J-
1)*10);
crosshb(J)=bend(1+(J-1)*10:2500)'*heave(1:2500-(J-1)*10)/(2500-(J-
1)*10);
end
MX=max(crosshh);
crosshh=crosshh/MX;
crosshp=crosshp/MX;
crosshb=crosshb/MX;
% Calculation of Velocity & Acceleration
for K=1:48
      I=K+1;
      dhh(K)=crosshh(I);
      vhh(K)=(crosshh(I+1)-crosshh(I-1))/(2*0.2);
      ahh(K)=(crosshh(I+1)-2*crosshh(I)+crosshh(I-1))/(0.2)^2;
      dhp(K)=crosshp(I);
      vhp(K)=(crosshp(I+1)-crosshp(I-1))/(2*0.2);
      ahp(K)=(crosshp(I+1)-2*crosshp(I)+crosshp(I-1))/(0.2)^2;
      dhb(K)=crosshb(I);
      vhb(K)=(crosshb(I+1)-crosshb(I-1))/(2*0.2);
      ahb(K)=(crosshb(I+1)-2*crosshb(I)+crosshb(I-1))/(0.2)^2;
end
t=[1:48]/5;
result=[dhh' vhh' ahh' dhp' vhp' ahp' dhb'];
```

s5test3.m

```
% An M-file for Random Test Verification (Towing Test 0.5m/sec)
series=[];
calm=c05c;
data=s5j7r1;
s5sample
series=[series;sample];
data=s5j7r2;
s5sample
series=[series;sample];
data=s5j7r3;
s5sample
series=[series;sample];
data=s5j7r4;
s5sample
series=[series;sample];
calm=c05d;
data=s5j7r5;
s5sample
series=[series;sample];
data=s5j7r6;
s5sample
series=[series;sample];
data=s5j7r7;
s5sample
series=[series;sample];
%Read Data from Joined Time Series
wave=series(:,1);
heave=series(:,2);
pitch=series(:,3);
bend=series(:,4);
% Resampling
N
crosshh=heave(N+1:N+500);
crosshp=pitch(N+1:N+500);
crosshb=bend(N+1:N+500);
MX=max(crosshh);
crosshh=crosshh/MX;
crosshp=crosshp/MX;
crosshb=crosshb/MX;
% Calculation of Velocity & Acceleration
for K=1:480
      I=K+10;
      dhh(K)=crosshh(I);
      vhh(K)=(crosshh(I+10)-crosshh(I-10))/(2*0.2);
      ahh(K)=(crosshh(I+10)-2*crosshh(I)+crosshh(I-10))/(0.2)^2;
      dhp(K)=crosshp(I);
      vhp(K)=(crosshp(I+10)-crosshp(I-10))/(2*0.2);
      ahp(K)=(crosshp(I+10)-2*crosshp(I)+crosshp(I-10))/(0.2)^2;
      dhb(K)=crosshb(I);
end
t=[1:480]/50;
```

```
%Frequency-domain Filter Implementation
fbend=fft(bend);
nfbend=zeros(size(fbend));
nfbend(1:1000)=fbend(1:1000);
nfbend(16502:17500)=fbend(16502:17500);
nbend=ifft(nfbend);
nbend=real(nbend);
fheave=fft(heave);
nfheave=zeros(size(fheave));
nfheave(1:1000)=fheave(1:1000);
nfheave(16502:17500)=fheave(16502:17500);
nheave=ifft(nfheave);
nheave=real(nheave);
fpitch=fft(pitch);
nfpitch=zeros(size(fpitch));
nfpitch(1:1000)=fpitch(1:1000);
nfpitch(16502:17500)=fpitch(16502:17500);
npitch=ifft(nfpitch);
npitch=real(npitch);
% Calculation for Filtered Values
for J=1:500
      ncrosshh(J)=nheave(1+N+(J-1));
      ncrosshp(J)=npitch(1+N+(J-1));
      ncrosshb(J)=nbend(1+N+(J-1));
end
ncrosshh=ncrosshh/MX;
ncrosshp=ncrosshp/MX;
ncrosshb=ncrosshb/MX;
% Calculation of Filtered Velocity & Acceleration
for K=1:480
      I=K+10;
      ndhh(K)=ncrosshh(I);
      nvhh(K)=(ncrosshh(I+10)-ncrosshh(I-10))/(2*0.2);
      nahh(K)=(ncrosshh(I+10)-2*ncrosshh(I)+ncrosshh(I-10))/(0.2)^2;
      ndhp(K)=ncrosshp(I);
      nvhp(K)=(ncrosshp(I+10)-ncrosshp(I-10))/(2*0.2);
      nahp(K)=(ncrosshp(I+10)-2*ncrosshp(I)+ncrosshp(I-10))/(0.2)^2;
      ndhb(K)=ncrosshb(I);
end
result=[ndhh' nvhh' nahh' ndhp' nvhp' nahp' ndhb'];
```

s5simu.m

```
%Simulation of Ship Motions and Bending Moment (Towing Test 0.5m/sec)
%JONSWAP Wave Spectrum
f1=0.5:0.01:0.7;
s1=0.21*7.5^2*0.7^4./f1.^5.*exp(-1.25*0.7^4./f1.^4).*3.3.^exp(-(f1-
0.7).^2/2/(0.07*0.7)^2);
f2=0.71:0.01:1.0;
s2=0.21*7.5^2*0.7^4./f2.^5.*exp(-1.25*0.7^4./f2.^4).*3.3.^exp(-(f2-
0.7).^2/2/(0.09*0.7)^2);
f0=[f1,f2]';
f=f0+2*pi*f0.^2/9.8*0.5;
s=[s1,s2]';
%Wave Simulation
phasew=rand(size(f))*2*pi;
ampliw=sqrt(2*s*0.01);
%Experimental Frequency Transfer Functions
F=[0.573,0.702,0.84,0.987,1.135,1.292,1.454]';
Magh=[0.97,0.8,0.67,0.96,0.12,0.13,0.08]';
Angleh=[10.56,7.56,8.43,-53.1,-3.7,76.95,108.3]';
Magp=[0.63,0.74,1.11,2.34,0.68,0.08,0.06]';
Anglep=[98.7,99.2,103,24.3,23.6,64.7,159.2]';
Magb=[2.24,3.22,4.2,9.55,1.68,2.37,1.49]';
Angleb=[207.8,190,167.6,79.7,-4.6,-108.1,-113.2]';
%Heave Simulation
raoh=interp1(F,Magh,f);
phaseh=interp1(F,Angleh,f)*pi/180;
t=[0.02:0.02:450]';
heave=zeros(size(t));
for k=1:size(f)
   heave=heave+ampliw(k)*raoh(k)*cos(2*pi*f(k)*t+phasew(k)+phaseh(k));
end
%Pitch Simulation
raop=interp1(F,Magp,f);
phasep=interp1(F,Anglep,f)*pi/180;
pitch=zeros(size(t));
for k=1:size(f)
   pitch=pitch+ampliw(k)*raop(k)*cos(2*pi*f(k)*t+phasew(k)+phasep(k));
end
%Bending Moment Simulation
raob=interp1(F,Magb,f);
phaseb=interp1(F,Angleb,f)*pi/180;
bend=zeros(size(t));
for k=1:size(f)
   bend=bend+ampliw(k)*raob(k)*cos(2*pi*f(k)*t+phasew(k)+phaseb(k));
end
% Estimation of Correlation Functions
for J=1:500
crosshh(J)=heave(1+(J-1):22500)'*heave(1:22500-(J-1))/(22500-(J-1));
crosshp(J)=pitch(1+(J-1):22500)'*heave(1:22500-(J-1))/(22500-(J-1));
crosshb(J)=bend(1+(J-1):22500)'*heave(1:22500-(J-1))/(22500-(J-1));
end
MX=max(crosshh);
```

```
crosshh=crosshh/MX;
crosshp=crosshp/MX;
crosshb=crosshb/MX;
% Calculation of Velocity & Acceleration
for K=1:480
      I=K+10;
      dhh(K)=crosshh(I);
      vhh(K)=(crosshh(I+10)-crosshh(I-10))/(2*0.2);
      ahh(K)=(crosshh(I+10)-2*crosshh(I)+crosshh(I-10))/(0.2)^2;
      dhp(K)=crosshp(I);
      vhp(K)=(crosshp(I+10)-crosshp(I-10))/(2*0.2);
      ahp(K)=(crosshp(I+10)-2*crosshp(I)+crosshp(I-10))/(0.2)^2;
      dhb(K)=crosshb(I);
end
T=[1:480]/50;
result=[dhh' vhh' ahh' dhp' vhp' ahp' dhb'];
```

Appendix III Data Analysis Results

The RAOs results obtained from both the regular wave tests and the random wave tests are presented in this Appendix.

In the following figures, the circle points represent the RAOs values from the regular wave tests.

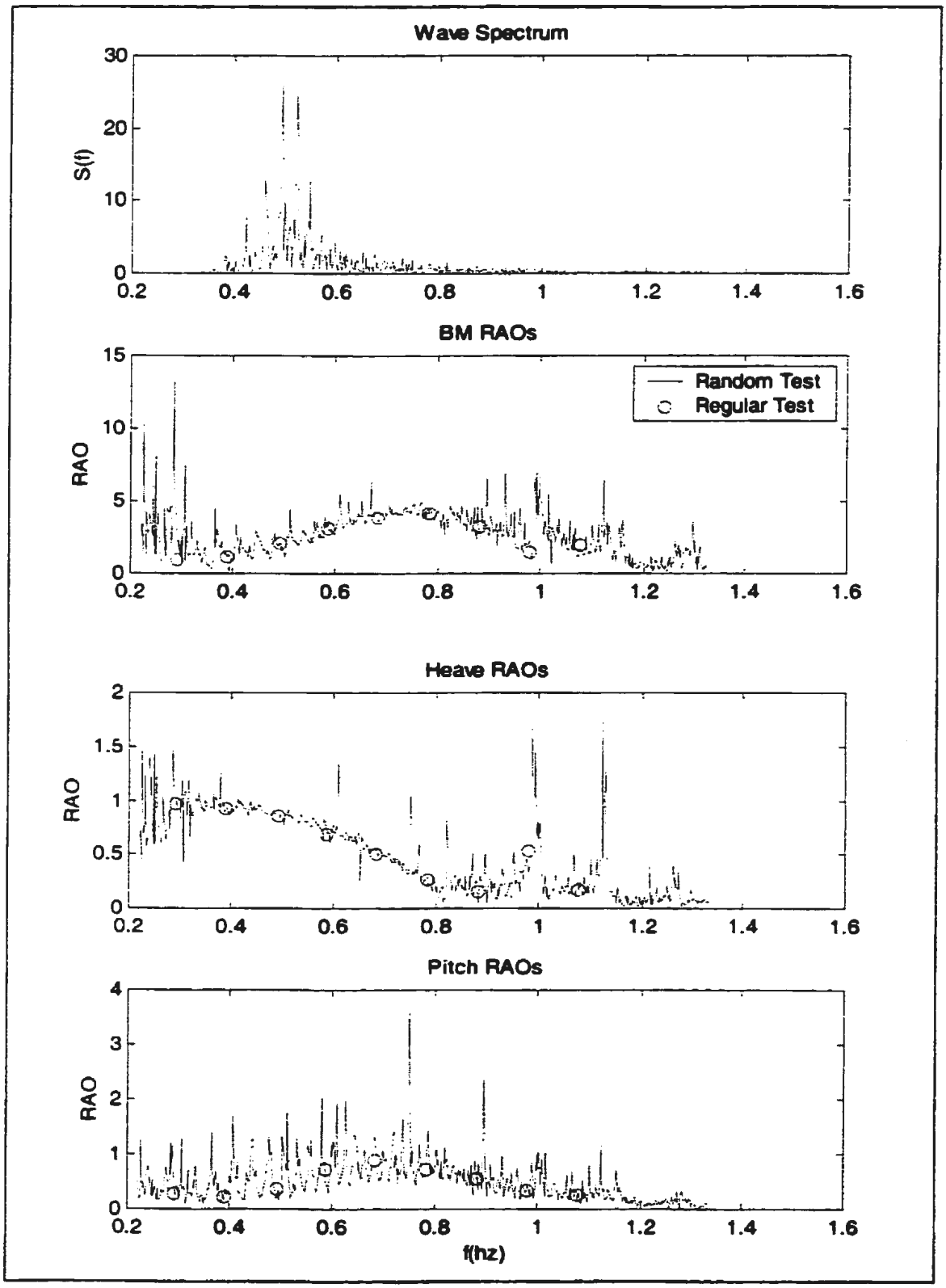

Figure 38: Spectral Analysis Results of J5h5a

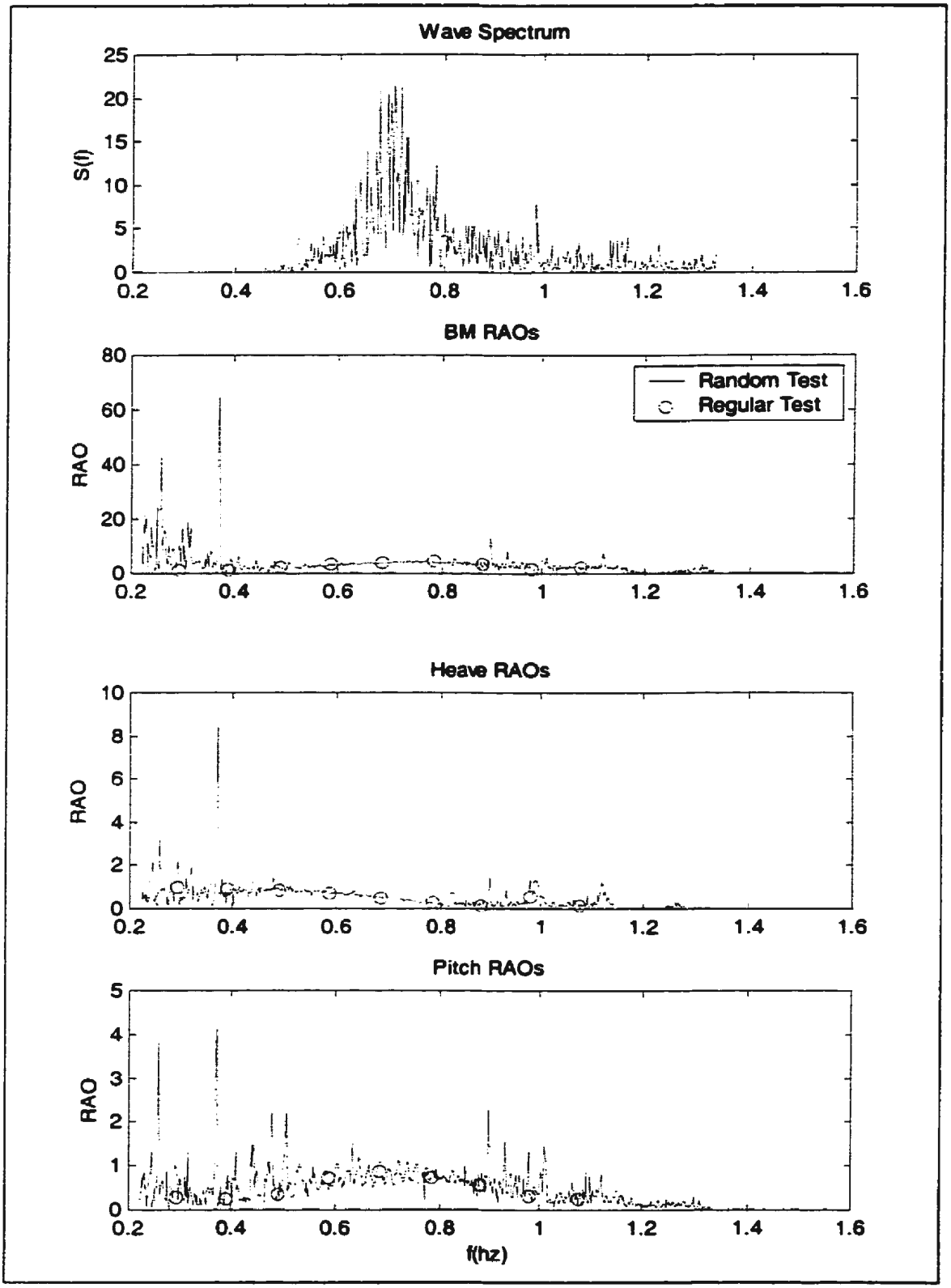

Figure 39: Spectral Analysis Results of J5h75b.dat

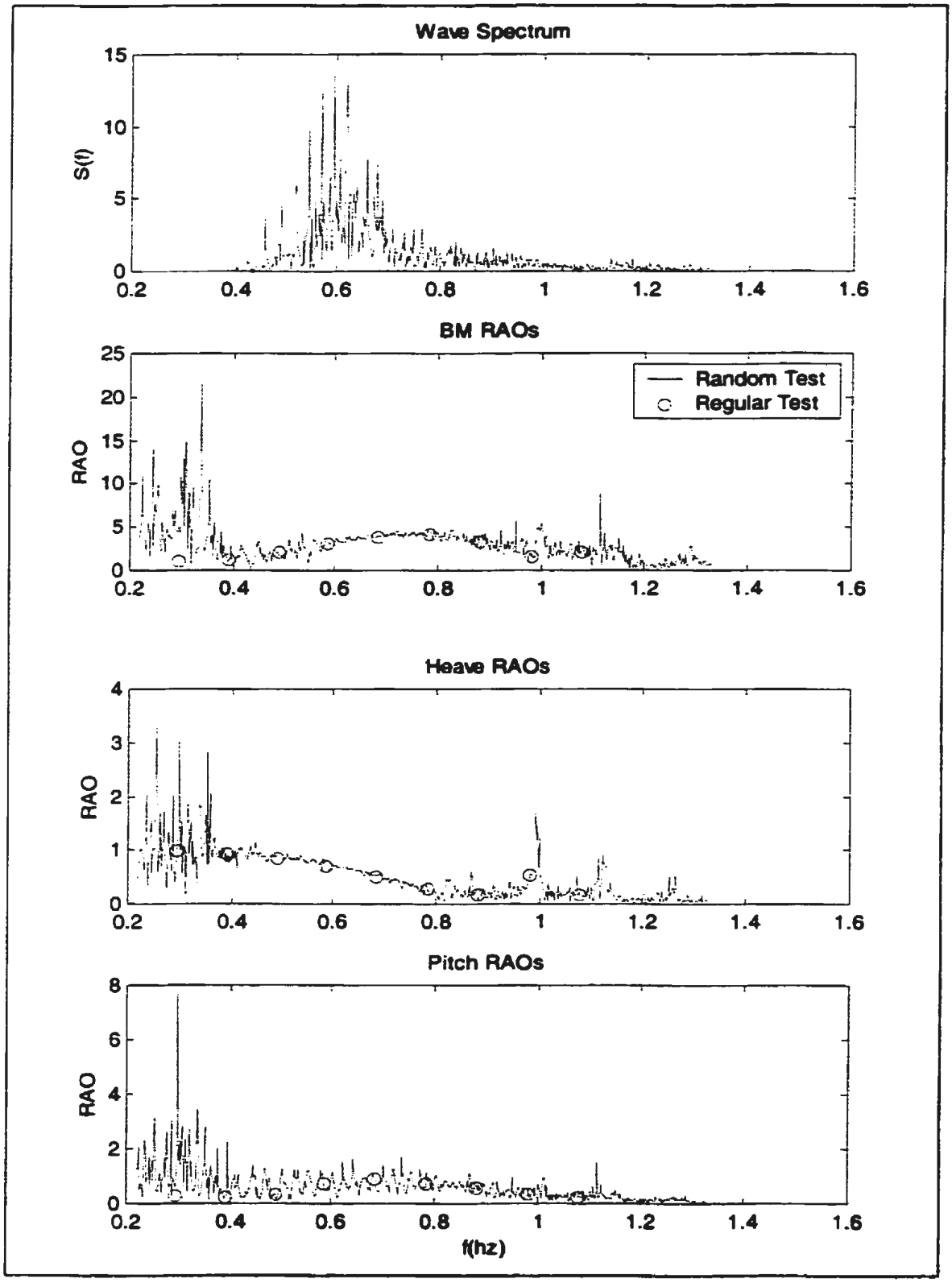

Figure 40: Spectral Analysis Results of J6h5a.dat

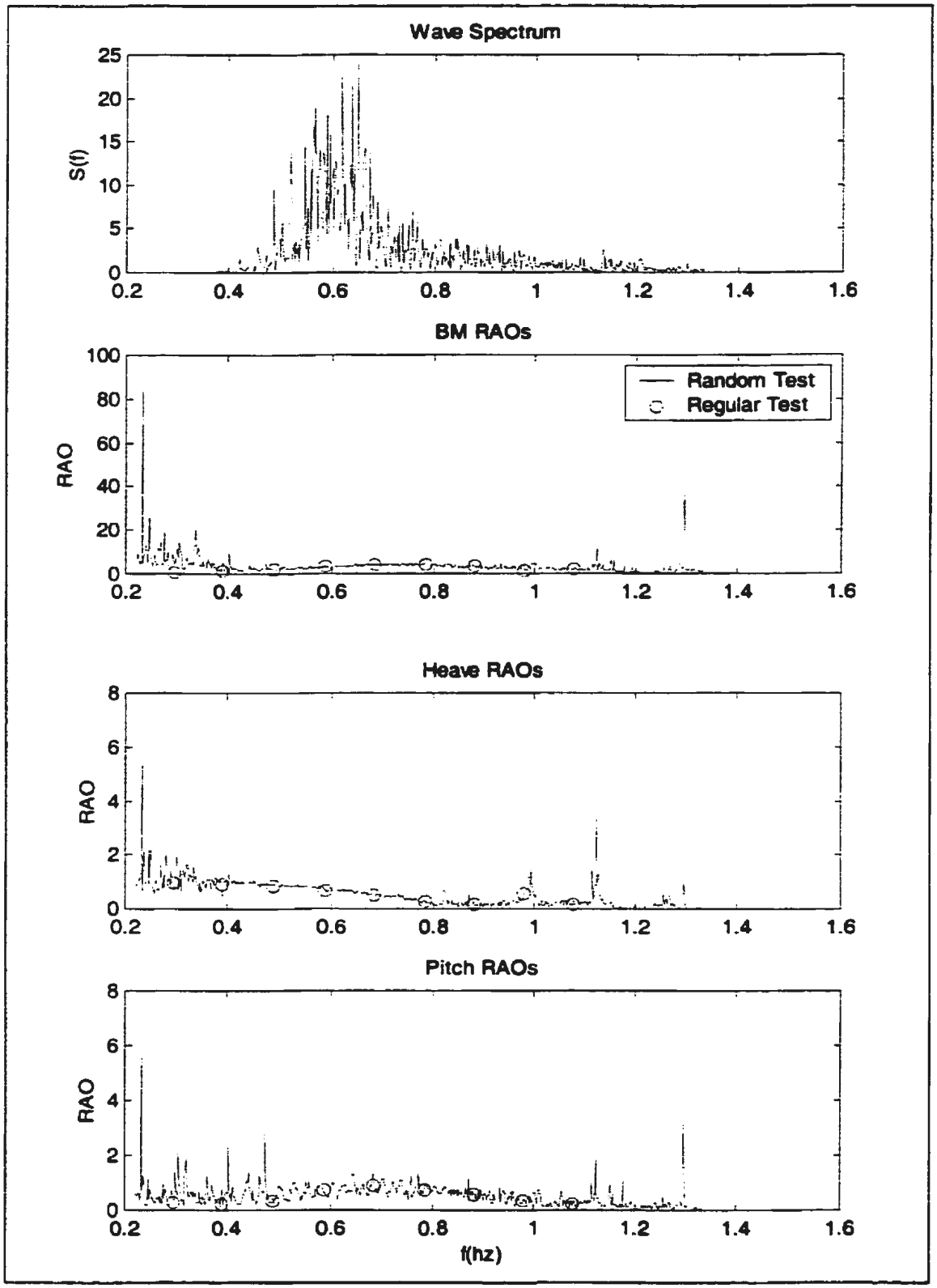

Figure 41: Spectral Analysis Results of J6h75a.dat

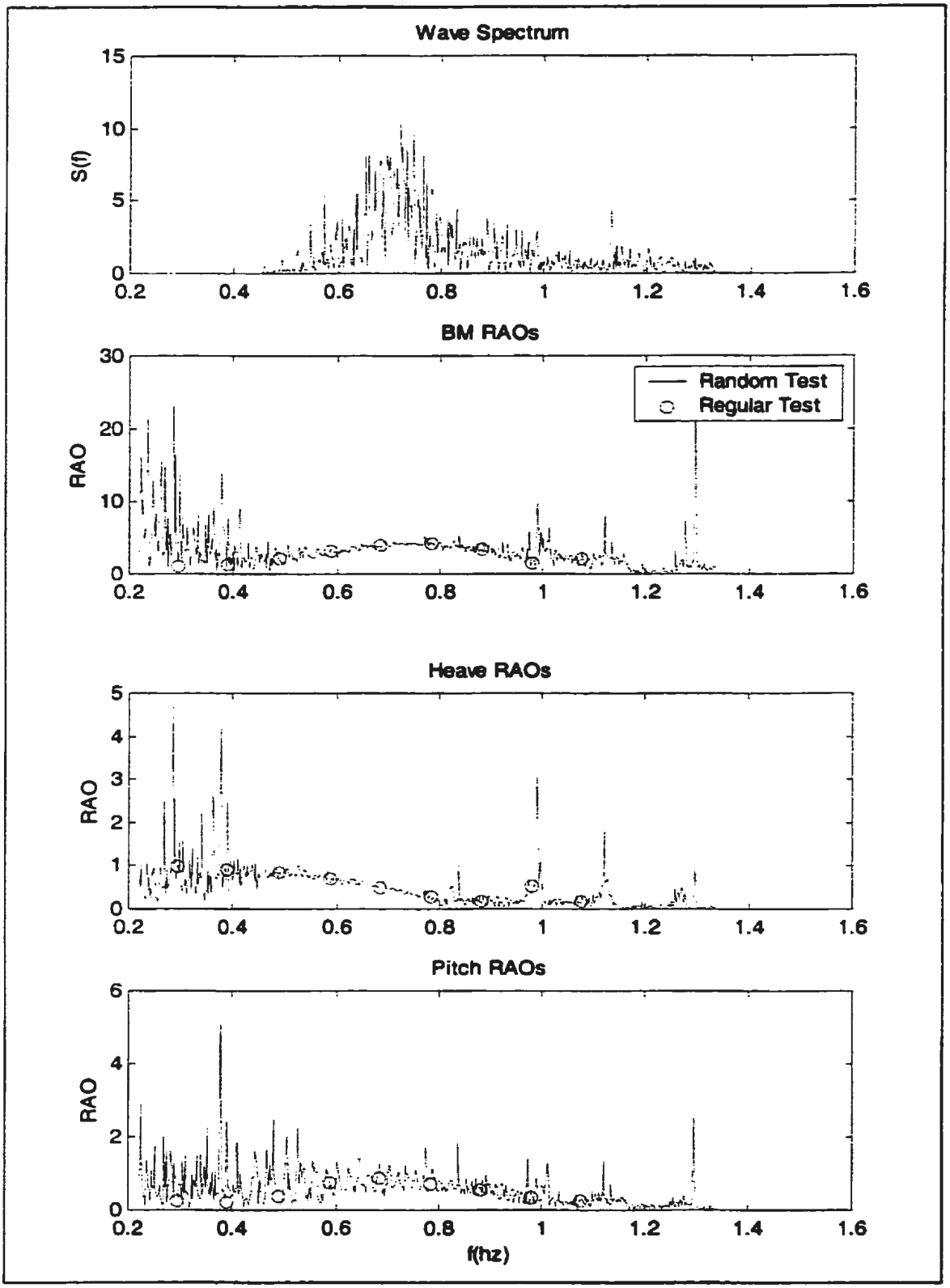

Figure 42: Spectral Analysis Results of J7h5c.dat

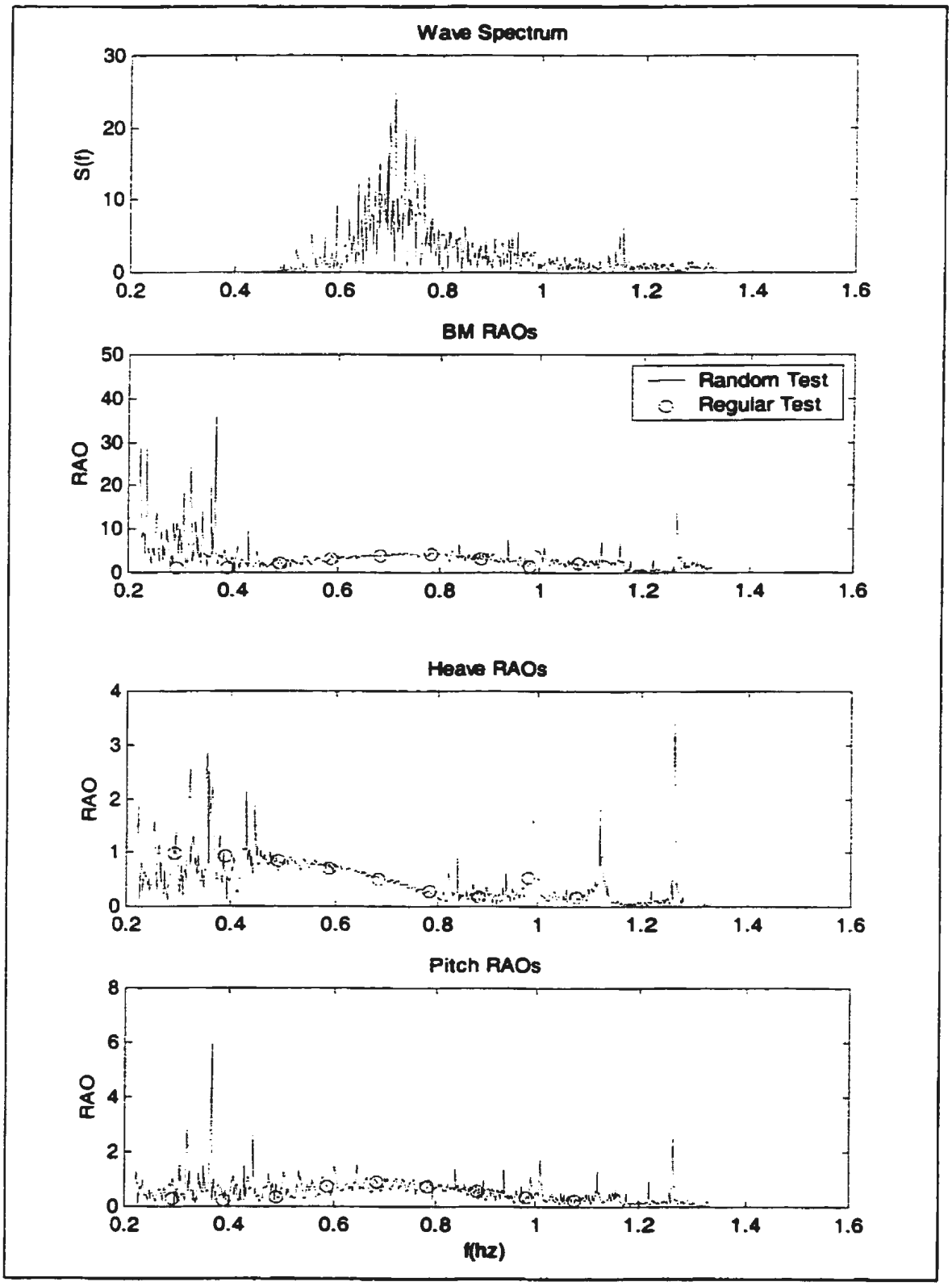

Figure 43: Spectral Analysis Results of J7h75a.dat

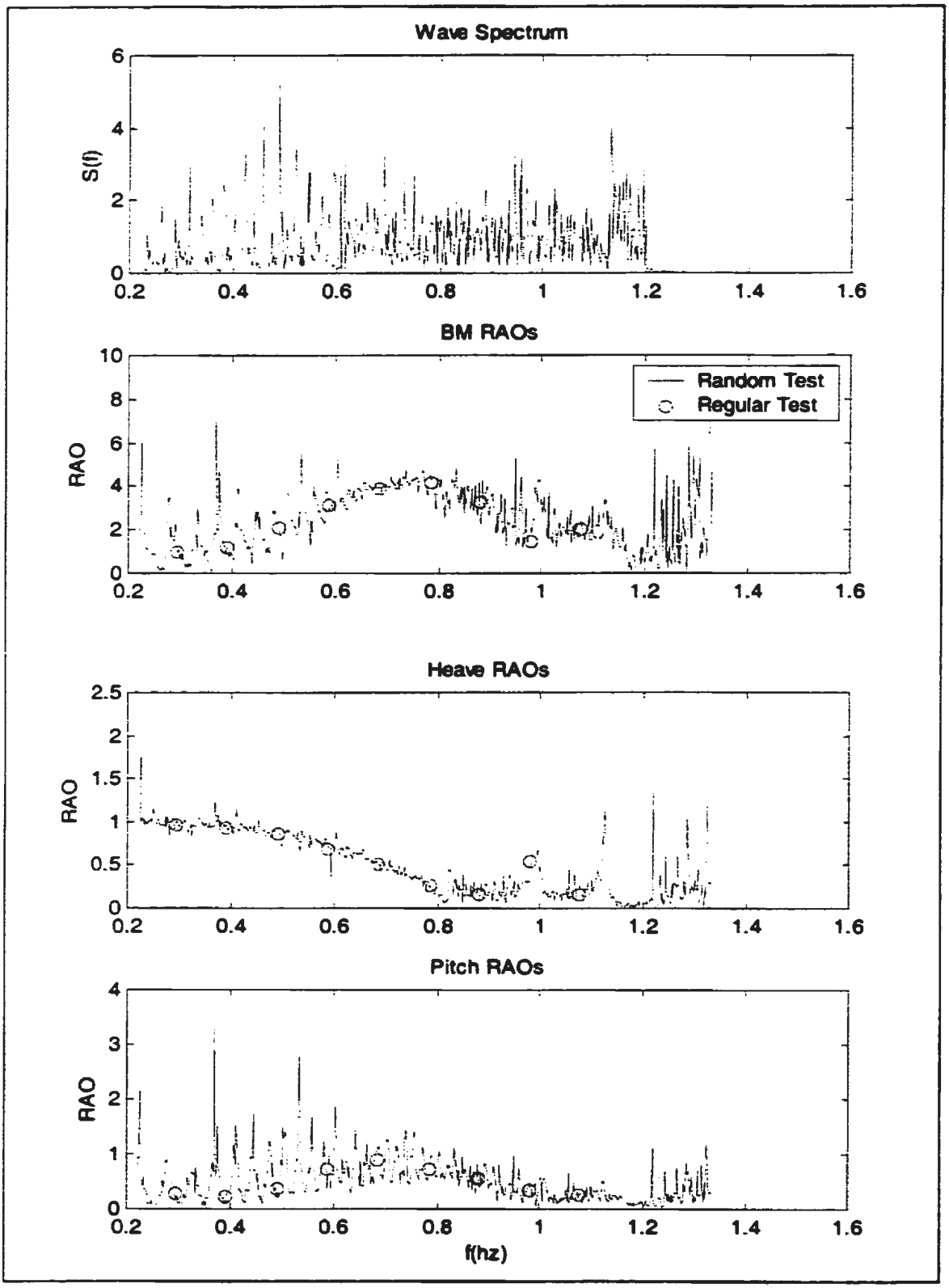

Figure 44: Spectral Analysis Results of B5a.dat

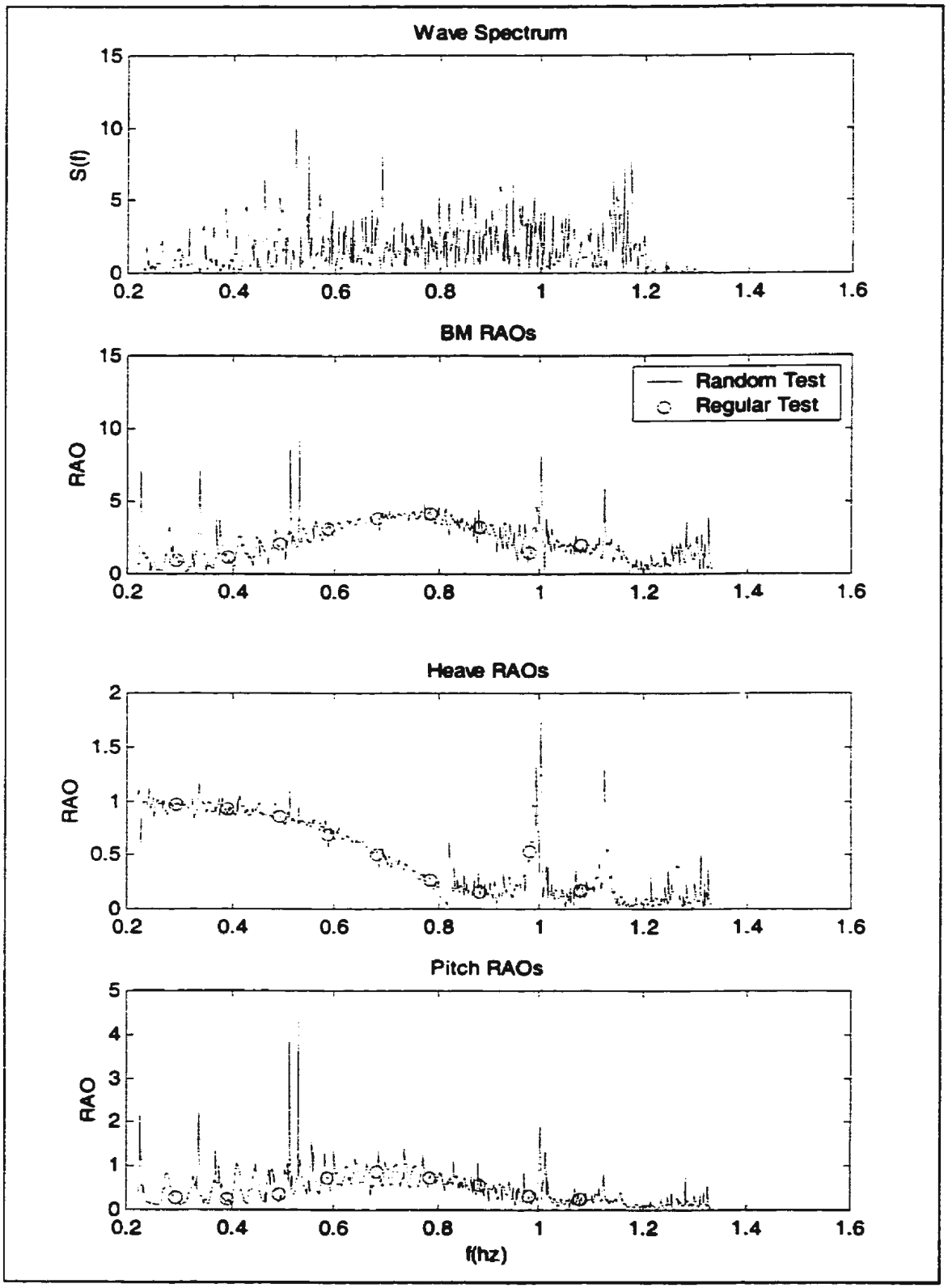

Figure 45: Spectral Analysis Results of B75b.dat

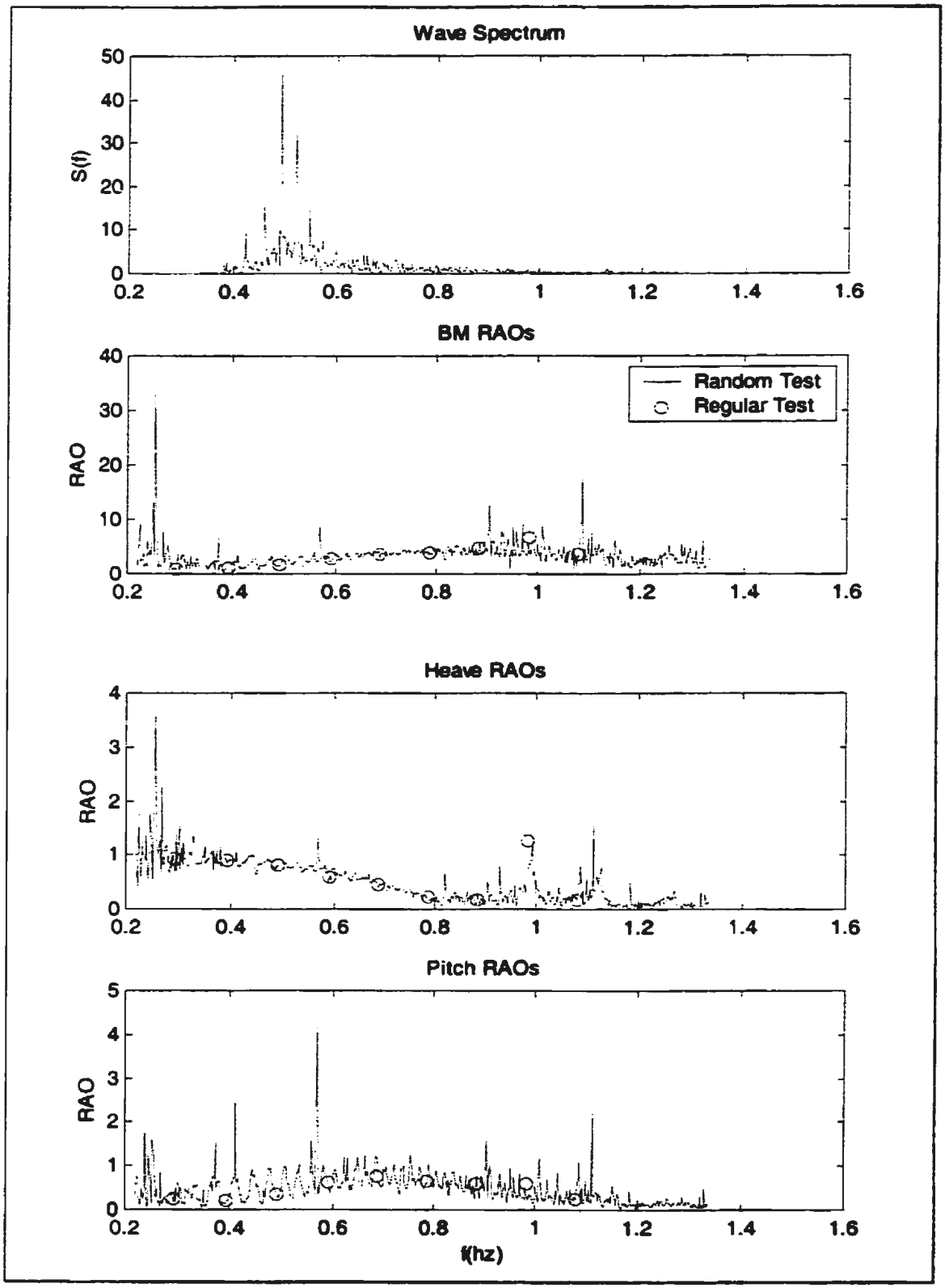

Figure 46: Spectral Analysis Results of Fj5h5a.dat

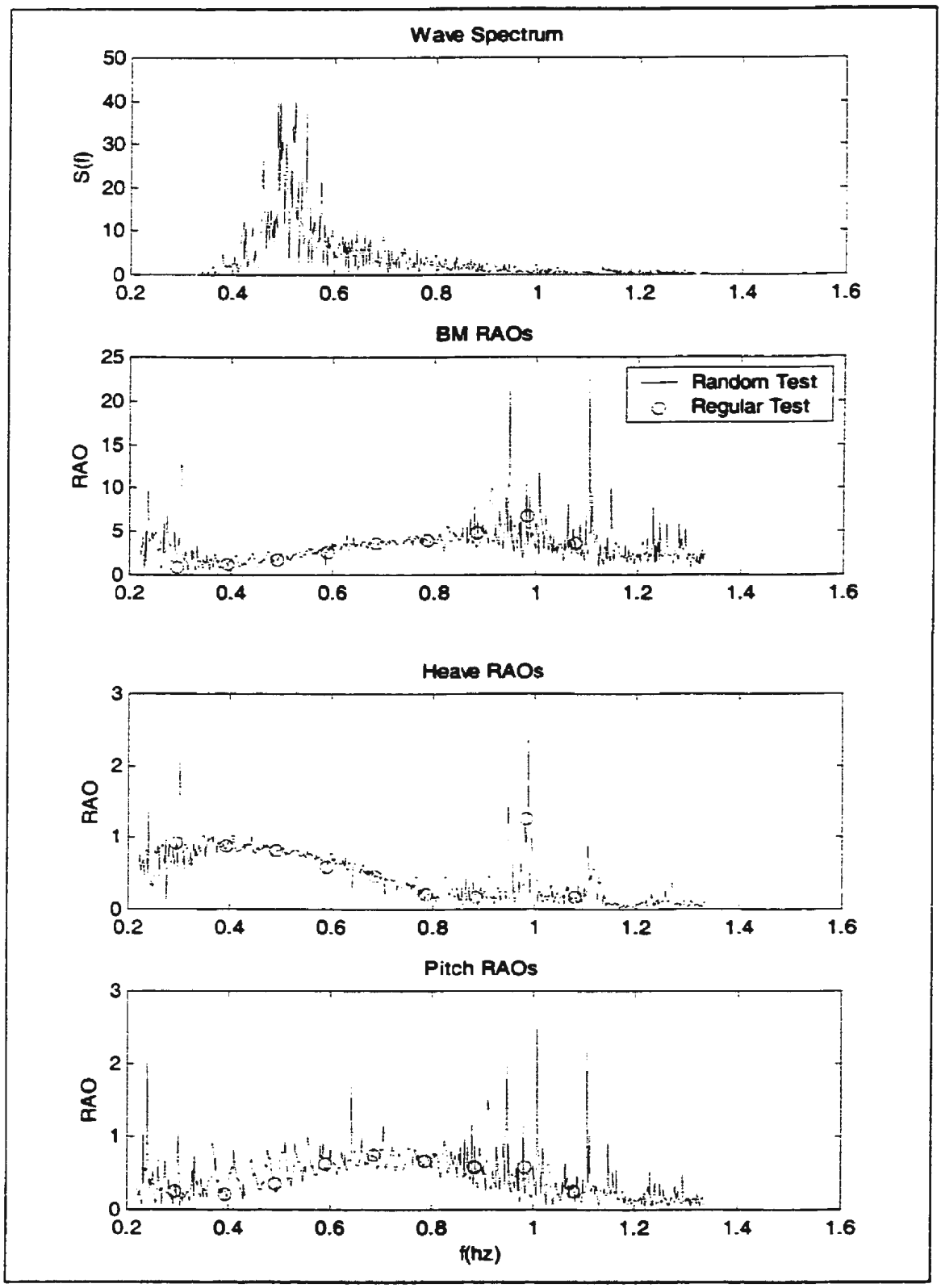

Figure 47: Spectral Analysis Results of Fj5h75b.dat

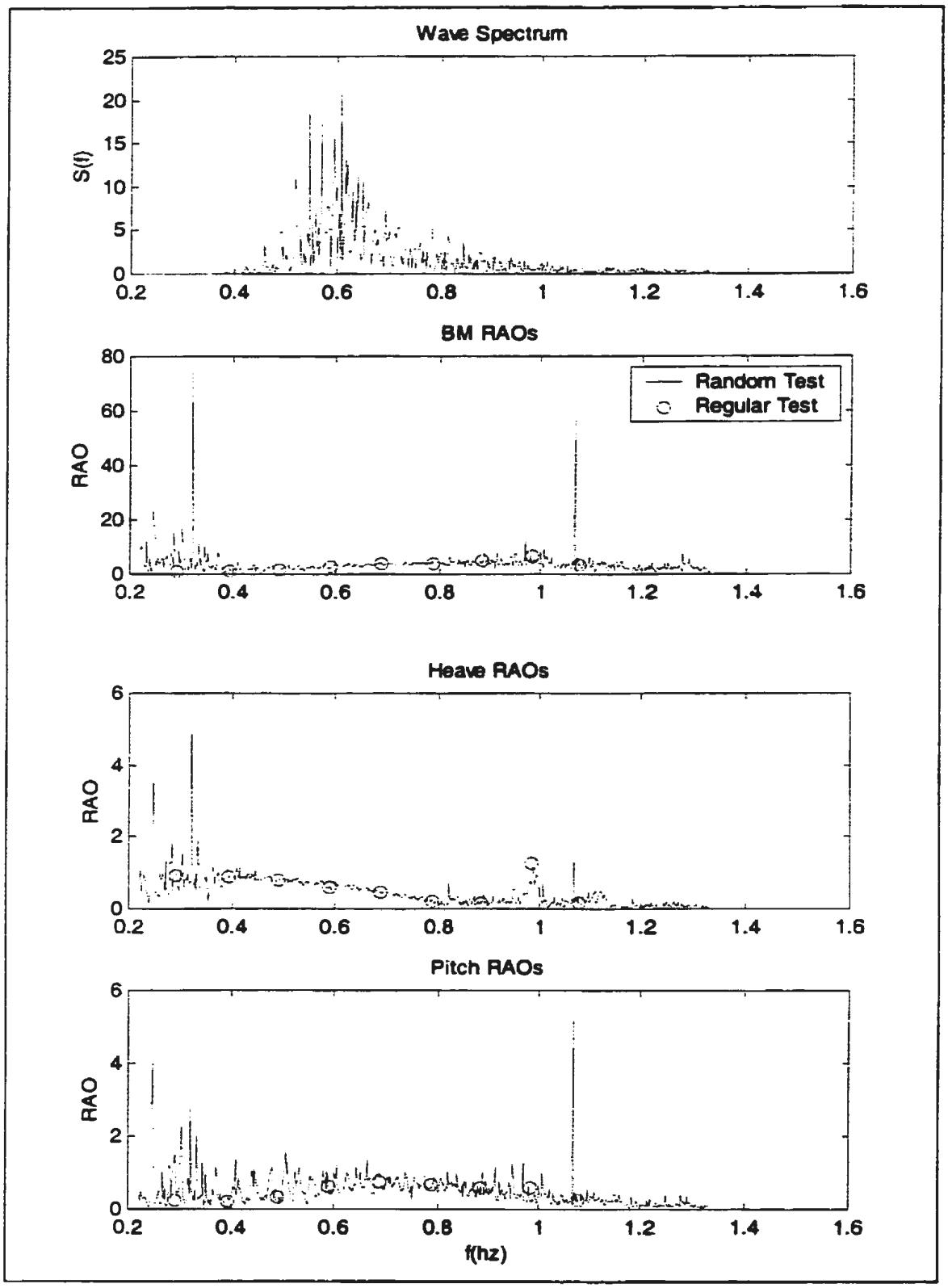

Figure 48: Spectral Analysis Results of Fj6h5a.dat

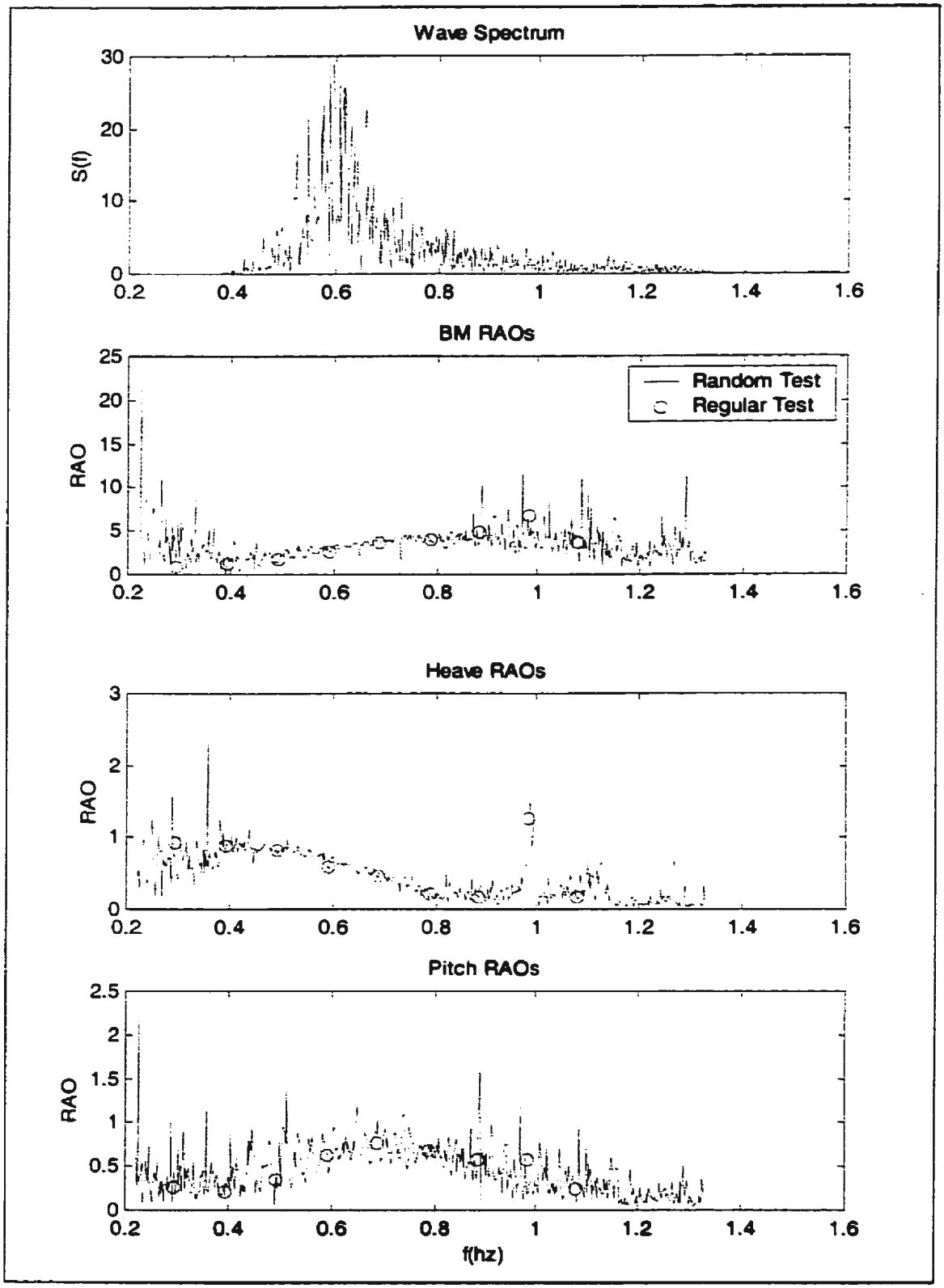

Figure 49: Spectral Analysis Results of Fj6h75a.dat

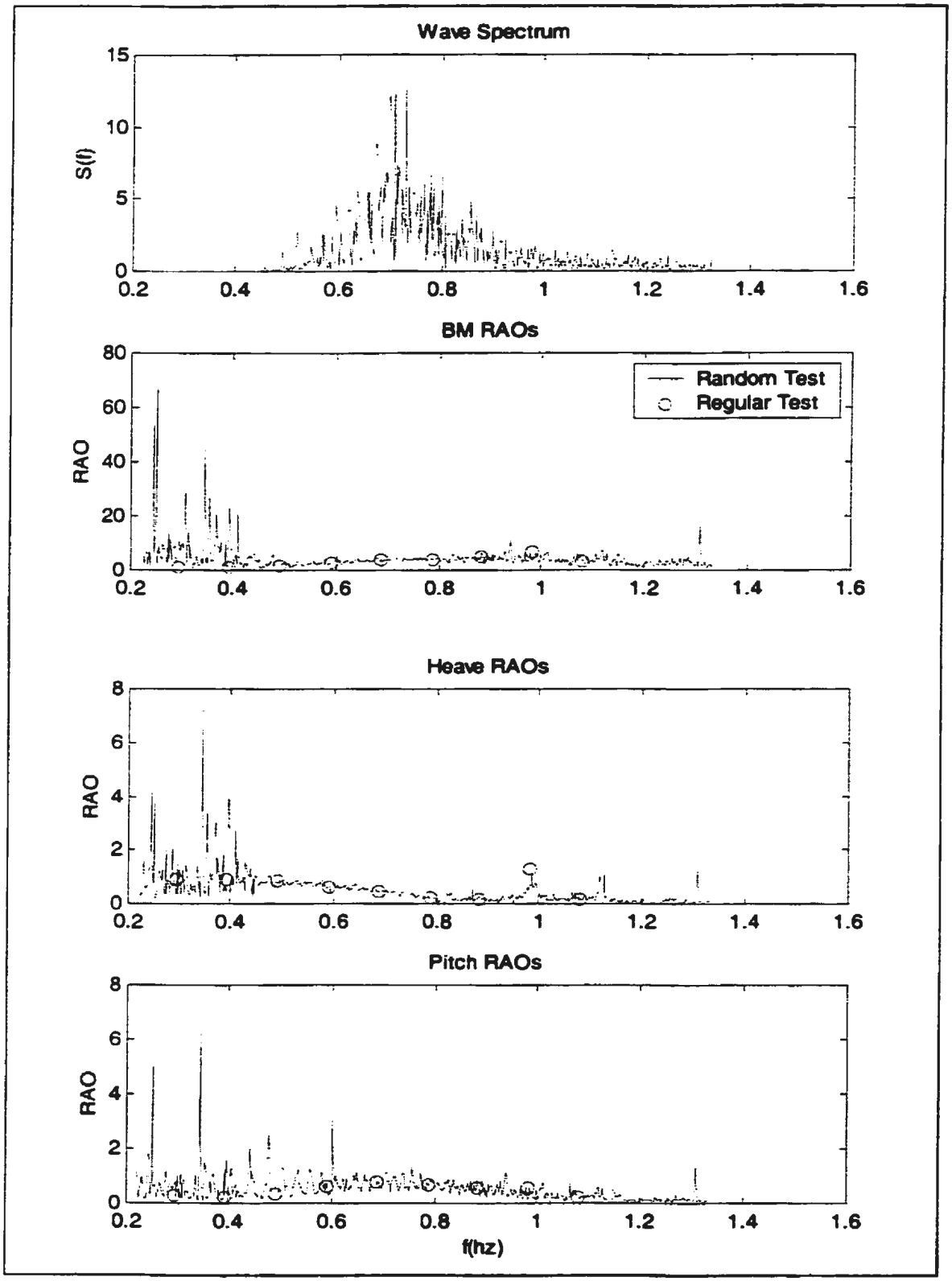

Figure 50: Spectral Analysis Results of Fj7h5a.dat

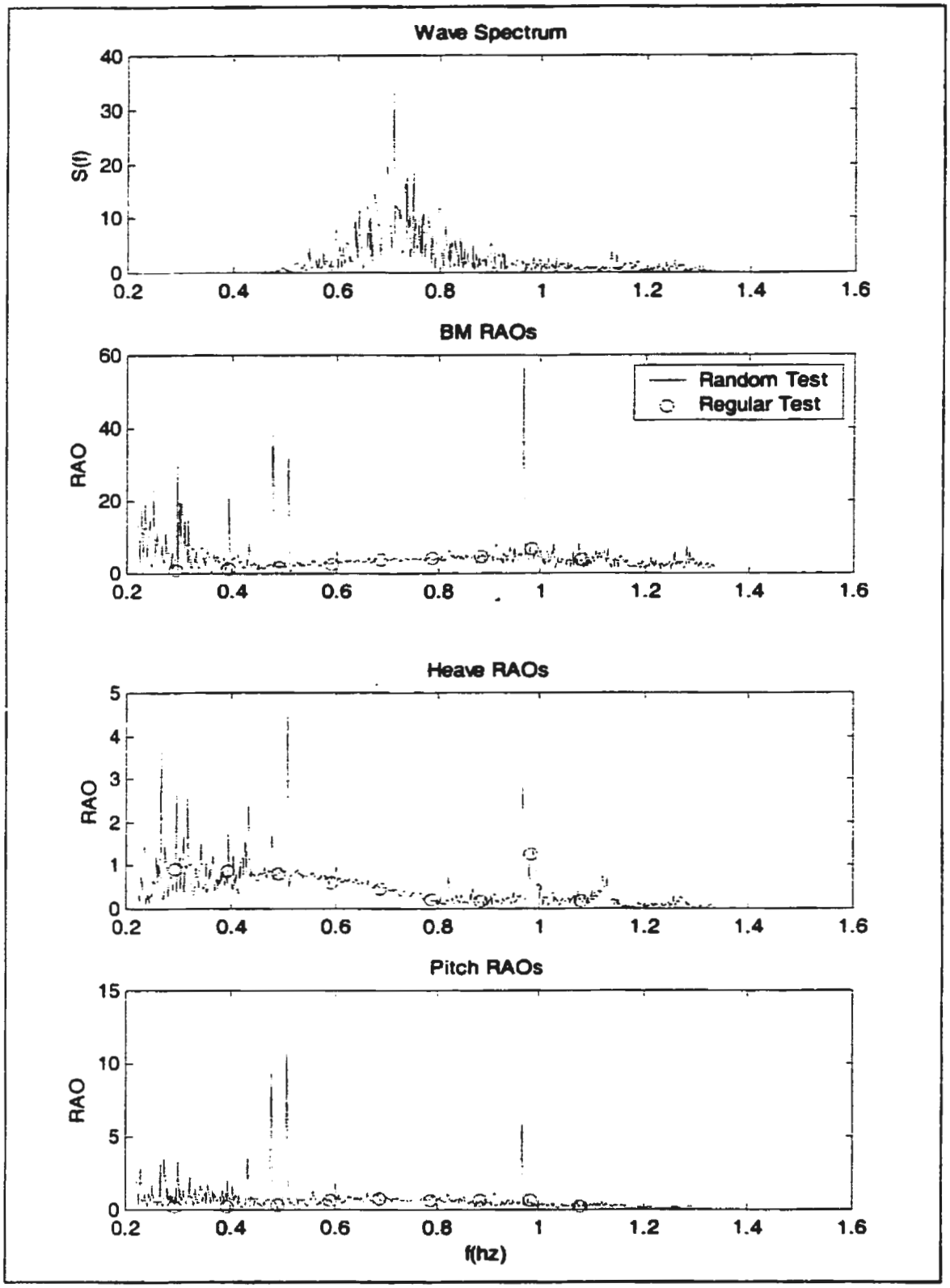

Figure 51: Spectral Analysis Results of Fj7h75a.dat

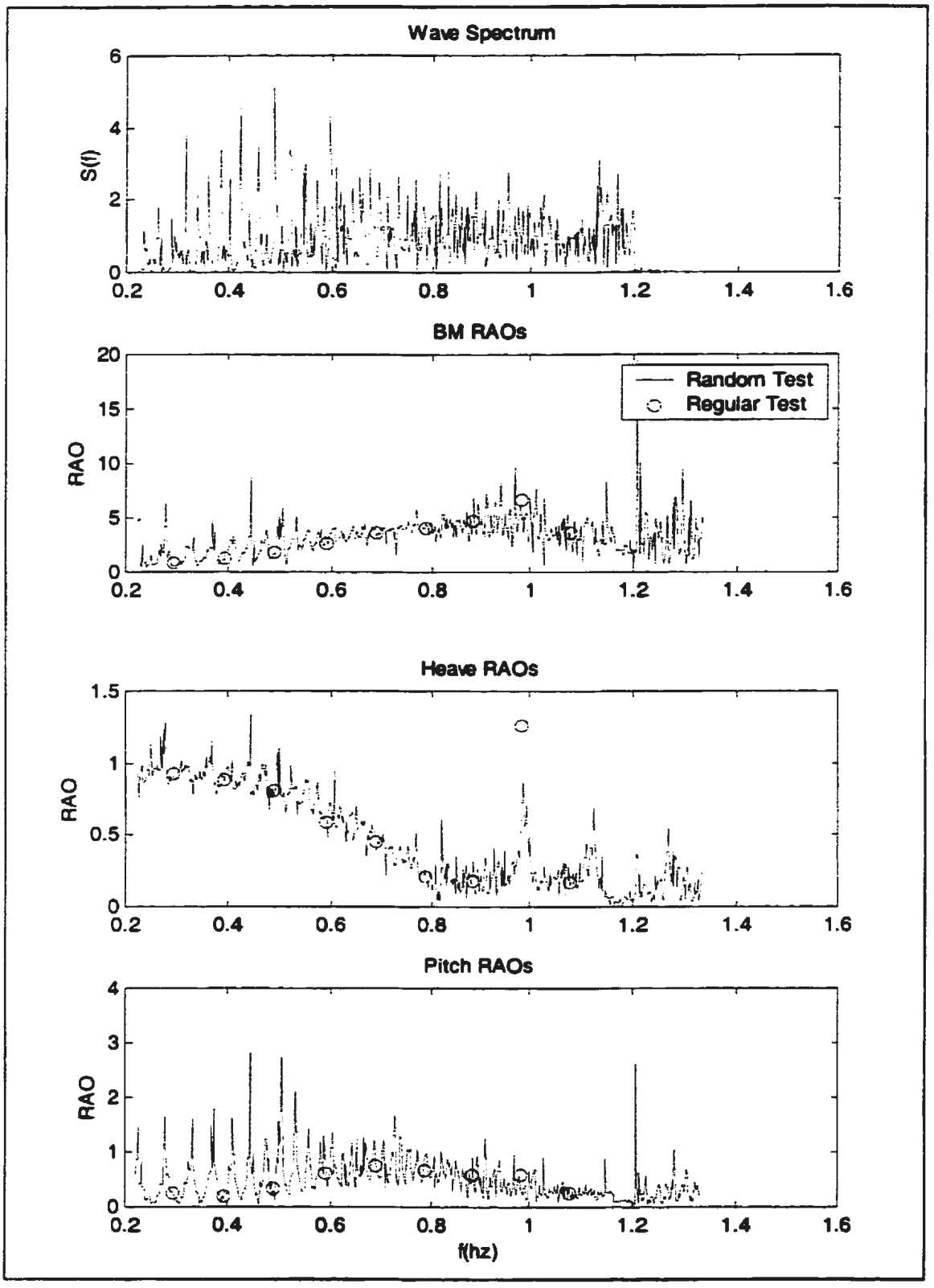

Figure 52: Spectral Analysis Results of Fb5a.dat

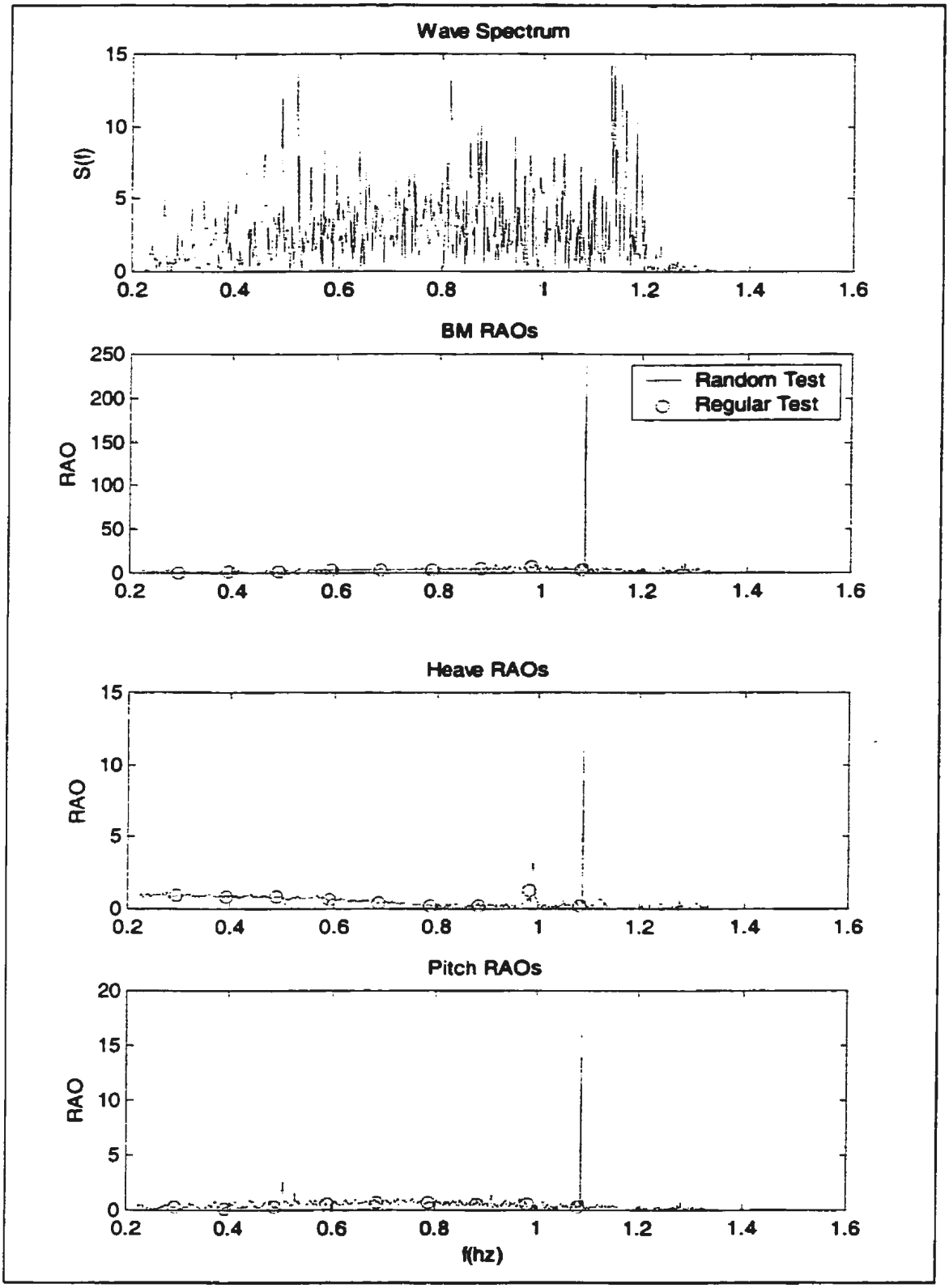

Figure 53: Spectral Analysis Results of Fb75a.dat